T.C.

TOKAT GAZİOSMANPAŞA ÜNİVERSİTESİ

LİSANSÜSTÜ EĞİTİM ENSTİTÜSÜ

BİYOLOJİ ANABİLİM DALI

MOLEKÜLER BİYOLOJİ DOKTORA PROGRAMI

GSDMC- AND GSDMD-MEDIATED PYROPTOTIC CELL DEATH IN OVARIAN CANCER AND THE ROLE OF ESTROGEN ON THIS CELL DEATH MECHANISM

DOKTORA TEZİ

Çağlar BERKEL

Danışman: Doç. Dr. Ercan ÇAÇAN

TOKAT – 2023

Bu tez çalışması, Tokat Gaziosmanpaşa Üniversitesi Bilimsel Araştırma Projeleri (BAP) (2021/87) ve TÜBİTAK (1001-122S735) tarafından desteklenmiştir. Ayrıca, Çağlar BERKEL, TÜBİTAK 2211-E programı tarafından desteklenmiştir.

This study has been supported by Tokat Gaziosmanpasa University Independent Research Projects program (2021/87) and TUBITAK (The Scientific and Technological Research Council of Turkey) (1001-122S735). In addition, Caglar BERKEL has been supported by TUBITAK 2211-E program.

ETİK SÖZLEŞME

Tokat Gaziosmanpaşa Üniversitesi Lisansüstü Eğitim Enstitüsü tez yazım kılavuzuna göre, Doç. Dr. Ercan ÇAÇAN danışmanlığında hazırlamış olduğum "OVER KANSERİNDE GSDMC- VE GSDMD-ARACILI PİROPTOTİK HÜCRE ÖLÜMÜ VE BU HÜCRE ÖLÜM MEKANİZMASINA ÖSTROJENİN ETKİSİ" adlı doktora tezinin bilimsel etik değerlere ve kurallara uygun, özgün bir çalışma olduğunu, aksinin tespit edilmesi halinde her türlü yasal yaptırımı kabul edeceğimi beyan ederim.

…/…/…

Çağlar BERKEL

ÖNSÖZ/TEŞEKKÜR

Bu tez çalışmasının gerçekleştirilmesinde büyük katkıları olan danışmanım **Doç. Dr. Ercan ÇAÇAN**'a, iş arkadaşlarım **Arş. Gör. Burak KÜÇÜK**'e, **Arş. Gör. Dr. Feyzanur ÇALDIRAN**'a, **Arş. Gör. Habeş Bilal AYDEMİR**'e, tez izleme komitesi üyeleri **Doç. Dr. Aykut Özgür**'e ve **Doç. Dr. Ali AYDIN**'a, başta **Aysun KESKİN, Fatma Nihan ÇELİK, Çağla SEVİNÇ, Burcu BAL, Muhsine ÖZEN** ve **Bahra NAJI** olmak üzere Çaçan lab'ın tüm eski ve yeni üyelerine teşekkür ederim.

ÖZET

OVER KANSERİNDE GSDMC- VE GSDMD-ARACILI PİROPTOTİK HÜCRE ÖLÜMÜ VE BU HÜCRE ÖLÜM MEKANİZMASINA ÖSTROJENİN ETKİSİ

Berkel, Çağlar
Doktora, Biyoloji Anabilim Dalı, Moleküler Biyoloji Programı
Tez Danışmanı: Doç. Dr. Ercan ÇAÇAN
Temmuz 2023, xii + 120 sayfa

Over (yumurtalık) kanseri, jinekolojik maligniteler arasında en yüksek ölüm oranlarına sahip ve kadınlarda en yaygın gözlenen yedinci kanser tipidir. Piroptozis, N-terminal bölgeleri ile membranı hedef alan, lipitlere bağlanan ve ardından por oluşturan gasdermin (GSDM) proteinlerinin aracılık ettiği pro-inflammatuar bir programlı hücre ölüm şeklidir. Bu tez çalışmasında, seröz over kanserinde, sağlıklı over dokusuna kıyasla, GSDMD ve GSDMC mRNA ekspresyonunda artış olduğunu ancak GSDME ve PJVK ekspresyonunda düşüş olduğunu gösterdik. GSDMB ve GSDMD gen ifadelerinin epitel over kanserinin çeşitli histolojik tipleri arasında farklılık gösterdiğini bulduk. GSDMC ve GSDMD genlerinde kopya sayısı kazanımlarının over kanseri hastalarında oldukça yaygın olduğunu (hastaların yaklaşık %50'sinde) gösterdik. TP53 mutasyonuna sahip over kanseri hastalarında, yüksek GSDMD ve GSDMC ekspresyonunun daha kısa progresyonsuz (ilerlemesiz) sağkalım süresi (PFS) ile ilişkili olduğunu ortaya koyduk. Dahası, over tümörlerinde, tümör mikroçevresindeki non-malignant stroma hücrelerine kıyasla, GSDMD protein seviyelerinin daha yüksek olduğunu ve GSDME protein seviyelerinin ise daha düşük olduğunu bulduk. Piroptozisi takiben hücre zarının parçalanmasından sorumlu bir protein olan NINJ1'in ekspresyonunun over kanserinde erken tümör evresinden geç tümör evresine geçerken düştüğünü gösterdik. NINJ1 kopya sayısı kaybı olaylarının over kanserinde diğer kanser tiplerine kıyasla daha yüksek olduğunu ve over kanseri hastalarında yüksek NINJ1 ekspresyonunun daha iyi sağkalım oranları ile ilişkili olduğunu bulduk. Aynı zamanda, *in vitro* olarak NINJ1 mRNA ifadesinin sisplatin-dirençli over kanseri hücrelerde sisplatin-sensitif olanlara göre daha düşük olduğunu ortaya koyduk. Dahası, östrojen uygulamasının, kemosensitif A2780 over kanseri hücrelerinde, GSDMC ve GSDMD ekspresyonunu transkript seviyesinde arttırdığı ama aynı durumun kemodirençli A2780-AD hücrelerinde gözlemlenmediğini ortaya koyduk. GSDMC overekspresyonunun, nigericin (bir piroptozis uyaranı) uygulanmış A2780-AD hücrelerinde hücre canlılığındaki düşüşü negatif kontrol hücrelerine kıyasla daha az kayda değer bir seviyeye indirdiğini gösterdik. Ek olarak, GSDMC ya da GSDMD overekspresyonunun nigericin uygulanmamış A2780 hücrelerinde hücre canlılığını arttırdığını bulduk. A2780 hücrelerinde GSDMD geni susturulduğunda, nigericine bağlı hücre canlılığındaki düşüşün, negatif siRNA uygulanmış hücrelere kıyasla, daha az kayda değer bir seviyeye indiğini ortaya koyduk. A2780-AD hücrelerinde GSDMC geni susturulduğunda ise, nigericine bağlı hücre canlılığındaki düşüşün, negatif siRNA uygulanmış kontrol hücrelere kıyasla, kayda değer olmayan bir seviyeye indiğini

bulduk. A2780 hücre hattında, belirli kaspazların (kaspaz-1, -4, -6 ya da -8) spesifik kaspaz inhibitörleri ile inhibisyonunun hücre canlılığında nigericine-bağlı düşüşü ortadan kaldırdığını gösterdik. Aksine, sadece kaspaz-1'in inhibisyonu, kemodirençli A2780-AD hücre hattında nigericine bağlı hücre canlılığındaki düşüşü ortadan kaldırdı. Ayrıca, kaspaz-1, -4 ya da -8 inhibisyonunun nigericin uygulanmış A2780 hücre hattında, hücre dışına IL-18 salınımını, nigericin uygulanmış ama kaspaz inhibitörü uygulanmamış hücrelere göre düşük bir oranda azalttığını bulduk. Sonuç olarak, bu çalışma, proptotik hücre ölümünün, bu hücre ölüm mekanizmasına aracılık eden belirli proteinlerin ve bu mekanizmanın moleküler boyutta düzenlenmesinin, over kanseri bağlamında daha iyi anlaşılmasına katkıda bulunmaktadır.

Anahtar Kelimeler: Piroptozis, Over kanseri, GSDMC, GSDMD, NINJ1, Hücre ölümü, Östrojen

ABSTRACT

GSDMC- AND GSDMD-MEDIATED PYROPTOTIC CELL DEATH IN OVARIAN CANCER AND THE ROLE OF ESTROGEN ON THIS CELL DEATH MECHANISM

Berkel, Çağlar
PhD Thesis, Molecular Biology
Advisor: Assoc. Prof. Dr. Ercan Çaçan
July 2023, xii + 120 pages

Ovarian cancer is the leading cause of death among gynecological malignancies, and it is the seventh most common cancer among women. Pyroptosis is a form of regulated pro-inflammatory cell death mechanism mediated and executed by the membrane-targeting (via their NT domains), lipid-binding, pore-forming gasdermin (GSDM) family of proteins. In this thesis, we found that mRNA expression of GSDMD and GDMDC is up-regulated in serous ovarian cancer compared to healthy ovaries, and that expression of GSDME and PJVK is down-regulated in serous ovarian cancer. GSDMB and GSDMD expressions showed differences among various histological subtypes of epithelial ovarian cancer. Copy number gains (CNV gains) were highly frequent (around %50) in genes encoding GSDMC and GSDMD in ovarian cancer patients. High expression of GSDMD and GSDMC was associated with shorter progression-free survival (PFS) in TP53-mutated ovarian cancer patients. Furthermore, we observed higher GSDMD and lower GSDME protein levels in ovarian tumors compared to surrounding/adjacent non-malignant stromal cells in the tumor microenvironment. Expression of NINJ1, a protein which mediates plasma membrane rupture following pyroptosis, decreased from early stage to late stage in serous ovarian cancer. The percentage of NINJ1 copy number loss events was the highest in ovarian cancer among other cancers. High expression of NINJ1 was associated with favorable overall survival (OS) in patients with ovarian cancer. NINJ1 mRNA expression was lower in cisplatin-resistant cells compared to cisplatin-sensitive ovarian cancer cells *in vitro*. Moreover, we showed that estrogen treatment increases the expression of GSDMC and GSDMD at the transcript level in chemosensitive (A2780) but not in chemoresistant (A2780-AD) ovarian cancer cell lines *in vitro*. We found that upon GSDMC overexpression, the decrease in cell viability in nigericin (a pyroptosis inducer)-treated A2780-AD cells reduces to a less significant level compared to that in A2780-AD negative control cells. Besides, we reported that GSDMC or GSDMD overexpression increases cell viability in untreated (without nigericin treatment) A2780 cells. We found that when GSDMD gene is silenced in A2780 cells, the decrease in cell viability in response to nigericin is reduced to a less significant level compared to that in negative siRNA-transfected A2780 cells. When GSDMC gene was silenced in A2780-AD cells, the decrease in cell viability in response to nigericin was reduced to a non-significant level compared to that in negative siRNA-transfected A2780-AD cells. In A2780 cell line, we found that inhibition of certain caspases (caspase-1, caspase-4, caspase-6 or caspase-8) using specific caspase inhibitors results in the loss of nigericin-induced decreases in cell viability. In contrast, the inhibition of only caspase-1, but not of any other caspases studied, led to a loss of

nigericin-induced decreases in cell viability in chemoresistant A2780-AD cell line. We showed that upon inhibition of caspase-1, -4 or -8, the levels of released IL-18 from A2780 cells treated with nigericin slightly decreases compared to A2780 cells treated only with nigericin but not with any of the specific caspase inhibitors. Combined, our work provides a better understanding of pyroptosis and its regulation, and of certain proteins that mediates this cell death mechanism in the context of ovarian cancer.

Keywords: Pyroptosis, Ovarian cancer, GSDMC, GSDMD, NINJ1, Cell death, Estrogen

CONTENT

Page

ETİK SÖZLEŞME SAYFASI.....
JÜRİ KABUL VE ONAY.....
ÖNSÖZ/TEŞEKKÜR.....
ÖZET i
ABSTRACT iii
CONTENT.....v
TABLES/DIAGRAM LIST.....vi
FIGURE LIST.....vii
ABBREVIATIONS LIST.....viii
INTRODUCTION.....1
MATERIALS AND METHODS.....18
RESULTS.....36
DISCUSSION.....75
REFERENCES.....83
SUPPLEMENTARY DOCUMENTS.....
Supp 1. Resume.....104

TABLE/DIAGRAM LIST

Table/Diagram No **Page**
Diagram 1.1: ……....….8
Table 2.1: ……....18

FIGURE LIST

Figure No **Page**

Figure 3.1: ……34
Figure 3.2: ……35
Figure 3.3: ……37
Figure 3.4: ……39
Figure 3.5: ……40
Figure 3.6: ……41
Figure 3.7: ……42
Figure 3.8: ……43
Figure 3.9: ……44
Figure 3.10: ……46
Figure 3.11: ……47
Figure 3.12: ……48
Figure 3.13: ……49
Figure 3.14: ……51
Figure 3.15: ……52
Figure 3.16: ……54
Figure 3.17: ……55
Figure 3.18: ……56
Figure 3.19: ……58
Figure 3.20: ……60
Figure 3.21: ……61
Figure 3.22: ……62
Figure 3.23: ……63
Figure 3.24: ……64
Figure 3.25: ……65
Figure 3.26: ……67
Figure 3.27: ……68
Figure 3.28: ……69
Figure 3.29: ……70
Figure 3.30: ……71
Figure 3.31: ……71
Figure 3.32: ……72
Figure 3.33: ……72

ABBREVIATIONS

7-AAD: 7-Aminoactinomycin
ASC: Apoptosis-Associated Speck-Like Protein Containing a CARD
ASR: Age-Standardized Rate
CNV: Copy Number Variation
DAMP: Damage-Associated Molecular Patterns
EOC: Epithelial Ovarian Cancer
ESCRT: Endosomal Sorting Complexes Required for Protein Transport
EtBr: Ethidium Bromide
FDA: Food and Drug Administration of US
FIGO: The International Federation of Gynecology and Obstetrics
GSDM: Gasdermin
GZMA: Granzyme A
HGSOC: High Grade Serous Ovarian Cancer
HMGB1: High Mobility Group Box 1
HR: Hazard Ratio
HRT: Hormone Replacement Therapy
IL-18: Interleukin-18
LPS: Lipopolysaccharide
MMR: DNA Mismatch Repair Deficiency
MSI: Microsatellite Instability
NINJ1: Ninjurin 1
NLRP1: NLR Family Pyrin Domain-Containing 1
NT: N-Terminal
OV: Ovarian Cancer
PAMP: Pathogen-Associated Molecular Pattern
PARP: Poly (ADP-Ribose) Polymerase
PARPi: PARP inhibitors
PFD: Pore-Forming Domain
PI: Propidium Iodide
PJVK: Pejvakin
PMR: Plasma Membrane Rupture
PS: Phosphatidylserine
TCGA: The Cancer Genome Atlas
TMB: Tumor Mutational Burden

1. INTRODUCTION

1.1 Ovarian Cancer

Ovarian cancer is the leading cause of death among gynecological malignancies and the seventh most common cancer among women, and it is responsible for more than 200,000 deaths worldwide with incidence rates expected to rise due to the aging population (Jayson et al., 2014; McMullen et al., 2021; Sung et al., 2021; Bray et al., 2018). A total around of 315,000 new cases of ovarian cancer was reported in women worldwide in 2020 with an ASR (age-standardized rate) incidence of 6.6 per 100,000. In parallel, a total of around 210,000 new deaths due to ovarian cancer was reported globally same year, with an age-standardized mortality of 4.2 per 100,000 women (Huang et al. 2022). In terms of geographic regions worldwide, the highest incidence of ovarian cancer was reported in populations from Central and Eastern Europe (ASR = 10.7) (countries including Latvia, Poland, Serbia, Croatia, Belarus, Slovakia, Lithuania, Hungary, Bosnia and Herzegovina, Montenegro, Russian Federation, Ukraine, Bulgaria, Romania, Georgia, Estonia and Slovenia), followed by Northern Europe (ASR = 8.8) (countries including Ireland, United Kingdom, Norway, Finland, Denmark), Polynesia (ASR = 8.8) (countries including Samoa, New Zealand), North America (ASR = 8.1) (countries including Canada, United States of America), and South East Asia (ASR = 8.1) (counties including Brunei Darussalam, Singapore, Indonesia, Philippines, Malaysia, Thailand). The lowest incidence was observed populations in Central Africa (ASR = 4.4) (countries including Republic of Congo, Guinea), the Caribbean (ASR = 4.6) (countries including Belize, Dominican Republic, Honduras), and Southern Africa (ASR = 4.9) (Huang et al. 2022). Based on the study by Huang et al., the highest incidence of ovarian cancer was found in countries with a high-income level (ASR = 8.0), followed by those countries with an upper–middle-income (ASR = 6.3), low–middle-income (ASR = 6.1), and lastly with low income (ASR = 5.3) levels (2022). The highest mortality of ovarian cancer was observed in populations from Micronesia (ASR = 7.3), followed by Polynesia (ASR = 6.6), Central and Eastern Europe (ASR = 5.6), South East Asia (ASR = 5.2), and Melanesia (ASR = 5.2). The lowest mortality of ovarian cancer was observed in populations from the Caribbean (ASR = 3.2), East Asia (ASR = 3.3), and Southern Africa (ASR = 3.3). The highest mortality was found in countries with a low–middle-income level (ASR = 4.3), followed by countries with high-income level (ASR = 4.1), low-income level (ASR = 4.1), and lastly countries with upper–middle-income level (ASR = 3.9) (Huang et al. 2022). In other words, it can be stated that both incidence and mortality in ovarian cancer is highly population- and income level-dependent.

There are multiple risk factors related to ovarian cancer (either protective or predisposing): age (increased incidence more pronounced in ages over 65), menstrual-related factors (inverse relationship between ovulation cycles and the risk of ovarian cancer), age of menarche and menopause, parity (the risk is reduced with live birth or induced abortion, and decreases with an increase in the number of live birth cases), pregnancy characteristics (preterm labor increases the risk of ovarian cancer), higher age of childbirth (older age in pregnancy is associated with a decreased risk), pelvic inflammatory disease, endometriosis, contraceptive methods (reduced risk in women with tubal ligation), hormone replacement therapy (HRT), infertility treatments, family history, BRCA mutations, Lynch syndrome (which is responsible for 10–15% of the total inherited OC cases), nutrition and diet, obesity (which reduces the survival in ovarian cancer) and physical activity, consumption of alcohol, caffeine and cigarettes, lactation and lower socioeconomic status (Momenimovahed et al., 2019; Mohammadian et al., 2012).

More than 3/4 of patients with ovarian cancer are currently diagnosed at late stage, and this cancer type has no effective screening strategy unlike some other cancer types for which effective screening strategies have significantly lowered mortality rates (Yokoi et al., 2017). The combinations of the tumor biomarker CA125 and pelvic imaging using transvaginal ultrasound scans (TVS) are being used in the screening of ovarian cancer; however, to date, there is no evidence that screening for ovarian cancer actually saves lives (Buys et al., 2011; Pinsky et al., 2016; Jacobs et al., 2016). The presenting symptoms of ovarian cancer (such as pelvic / abdominal pain, higher abdominal size / bloating and difficulties in eating / feeling full) are not much specific, and are usually viewed by ovarian cancer patients as normal and expected changes associated with aging, menopause or previous pregnancies (Fitch et al., 2002; Goff et al., 2004; Goff et al., 2007). Thus, ovarian cancer is many times referred to as the ‘silent killer’, and it is very often believed that no symptoms are evident in early stages of the disease. Besides, referral decisions for general practitioners are frequently hard due to the fact that the symptoms commonly observed in ovarian cancer patients (including pain the pelvic area/abdomen, larger abdominal size/bloating and problems in eating/feeling full) are similar to those observed in patients with gastrointestinal disease (Acheson and Chan, 2001). Women also frequently follow complex referral pathways until they are ultimately correctly diagnosed as having ovarian cancer, with around half of women not being referred directly to gynecological cancer clinics or oncology clinics in general. This is mostly due to the fact that both ovarian cancer patients and general practitioners are not able to precisely recognize the presenting symptoms of ovarian cancer, thus increasing the time period until being diagnosed and treated correctly (Chan, 2001; Goff et al., 2000). This also contributes to decreased

survival rates, to a certain extent. Therefore, due to the lack of highly specific symptoms and effective screening methods, ovarian cancer is frequently diagnosed at an advanced stage (as opposed to early stage), when the tumor has already disseminated into the peritoneum (serous membrane that lines the abdominal cavity) and when treatment options are highly limited and ineffective (Marchetti et al., 2021). 5-year survival rate of 48% among ovarian cancer patients (meaning that around half of patients with ovarian cancer dies 5 years after being diagnosed) is in part attributed to the diagnosis at late-stage disease (5-year survival rate of 29%); however, tumour biology and treatment differences, and also differences in the response to available treatments likely contribute (Siegel and Jemal, 2020). In more detail, stage I (cancer is present only in the ovaries) and II (cancer is present outside the ovaries and growing within the pelvis) ovarian cancer patients have 5-year survival rates of 90% and >70%, respectively; while 5-year survival rate drops to 39% for stage III (cancer even spread outside the pelvis into the abdominal cavity or to lymph nodes) patients and to 17% for stage IV (cancer spread to other organs which are distant from the ovaries) patients with ovarian cancer (Society AC, 2019). This data highlights the importance of successful diagnosis at earlier stages in order to improve the survival of ovarian cancer patients.

1.1.1 The treatment of ovarian cancer

Current frontline / standard treatment of ovarian cancer patients includes cytoreductive surgery (debulking surgery; i.e. the reducing the amount of cancer cells present in the abdominal cavity) and a platinum- and taxane-based chemotherapy (using platin derivatives such as cisplatin and carboplatin, and using taxane derivatives including paclitaxel and docetaxel, respectively), with some patients receiving PARP (a critical enzyme involved in DNA repair) inhibitors (PARPi) including olaparib (Armstrong et al., 2019; Morales et al., 2014; Mikuła-Pietrasik et al., 2019). Platinum-based standard of care in ovarian cancer (e.g. cisplatin or carboplatin + taxane) in most cases leads to robust initial clinical response; however, patients eventually succumb to chemoresistant recurrence due to the clinical development of resistance mechanisms to the drugs used (Jayson et al., 2014). Anti-angiogenics such as bevacizumab and PARP inhibitors such as olaparib have shown promising clinical results for the treatment of ovarian cancer (Chen and Du, 2018; Wang et al., 2020). The development of PARP inhibitors (known as PARPi) has transformed the management of patients with high-grade serous or endometroid ovarian, primary peritoneal or fallopian-tube cancers (later referred to as high-grade serous/endometroid ovarian cancer (HGSC or HGSOC)), in both relapsed / recurrence and first-line settings (Pujade-Lauraine et al., 2017; Coleman et al., 2017; Mirza et al., 2016) (Here, please note that serous and endometrioid represent

two different histological subtypes of epithelial ovarian cancer). Although these drugs were initially approved by the regulators as a maintenance treatment option of recurrent platinum sensitive BRCA1 or BRCA2 (BRCA1/2)-mutant epithelial ovarian cancer (EOC), further data obtained in the later years demonstrated a clinical benefit beyond those with a BRCA1/2 mutation. In other words, data pointed that ovarian cancer patients even without mutations in BRCA1 or BRCA2 genes might benefit from the inhibition of PARP enzymes in certain contexts. The key to this sensitivity to treatment based on PARP inhibition is considered to be homologous recombination (HR) deficiency, which is present in around 50 % of all patients with high-grade serous / endometrioid ovarian cancer (HGSOC) (Pennington et al., 2014; Miller et al., 2020). Most frequently, this is characterized by the absence of a functional copy of either BRCA1 or BRCA2 genes, both of which play crucial roles in genome integrity maintenance via the repair of double-strand (ds) DNA breaks by the homologous recombination repair (HRR) pathway (Mylavarapu et al., 2018). However, as stated above, patients with a functional copy of either BRCA1 or BRCA2 genes might still benefit from this treatment modality.

Furthermore, the development of chemoresistance to available drugs in the clinic in the treatment of ovarian cancer is one of the most important factors which contribute to ovarian cancer recurrence and mortality, in addition to early peritoneal dissemination (certain form of metastasis usually observed in patients with ovarian cancer) and the high frequency of tumor relapse following primary debulking surgery. Checkpoint blockade immunotherapy using immune checkpoint inhibitors such as PD-1 or PD-L1 inhibitors has so far only shown modest / limited efficacy in ovarian cancer patients unlike patients with some other cancer types (Barber and Matei, 2021; Chardin and Leary, 2021; Pujade-Lauraine et al., 2021). Therefore, there are currently no highly effective and approved immune therapies for ovarian cancer patients (There are currently three immunotherapy options (which are approved by FDA, Food and Drug Administration of US) with limited efficacy for different groups of ovarian cancer patients: Bevacizumab: a monoclonal antibody (Ab) which targets the VEGF/VEGFR pathway to inhibit the growth of tumor blood vessels; approved for women with newly-diagnosed and with relapsed/recurrent ovarian cancer; Dostarlimab: a checkpoint inhibitor that targets the PD-1/PD-L1 pathway (Programmed cell death protein 1/programmed death-ligand 1, which functions as a negative feedback loop to limit tumor immunity); approved for certain subsets of women with advanced ovarian cancer who also has deficiencies in DNA mismatch repair (dMMR) pathway; Pembrolizumab: similarly, a checkpoint inhibitor which targets the PD-1 / PD-L1 pathway; approved for certain subsets of women with advanced ovarian cancer who has high microsatellite instability (MSI-H), DNA mismatch repair

deficiency (dMMR), or high tumor mutational burden (TMB-H)). In terms of immunotherapy in ovarian cancer, the immune suppressive networks within the ovarian tumor microenvironment (TME) should be considered; therefore, a major direction in this research field is to develop and optimize biomarkers that would predict responsiveness of ovarian cancer patients to different types of immunotherapy strategies, and allow for treatment selection based on the results (Odunsi, 2017).

Chemoresistance has long been the bottleneck of ovarian cancer (OC) prognosis, leading to a significant decrease in the survival of ovarian cancer patients by limiting their responses to chemotherapies used. Most ovarian cancer patients show a good initial response to platinum-based chemotherapy (including those that use cisplatin and carboplatin) as mentioned above; however, platinum resistance leads to up to 80% of this responsive ovarian cancer patient cohort ultimately becoming refractory and not responding well to the treatment. In other words, the development of resistance by various molecular and cellular mechanisms to these chemotherapeutic agents ultimately results in the loss of efficacy of these drugs which has been previously observed in ovarian cancer patients. There are basically four types of recurrent ovarian cancers (ROC), which are: platinum-sensitive cancer (ovarian cancer patients with tumors that are sensitive to platinum-derived drugs attain clinical remission after initial platinum-based combination chemotherapy, and have a recurrence 6 months after ending chemotherapy), platinum-resistant cancer (patients with platinum-sensitive ovarian tumors show clinical remission following the first platinum-based combination chemotherapy, but have relapse later within 6 months after ceasing chemotherapy), persistent ovarian cancer (patients exhibit a clinical response or obvious reaction to the initial platinum-based chemotherapy, but have residual lesions to be found following further examination) and refractory ovarian (patients who do not respond to platinum-based chemotherapy, including stabilization or progression during treatment) (Pujade-Lauraine et al., 2016; Guo et al., 2022). Therefore, there are multiple groups of ovarian cancer patients whose responses to the current treatment options highly vary mostly due to differential chemosensitivity profiles of these patients. Over the decades, extensive research efforts have been made to identify and detail key molecular and cellular events critical for the development of platinum resistance in patients with ovarian cancer and also to target these events with the ultimate aim of limiting the development of chemoresistance. However, the strategies developed until now have only achieved limited success and have not led to a highly significant improvements in patient outcomes (Matulonis et al., 2016). Indeed, the survival rates of ovarian cancer patients have remained almost the same in the last 40 years. The activity of platinum-based drugs against cancer cells is mediated primarily through the formation of persistent DNA interstrand crosslinks (ICLs), resulting in DNA damage and apoptosis

(Siddik 2003; Murata et al., 2004). This happens mostly due to the formation of the 1,2-intrastrand [d(GpG) and d(ApG)] adducts of purines, in addition to other chemical changes in DNA induced by cisplatin. Despite the fact that around 3000 platinum-derived molecules have been developed by researchers in the past, and 13 of these drugs underwent further clinical trials, only one of these platinum analogs (carboplatin (also known as 1,1-cyclobutyldicarboxylate)) has demonstrated an advantage clinically compared to cisplatin, and therefore gained widespread acceptance. In the context of these chemotherapeutic drugs, chemotherapy resistance can be basically categorized in two groups: intrinsic chemoresistance, where the cancer / tumor cells are inherently resistant to drug treatment, and acquired chemoresistance, which can be developed at any time during the course of treatment with chemotherapeutics (Rubin et al., 1999). Intrinsic chemoresistance is caused due to cancer cells already possessing several biological modifications / characteristics such as limited drug uptake (influx), increased drug efflux outside the cell, enhanced detoxification of chemotherapeutic drugs (thus decreased efficacy), inactivation of the drug, inhibition of apoptosis by molecular mechanisms (Armstrong, 2002). While acquired chemoresistance can arise due to genetic and/or epigenetic alternations (DNA or histone modifications or changes in the chromatin structure etc.) that help cancer cells to adapt to changes induced by chemotherapy including stress, DNA damage and cell death mechanisms including apoptosis and pyroptosis (Armstrong, 2002; Ali et. al., 2013; Cacan et. al., 2014).

1.1.2 Classification and subtyping of ovarian cancer

Ovarian cancer can be classified based on cell type of tumor origin into different subtypes: epithelial (around 90% of all cases of ovarian cancer (Sankaranarayanan and Ferlay, 2006), sex cord / stromal (5–6%) and germ cell (2–3%). Worldwide, around 250,000 women are diagnosed with epithelial ovarian cancer (EOC) annually, and around 150,000 patients die due to epithelial ovarian cancer each year (Sankaranarayanan and Ferlay, 2006). One of the main factors contributing to the high death-to-incidence rate, compared to other cancer types, is the advanced stage at diagnosis (~75% of EOC patients), as mentioned above for ovarian cancer in general. Late-stage EOC has a 5-year survival rate of 29%, in contrast with 92% for early-stage EOC (Chen et al., 2016), highlighting that survival decreases dramatically (around 3-fold) from early to late stage in patients EOC.

The epithelial ovarian cancer differentiates into five main histological subtypes (also called histotypes) such as high-grade serous carcinomas (HGSC or HGSOC), which is the most frequent

subtype (~80% of all ovarian cancer) (Seidman et al., 2004), low-grade serous carcinomas (LGSC or LGSOC), mucinous, endometrioid and clear cell ovarian cancers (Kurman et al., 2014). Women diagnosed with advanced HGSC currently have a 5-year survival rate of 41%, and less than 15% of patients survive more than 10 years (Hoppenot et al., 2018; Millstein et al, 2020). Rarer forms of epithelial ovarian cancer including transitional cell (which include pure transitional cell carcinomas (TCCs) and Brenner tumors) or mesenchymal and mixed-epithelial carcinomas may also occur; however, based on their low incidence, they are relatively less studied and thus less characterized (Hoppenot et al., 2018; Millstein et al, 2020). TCCs are high-grade tumors originated from surface epithelium, as different from benign, malignant or borderline Brenner tumors (Boyraz et al., 2017). Based on their differences in morphological, molecular and clinical characteristics including prognosis (Shih and Kurman, 2004), ovarian cancer histotypes are generally considered as different diseases rather than a single disease (Köbel et al., 2008). Besides, drug response or resistance to the chemotherapy also differs widely based on histological subtypes in EOC patients. For instance, high grade serous ovarian cancer patients respond well to platinum-based chemotherapy (such as carboplatin treatment), whereas rarer clear cell and mucinous types are known to be remarkably resistant to platinum-based drugs (Sugiyama et al., 2000; Itamochi et al., 2002; Mabuchi et al., 2016). This and other facts support the observation that different histological subtypes of ovarian cancer should be considered as different malignancies which require specialized and distinct treatment strategies, rather than a single treatment approach for all subtypes. For this reason, a better understanding of ovarian cancer subtypes in terms of both molecular changes taking place during initiation and progression and of clinical responses is urgently required.

1.2 Pyroptosis

1.2.1 Gasdermin protein family

Gasdermins are members of a family of pore-forming effector and lipid-binding proteins (Kayagaki et al., 2015; Shi et al., 2015; He et al., 2015; Broz et al., 2020). This protein family and their cellular functions have been mostly studied in the last 10 years. Until today, several gasdermin family members and also gasdermin-like proteins have been identified by the researchers based on sequence homology, and their molecular roles in different cell types and various contexts have been determined to a certain level. Gasdermin protein family in *Homo sapiens* currently has six paralogous members, namely GSDMA (GSDM1), GSDMB (GSDML), GSDMC (MLZE), GSDMD (GSDMDC1), GSDME (DFNA5) and PJVK (Pejvakin, DFNB59), of which GSDME and PJVK

cluster closely together, distant from other gasdermins (Broz et al., 2020). All of these proteins, with the exception of PJVK (Pejvakin, DFNB59), lead to membrane permeabilization through the formation of pores and pyroptosis, a lytic cell death with pro-inflammatory characteristics, which will be detailed below (Kayagaki et al., 2015; Shi et al., 2015; He et al., 2015; Broz et al., 2020). Aside from PJVK, they share sequence homology (Broz et al., 2020). These forms of proteins constitute the inactive precursors of later pore-forming proteins. At present, gasdermin D (GSDMD) (53 kD cytoplasmic protein) is the best characterized and studied of the GSDMs, and it is mainly expressed by esophagus, stomach, skin and immune cells (Katoh and Katoh, 2004). However, in general, these membrane-targeting and pore-forming proteins are expressed in both immune and non-immune cells including ovarian cells. In their structure, gasdermins contain a cytotoxic (lytic) N-terminal domain (NT) which has an intrinsic pore-forming activity (NT domain is also known as pore-forming domain, PFD), and a C-terminal domain which represses / limits the pore-forming activity of N-terminal domain in the absence of an activating signal such as the presence of a pathogen (Kayagaki et al., 2015; Shi et al., 2015; He et al., 2015; Broz et al., 2020). Structural mechanisms regulating the change from inactive to active forms of gasdermins have been studied and determined to a certain detail for certain members of the family. The observation that C-terminal domain which represses the pore-forming function of NT domain is true for all gasdermin proteins except for PJVK, whose NT domain is directly connected to a shorter C-terminal domain (Ding et al., 2016). These gasdermin protein domains, i.e. C- and N-terminal domains, are connected by a central flexible linker (which have specific amino acid sequences) which is cleaved by certain caspases upon induction by either pathogen-derived or host-derived danger signals, such as PAMPs or DAMPs. Once inhibition of the C-terminal domain on NT is released by the cleavage of the central linker region between these domains by specific caspases, the N-terminal domains are able to bind to the negatively charged lipids in the plasma membrane (for instance, NT GSDMD binds to monophosphorylated phosphatidylinositols including phosphatidylinositol 4-phosphate, bisphosphorylated phosphatidylinositols including phosphatidylinositol (4,5)-bisphosphate, also phosphatidylinositol (3,4,5)-bisphosphate, and relatively more weakly to phosphatidic acid and phosphatidylserine) and undergo extensive conformational changes, form homo-oligomers and insert within the membrane to form large oligomeric pores, which results in the disruption of ion homeostasis and in the induction of pro-inflammatory cell death (Ding et al., 2016; Aglietti et al., 2016; Liu et al., 2016; Sborgi et al., 2016; Liu et al., 2019; Mulvihill et al., 2018; Chai et al., 2022). In other words, activated gasdermins insert into cell membranes by binding to specific lipids in the plasma membrane, where they form pores that lead to the secretion of cytokines (such as pro-inflammatory IL-18), alarmins and damage-associated molecular patterns (DAMPs) and cause cell

membrane rupture. The C-terminal domain of gasdermins is almost exclusively composed of α-helical structures to form a globular conformation to fully mask the N-terminal hydrophobic pocket that attaches to specific lipids; therefore, for GSDM proteins to be able to bind lipids on PM, CT domain should be removed (Ding et al., 2016). The *in vitro* ability to form pores within liposomal membranes has been experimentally shown for the N-terminal domains of GSDMA to GSDME, whereas PJVK has lost these pore-forming capabilities unlike the other members of the family, although it still retains certain functions in inflammation and cellular responses to infections (Ding et al., 2016; Angosto-Bazarra et al., 2022). Several studies showed that gasdermin pores form inner diameters in the membrane ranging in size from 10 to 18 nm based on the composition of lipids in which they insert themselves (such as those lipids mentioned above); and this pores, for instance, enables the release of certain pro-apoptotic molecules such as Cyt c which has a diameter of around 3 nm (Ding et al., 2016; Ruan et al., 2018; Papadopoulos et al., 2020). Molecules that are larger in size than gasdermin pores can still be released in the lytic phase of pyroptotic cell death, whose recently identified mechanisms and regulation are further given below in this section.

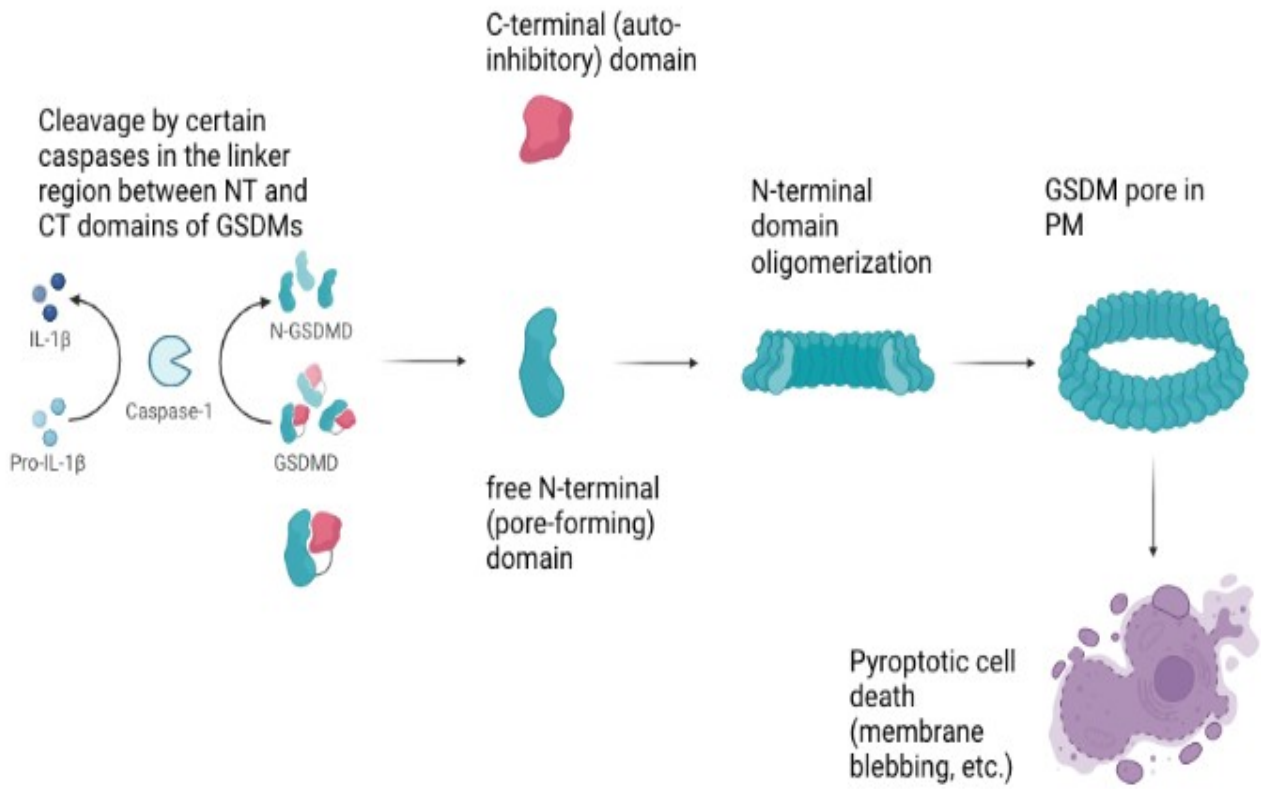

Diagram 1.1. Gasdermin (GSDM) pore formation

Following the cleavage of central linker regions between C- and N-terminal domains (CT and NT) of GSDMs by specific caspases (here, shown by caspase-1), free NT-domains oligomerize in the plasma membrane to form pores to release certain pro-inflammatory molecules such as IL-18. If not repaired, these pores ultimately lead to pyroptotic cell death with certain morphological characteristics such as membrane blebbing. (Illustration was performed using BioRender).

Multiple studies have identified caspases responsible for the cleavage and thus activation of certain gasdermins within their central flexible linker regions between NT and CT domains. For instance, in order to be in the active form, GSDMD should be cut enzymatically at a certain amino acid position in its central linker region between its NT and CT domains by certain inflammatory caspases including caspase-1, caspase-4, caspase-5, and caspase-11, and as shown more recently, by the activity of caspase-8 (Broz et al., 2020; Demarco et al., 2020; Chen et al., 2019; Orning et al., 2018; Sarhan et al., 2018; Sanjo et al., 2019). Similarly, caspase-3 and caspase-8 have been reported to be the enzymes responsible for the cleavage of linker regions of GSDME and GSDMC,

respectively, to promote GSDME- and GSDMC-mediated cell death pathways (Wang et al., 2017; Rogers et al., 2017; Hou et al., 2020). In other words, the cleavage of central linker region of these proteins by caspase-3 and caspase-8 at a certain location enables the freeing of NT region, thereby allowing its binding to plasma membrane lipids and ultimately the formation of pores (Wang et al., 2017; Rogers et al., 2017; Hou et al., 2020). Here, it should be noted that NT domains of gasdermins proteins are able to bind to cellular membranes other than plasma membrane, such as mitochondrial membrane. However, the binding of active forms of gasdermins to organelle membranes and the formation of pores in these membranes have been relatively much less studied. Similarly, lipids to which NT domains of gasdermins can bind in organelle membranes and how pore formation is different than that in plasma membrane remains mostly to be determined.

Besides their role in inflammasome-dependent cell death (i.e. pyroptotic cell death), gasdermins can also be activated independently of caspase and inflammasome activity in the cell, and may not necessarily lead to lytic and pro-inflammatory cell death. Although GSDMs are primarily known for their roles as mediators of pyroptosis (since they are mostly studied in the context of pyroptotic cell death); however, other cellular functions including the non-lytic release of inflammatory cytokines (as opposed to lytic release observed in pyroptosis), regulation of vital cell functions, facilitation of other forms of regulated cell death (i.e. other than pyroptosis) and targeted bactericidal effects have been also reported in the previous studies. As an example, caspase-3-mediated GSDME cleavage can result in secondary necrosis in apoptotic cells, showing the function of GSDME in cell death mechanisms different than pyroptosis (Rogers et al., 2017). In human cells lines *in vitro*, GSDMD-NT and GSDME-NT can promote apoptosis by releasing mitochondria-derived caspase 3 (Rogers et al., 2017). The considerable crosstalk between pyroptosis and other cell death pathways including apoptosis is increasingly recognized by researchers based on recent studies (Elias et al., 2023). As an example to non-pyroptotic biological functions of full-length GSDMs (their inactive forms in pyroptosis), in intestinal epithelial cells, full length GSDMB (FL-GSDMB) moves to the plasma membrane (PM) and controls proliferation, migration and cellular adhesion *in vitro* (Rana et al., 2022). These studies highlight that gasdermins should be studied in great detail in the context of cell death based on their diverse functions in several cell death mechanisms in addition to pyroptosis. Besides cell death, their functions in other cellular pathways will certainly be detailed to a great extent in the future.

1.2.2 Pyroptotic cell death

Pyroptosis is a form of regulated pro-inflammatory cell death mechanism mediated and executed by the membrane-targeting (via their NT domains), lipid-binding, pore-forming gasdermin family of proteins mentioned above. Pyroptosis was initially described and identified as an inflammasome- and caspase 1-dependent cell death pathway which is characterized by the loss of cell membrane integrity (through the formation of pores in the PM) and the secretion of certain small molecules such as pro-inflammatory cytokines e.g. IL-1β and IL-18 from these pores. It was initially identified in bacteria-infected macrophages. This type of cell death was observed and reported to be highly different than apoptotic cell death with respect to multiple characteristics and outcomes, and was later termed '*pyroptosis'* ("*pyro*" Greek for fire or fever, and "*ptosis*" falling) (Brennan and Cookson, 2000; Watson et al., 2020; Cookson and Brennan, 2001). The discovery made in 2002 by Martinon et al. that oligomeric protein complexes comprising NLR family pyrin domain-containing 1 (NLRP1) and apoptosis-associated speck-like protein containing a CARD (ASC) act as a platform in order to induce the activation of caspase-1 identified pyroptosis as a downstream effector mechanism of this and some other inflammasomes; however, the regulation and molecular details of this cell death mechanism remained poorly understood back then (2002; Agostini et al., 2004; Miao et al., 2010; Kayagaki et al., 2011; Sagulenko et al., 2013). More than 10 years later, the discovery of GSDMD as the target protein (substrate) of inflammatory caspases 1, 4 and 5 (or caspase 11 in mice) induced by inflammasomes, and as the terminal effector molecule of pyroptosis has revolutionized fundamental concepts regarding mechanisms of programmed cell death (Kayagaki et al., 2015; Shi et al., 2015). Thenceforth, the research on pyroptosis and understanding of pyroptotic cell death has increased to a great extent. Gasdermins are now recognized as the principal effectors of this form of pro-inflammatory cell death. Pyroptotic pathway which involves the activation of caspase-1 is now known as the canonical pathway, and whereas the non-canonical pathway involves the activation and functionality of caspases -4, -5 and -11. The canonical pyroptotic pathway is initiated by the detection of PAMPs and DAMPs by various inflammasomes such as NLRP3. However, non-canonical pyroptotic pathway is primarily initiated by the recognition of lipopolysaccharides (LPS) by the CARD domains of caspase-4, -5 and -11 in the cytosol (Jia et al., 2019; Shi et al., 2014). Pyroptosis and gasdermins participate in host antimicrobial defense and in the pathogenesis of many non-microbial diseases such as cancer, gastrointestinal disease and kidney disease. The contrasting roles of gasdermins in the context of cancer will be detailed and discussed further below.

After the formation of gasdermin pores following the initiation by either canonical or non-canonical pathways, the imbalanced flow of ions through pores that eventually leads to pyroptotic cell death

can be counterbalanced by membrane repair mechanisms via the endosomal sorting complexes required for protein transport (ESCRT) III. The ESCRT machinery which can be activated in response to increased levels of cytosolic Ca^{2+} (i.e. calcium influx through GSDMD pores), is then recruited to the site of gasdermin pores, where damage is repaired by the budding of pore-containing membranes (Rühl et al., 2018). Inhibition of the ESCRT-III machinery significantly increases the number of pyroptotic events and IL-1β release in both human and mouse cells upon activation of either canonical or noncanonical pathways of inflammasome activation. The choice between gasdermin pore formation and membrane repair by ESCRT machinery ultimately determines the fate of the cell with the activated inflammasomes (pyroptotic cell death vs cell survival). For instance, it not repaired or removed, gasdermin pores may ultimately lead to lytic cell death which is irreversible at most cases. In parallel, GSDMD pores are dynamic structures whose open or closed status occurs at irregular intervals, with varying pore sizes over time (Santa Cruz Garcia et al., 2022).

There are certain similarities between pyroptosis and another form of programmed cell death, apoptosis, including the presence of DNA damage and chromatin condensation (Kerr et al., 1972). Cells undergoing pyroptosis emerge swelling, and many bubble-like protrusions (termed pyroptotic bodies) appear on the cellular membrane surface before its ultimate rupture (Chen et al., 2016). Pyroptosis also results in the flattening of cells. In a similar manner, membrane blebbing also occurs in cells undergoing apoptotic cell death, and caspase-3 is known to be necessary for this process (Tomiyoshi et al., 2004). However, the unique morphological characteristics of pyroptotic cell death are clearly distinct from those of apoptotic cell death. It is commonly thought that apoptosis is a safe form of cell death (with no pro-inflammatory potential); however, pyroptosis can lead to inflammation, activated by certain extracellular or intracellular stimuli, such as bacteria, viruses, toxins (e.g. nigericin, LPS) and chemotherapy drugs, DAMPs (Tang et al., 2020). In contrast to the explosive rupture observed in the case of necrosis, pyroptosis results in flattening of the cytoplasm due to leakage in the plasma membrane via gasdermin pores as we previously mentioned (Chen et al., 2016). Besides, caspase activation or release of granzymes results in the oligomerization of gasdermin NT domains and pore formation (around 1–2 μm in diameter) in the plasma membrane, which allows mature IL-1β or IL-18 (processed by certain caspases) with a diameter of 4.5 nm and caspase-1 with a diameter of 7.5 nm to pass through, respectively (Ding et al., 2016). At the same time, the water entering through the gasdermin pores leads to swelling of the cell and osmotic lysis, thus resulting in the rupture of the plasma membrane and the release of proinflammatory molecules such as IL-1β and IL-18 (Fink and Cookson, 2006). However, lytic cell death following pyroptosis

is not a passive or unregulated process as previously thought (as identified recently), and we will give details on it in the following pages. Therefore, the pyroptotic cells are permeable to low molecular weight dye molecules such as 7-aminoactinomycin (7-AAD), propidium iodide (PI), and ethidium bromide (EtBr) (Fink and Cookson, 2006). In contrast, compared to pyroptotic cells, apoptotic cells maintain the integrity of their plasma membrane, not allowing the entry of these dyes inside the cells, enabling the differentiation of them from pyroptotic cells based on this feature (Zhang et al., 2018; Ray et al., 2012). Similar to apoptotic cells, Annexin V also stains pyroptotic cells, and the dye binds to phosphatidylserine (PS) molecules exposed on the outer surface of the membrane following pyroptosis (Siegel, 2006). Therefore, using Annexin V, apoptotic cells and pyroptotic cells can not be correctly distinguished. Furthermore, the diameter of pyroptotic bodies is similar to that of apoptotic bodies, which are both 1–5 μm in size; and therefore, similarly, pyroptotic and apoptotic bodies can not be differentiated just based on their sizes (Zhang et al., 2018; Chen et al., 2016).

1.2.3 Pyroptosis and cancer

Some studies previously reported the involvement of gasdermins in the initiation and progression of certain cancer types. For instance, expression of GSDMA was shown to be downregulated / decreased in primary gastric cancers and gastric cancer cell lines *in vitro*, more than 20 years ago (Saeki et al., 2000; this was also the first study naming the mouse gene as Gasdermin (Gsdm) due to its observed restricted expression to both upper gastrointestinal tract (gas-) and skin (-dermin)). Another gasdermin protein, GSDMB, was also reported to be involved in tumor progression in multiple cancer types incl. gastric cancer, hepatocarcinoma, cervix and breast cancers (Carl-McGrath et al., 2008; Sun et al., 2008; Hergueta-Redondo et al., 2014). For instance, Hergueta-Redondo et al. showed that GSDMB is upregulated in breast cancer cells compared to normal breast tissue, being the isoform 2 (GSDMB-2) the most differentially expressed in breast cancer among the other GSDMB isoforms (Hergueta-Redondo et al., 2014). They also showed that GSDMB-2 induces invasion, tumor progression and metastasis in MCF7 breast cancer cells *in vitro* (Hergueta-Redondo et al., 2014). In another study, expression of GSDMC (termed MLZE at that time) was found to be increased in metastatic melanoma cells (Watabe et al., 2001). Authors found by performing IHC experiments that the number of GSDMC-positive cases is remarkably larger in melanomas with Clark levels III, IV and V compared to melanomas with Clark levels I and II, and the strength of antibody staining increased significantly in the deep component of the melanoma tumor (Watabe et al., 2001). Saeki et al. analyzed the expression patterns of different gasdermin

family members in esophageal and gastric cancers, and suggested that GSDMC, GSDMD and GSDMA may be tumor suppressors, and GSDMB, which was amplified and overexpressed in some gastric cancers, could function as an oncogene, pointing to the distinct and possibly opposite functions of gasdermin family members in the upper gastrointestinal epithelium (2009). At that time (around 2009), all the current six members of the gasdermin protein family were not known. In contrast to the previous study, GSDMC was found to be pro-tumorigenic in colorectal cancer cells, since its knockdown resulted in decreased proliferation of colorectal cancer cell lines *in vitro*, whereas its overexpression enhanced cell proliferation (Miguchi et al., 2016). Another relatively recent study showed that GSDME is able to limit tumor growth by triggering pyroptosis which activates anti-tumor immunity through the enhancement of the phagocytosis of tumor cells by tumor-associated macrophages and of the number and functions of tumor-infiltrating natural-killer and CD8+ T lymphocytes (Zhang et al., 2020). Knocking out GSDME in GSDME-expressing tumors enhances tumor growth, whereas ectopic expression in GSDME-repressed tumors inhibits it in mice (Zhang et al., 2020). Besides, non-cleavable or pore-defective (thus inactive) GSDME was found to not functioning as a tumor suppressor unlike active GSDME. Therefore, authors stated that GSDME might function as a tumor suppressor since it can activate pyroptosis, which ultimately enhances anti-tumor immunity (Zhang et al., 2020). Similarly, supporting the role of GSDME as a tumor suppressor, previous studies found that GSDME expression is downregulated in many other cancer types, and lower GSDME expression is associated with decreased breast cancer survival (de Beeck et al., 2012; Xia et al., 2019). Similar to GSDME, GSDMB was also reported to enhance anti-tumor immunity in another study. Zhou et al. showed that lymphocyte-derived granzyme A (GZMA) cleaves GSDMB in target cells to promote its pore-forming activity, and that this cleavage event thus ultimately results in pyroptotic cell death (2020). In this study, authors also reported that interferon-γ can increase the expression of GSDMB and ultimately promote pyroptotic cell death, and that GSDMB expression is high in certain tissues, especially in digestive tract epithelia, including tumor cells derived from these tissues. When they introduced GZMA-cleavable GSDMB into mouse cancer cells, they found that this results in tumor clearance in mice. Therefore, we can state that GSDMB-mediated pyroptosis can function as a cytotoxic lymphocyte-killing mechanism, which may enhance antitumor immunity in certain contexts (Zhou et al., 2020).

Lou et al. showed generally increased expression of 17 pyroptosis-associated genes in tumor patients with high-immune-activity and a reduced pyroptosis in low-immune-activity tumors (Lou et al., 2022). Moreover, pyroptosis was found to be positively correlated with immune infiltration and immune-related signatures in 30 different types of cancer (Lou et al., 2022). They also

suggested that pyroptotic cell death can directly modulate the expression of immune checkpoint molecules and cytokines (Lou et al., 2022). Since pyroptosis promotes anti-tumor immune response in tumor cells through the release of pro-inflammatory cytokines such as IL-18 and immunogenic substances following cell rupture, and ESCRT III-mediated plasma membrane repair remarkably limits pyroptosis in tumor cells via the repair and subsequent removal of gasdermin pores, others showed that blocking calcium influx-triggered ESCRT III-dependent membrane repair strongly enhances the intracellularly delivered GSDMD-induced tumor pyroptosis (Li et al., 2022). This year, Lin et al. reported that oncolytic parapoxvirus induces GSDME-mediated pyroptosis and thus activates anti-tumor immunity (2023). In support, they showed that GSDME depletion decreases the percentage of cytotoxic T lymphocytes in the tumor microenvironment, pyroptotic cell death and the success of tumor virotherapy. Authors found that oncolytic viruses preferentially accumulate in the tumor upon systemic delivery and enhances pyroptotic tumor cell death, which sensitizes immunologically cold tumors to checkpoint blockade, highlighting the critical role of GSDME-mediated pyroptosis in oncolytic virus-based anti-tumor immunity (Lin et al., 2023). Combined, these studies might point out that pyroptosis might be manipulated clinically by various means to increase anti-tumor immunity, especially in cancer types for which current checkpoint blockade therapies is not that effective, such as ovarian cancer.

Peng et al. found that predominant localization of GSDMD in the nucleoplasm *in vivo* indicates favorable clinical outcomes in colorectal cancer, while a lack of nuclear localization of GSDMD is associated with unfavorable outcomes (Peng et al., 2022). This study highlighted that in addition to their cellular levels, cellular localization of gasdermin proteins might be of importance in cancer. In another study, after proving that the presence of exon 6 in GSDMB isoforms dictates their pore-forming and pyroptotic activity, Zhong et al. showed that different cancer cell lines have significantly different GSDMB isoform compositions, correlating with the onset and extent of pyroptosis following the stimulation by granzyme A which cleaves GSDMB to trigger target cell pyroptosis, pointing that the levels of pyroptosis-competent GSDMB isoforms in target tumors may better guide cancer immunotherapy selection, rather than other isoforms (Zhong et al. 2023). Similarly, Oltra et al. showed that exon 6 of GSDMB translation is essential for GSDMB-mediated pyroptotic cell death, and thus, GSDMB isoforms lacking this exon (GSDMB1-2) can not provoke cancer cell death by pyrotosis (2023). Consistently, the expression of GSDMB2, and not exon 6-containing variants (GSDMB3-4), was found to be associated with unfavorable clinical-pathological parameters in breast cancer. Also, they found that GSDMB can lead to cancer cell death in an isoform-dependent manner. Mechanistically, they showed that GSDMB NT constructs

containing exon-6 promote cell membrane lysis and a concomitant mitochondrial damage (Oltra et al., 2023). Collectively, studies mentioned above show that functions of gasdermin proteins in cancer might depend on the particular isoforms; therefore, isoform specificity should be taken into account when designing experiments and by performing clinical analyses.

1.2.4 NINJ1 and plasma membrane rupture

A recent study identified cell-surface protein NINJ1 (Ninjurin 1) as an important mediator of plasma membrane rupture (PMR) during lytic cell death including pyroptosis, and showed that NINJ1 is an essential protein for pyroptosis-related plasma membrane rupture (Kayagaki et al., 2021; Wang and Shao, 2021). Since plasma membrane rupture is a subsequent event following the initial formation of small pores in plasma membrane by certain gasdermins, NINJ1 and lytic phase mediated by NINJ1 should also be given attention in the context of pyroptotic cell death. Eukaryotic cells can experience different forms of programmed cell death, many of which result in plasma membrane rupture as the defining terminal lytic event (Zhang et al., 2018; Galluzzi et al., 2018; Don et al., 1977; Fink and Cookson, 2006; Vercammen et al., 1997; Stockwell et al., 2017; Yacobi-Sharon et al., 2013). Plasma membrane rupture was considered to be mediated by osmotic pressure and to be a passive and unregulated event for a long time; however, as we mentioned, it has recently been reported to be, in many cases, an active and regulated process, mediated by the protein ninjurin-1 (NINJ1) (Kayagaki et al., 2021). Studies showed that during lytic cell death, the extracellular α-helices of NINJ1 insert into the plasma membrane (PM) to polymerize NINJ1 monomers into amphipathic filaments that are able to rupture the plasma membrane. Authors of these studies suggested that the membrane protein NINJ1 is therefore an interactive component of the eukaryotic cell membrane that functions as an in-built breaking point in response to activation of cell death such as pyroptosis (Degen et al. 2023; Whisstock and Law, 2023; Kayagaki et al., 2023).

2 MATERIALS AND METHODS

2.1 Datasets and Data Analysis and Visualization

2.1.1 Data analysis and visualization

All data analysis and visualization steps in this study was performed in R programming environment (R version 4.2.1 (2022-06-23)) (R Core Team, 2022). Following R and Bioconductor packages were used throughout the study: readxl (Wickham and Bryan, 2022), tidyverse (Wickham et al., 2019), magick (Ooms, 2021), ggpubr (Kassambara, 2022), tidytext (Silge and Robinson, 2016), GGally (Schloerke et al., 2021), rmarkdown (Allaire et al., 2022; Xie et al., 2018; Xie et al., 2020), knitr (Xie, 2022; Xie, 2015; Xie, 2014), gridExtra (Auguie, 2017), ggtext (Wilke and Wiernik, 2022), glue (Hester and Bryan, 2022), ExperimentHub (Morgan and Shepherd, 2022), SummarizedExperiment (Morgan et al., 2022) and curatedOvarianData (Ganzfried et al., 2013).

The Bioconductor project (https://www.bioconductor.org/), which uses R statistical programming language (R Core Team, 2022) and which is open source and open development project, is an initiative for the collaborative creation of extensible software for computational biology, bioinformatics and biological data science with the goals of fostering collaborative development and common use of innovative software, reducing barriers to entry into interdisciplinary scientific research, and encouraging the achievement of remote reproducibility of results obtained from scientific research (Gentlemen et al., 2014).

The normality test for each dataset / experimental data was performed using ggqqplot() (quantile-quantile plot) and shapiro.test() (Shapiro-Wilk normality test) functions in R (from ggpubr (Kassambara, 2022) and stats (R Core Team, 2022) R packages, respectively). When data is normally distributed (p value from Shapiro-Wilk normality test > 0.05), we used Student's t test to compare group means; otherwise (i.e. p value from Shapiro-Wilk normality test < 0.05), we performed the analysis using two-sample Wilcoxon test (Mann-Whitney test) (Kassambara, 2022; R Core Team, 2022).

In the boxplots, the bottom and top sides of the box represent the lower and upper quartiles. The box covers the interquartile interval, where half of the data is found. The vertical line that split the box in two is the median value of all the data points.

For more detail on R programming language and on how to use it can be found in R4DS book available online for free (https://r4ds.had.co.nz/; Wickham and Grolemund, 2023).

2.1.2 Gene expression datasets and transcriptome analysis

Following gene expression / transcriptomics datasets from Gene Expression Omnibus (GEO, https://www.ncbi.nlm.nih.gov/geo/) (Barrett et al., 2013) were used in the present study: GSE12470 (sample size (n) = 53) (Yoshihara et al., 2009), GSE18520 (n = 63) (Mok et al., 2009), GSE26712 (n = 195) (Bonome et al., 2008; Vathipadiekal et al., 2015), GSE6008 (n = 103) (Wu et al., 2016; Bommer et al., 2010) and GSE51088 (n = 172) (Karlan et al., 2014). These GEO datasets and The Cancer Genome Atlas (TCGA) RNA-Seq and meta data for ovarian cancer (n = 578) were loaded into R statistical computing environment using curatedOvarianData Bioconductor package which contains many clinically annotated ovarian cancer transcriptome datasets (Cancer Genome Atlas Research Network, 2011; Ganzfried et al., 2013; Huber et al., 2015). Ovarian cancer gene

expression datasets in this study were selected based on the criteria that they contain data for both "healthy" (non-malignant) and "tumor" sample types, and datasets containing data only for tumor samples were excluded. Expression data and clinical metadata were retrieved from large Expression Set objects using functions from Biobase R package which contains standardized data structures to represent genomic data (Huber et al., 2015). Gene expression datasets used in the study and their certain features are also listed in Table 2.1 below.

Table 2.1.

Datasets (GEO accession no)	Stage/grade/histotype	Gasdermins for which data is available
GSE12470	Serous ovarian cancer	GSDMD, GSDMC, GSDME, GSDMB, GSDMA
GSE18520	Serous, late stage, high grade ovarian cancer	GSDMD, GSDMC, GSDME, PJVK, GSDMB
GSE26712	Serous, late stage, high grade ovarian cancer	GSDMD, GSDME, GSDMB
GSE51088	Serous ovarian cancer	GSDMA
GSE6008	Epithelial ovarian cancer (histotypes: clearcell, endometrioid, mucinous, serous)	GSDMB, GSDMD, GSDME

2.1.3 Proteome data analysis

Proteomics data for high-grade serous ovarian carcinoma (HGSOC) patients, acquired using liquid chromatography (LC)-mass spectrometry (MS) from formalin-fixed, paraffin-embedded (FFPE) specimens, were accessed from MaxQB — the MaxQuant DataBase of Max-Planck-Institut für Biochemie (Eckert et al., 2019) (http://maxqb.biochem.mpg.de/mxdb/project/show/9373012627500). This proteome dataset (n = 11 patients with HGSOC) contains relative protein levels for tumor cells and surrounding non-malignant stromal cells at the tumor microenvironment at four different anatomical locations in HGSOC patients (namely, omental metastasis, serous tubal in situ carcinoma (STIC), invasive fallopian tube (FT) lesions, and invasive ovarian lesions) (Eckert et al., 2019). Sample sizes (n) for each protein are as follows in this dataset: GSDMD (n = 94), GSDME (n = 73), and GSDMA (n = 46). In creating this dataset, authors collected tissues prospectively during the initial debulking

surgery and they reported that all patients were chemotherapy-naive (Eckert et al., 2019). For each patient and all anatomic sites, both tumor and stromal compartments were microdissected, and proteins were then extracted using an optimized high-sensitivity, label-free proteomic workflow for low-input samples as detailed in the original paper (Eckert et al., 2019). Protein data for other gasdermin family members including GSDMC are not available in this dataset (Eckert et al., 2019).

2.1.4 Copy number variation (CNV) analysis

Copy number variation (CNV) data was obtained from Genomic Data Commons (GDC) Data Portal of National Cancer Institute (https://portal.gdc.cancer.gov/) (Grossman et al., 2016). Cancer types were ordered based on the percentage of total CVN events (both copy number gains and losses) in genes encoding gasdermins from the highest to the lowest, and only top 5 cancer types which have the highest percentage of total CNV events for each gene were shown in plots. The percentage of copy number gains and losses (i.e., the percentage of cancer patients affected by these copy number variation events) was colored differently in plots (in blue and yellow, respectively). OV at the x-axis represents ovarian cancer. Abbreviations for other cancer types were also given in the figure legend. Y-axis represents the percentage of cancer patients affected by CNV events in given genes.

2.1.5 Survival analysis

Kaplan-Meier / survival plots were drawn to show the progression-free survival (PFS) of serous ovarian cancer patients (TP53-mutated) with low and high expression of gasdermin proteins using Kaplan-Meier Plotter tool (Gyorffy et al., 2012; Gyorffy, 2023). Data for high expression cohorts was shown with red lines, data for low expression cohorts were given in black. Here, patients were split by median expression into low and high expression cohorts.

Furthermore, Kaplan–Meier plots were drawn to show the overall survival (OS) or recurrence-free survival (RFS) of ovarian (for all histotypes combined and only for serous histotype) or breast cancer patients with low and high expressions of NINJ1 (patients were split by median expression) using Kaplan–Meier Plotter tool (n = 1656) (Nagy et al., 2021; Gyorffy et al., 2012) (http://kmplot.com/analysis/index.php?p=service&cancer=ovar). We selected JetSet best probe set indicated in green as recommended, and we otherwise used the default values in the tool. We did not restrict the analysis to any subtypes and treatment groups, and used the default parameters in the

tool. Logrank p and false discovery rate (FDR) values were taken into account in the comparison of survival rates between low- and high-expression cohorts of NINJ1. Hazard ratio (HR) and logrank p values were given in the top right corner of each Kaplan–Meier plot. Hazard ratio is a measure of how often a particular event (here, death of the patient) happens in one group in relative to how often it happens in another group, over a period of time. A HR of 1 indicates that there is no difference in terms of survival between the two groups. A HR of greater than one or less than one means that survival was better in one of the groups compared to the other group.

We also calculated HR values for NINJ1 expression in ovarian cancer for different datasets independently and combined (overall) using curatedOvarianData Bioconductor package, after adjusting for the success of debulking surgery (debulking status defined as residual tumor smaller than 1 cm following cytoreduction surgery) and The International Federation of Gynecology and Obstetrics (FIGO) stage (Ganzfried et al., 2013). A forest plot (blobbogram) was drawn using these data (Ganzfried et al., 2013). For details of survival analysis using data from curatedOvarianData package, please see the vignette of the package which can be found at https://bioconductor.org/packages/release/data/experiment/html/curatedOvarianData.html.

2.2 Cell Culture

In this study, A2780 (chemosensitive) and A2780-AD (chemoresistance) ovarian cancer cell lines were used for *in vitro* analyses in cell culture. These cell lines were generously provided by Dr. Shelly B. Hooks, University of Georgia, USA. These cells were maintained in RPMI-1640 (different brands were used in the course of the study) medium supplemented with 10% fetal bovine serum (FBS), 5 mM L-glutamine and 5 mM penicillin/streptomycin (Pen/Strep) (1% v/v from stock), in humidified 5% CO_2 incubator at 37ºC. Chemoresistant cell line A2780-AD were continuously grown with 3 µM cisplatin to maintain their chemoresistant profile. Cisplatin was purchased from Kocak Pharma (Istanbul, Turkey) and diluted with DMSO when needed. A2780 cell line has the following characteristics: A2780 (age unspecified, endometrioid histotype, sequence variations: ATM p.Pro604Ser (c.1810C>T), PTEN p.Lys128_Arg130del (c.383_391del9)) (Takenaka et al., 2015.; Beaufort et al., 2014). A2780 human ovarian cancer cell line was established from an ovarian endometroid adenocarcinoma tumour in an untreated patient. A2780 is

the parent line to the doxorubicin (adriablastin; adriamycin)-resistant cell line A2780-AD (Tsuruo et al., 1986; Huxham et al., 1994).

Confluent cells were passaged as follows: Media were aspirated from T75 flasks (Corning or SPL Life Sciences (Korea), 75 cm^2 cell culture flask) and 5 mL trypsin (Biological Industries) pre-warmed to 37 ºC were added for a T75 cell culture flask (Before the addition of trypsin, plates can be washed with 1x PBS if needed, e.g. if the dead cell density is high; otherwise, this washing step can be omitted in regular passaging). Flasks were incubated for approximately 3-5 min at 37 ºC incubator until cells were completely detached from the surface of flasks (checked under the light microscope), and if all cells are detached, then 10 ml pre-warmed RPMI-1640 (37 ºC) media were added to each flask using sterile serological pipettes. After pipetting several times with a serological pipette to detach and mix all the cells, media + cell mixture was transferred to 50 ml canonical tubes and centrifuged at 2000-3000 rpm for 3-5 mins. After discarding supernatant, cell pellets were dissolved in 10 ml fresh media, and cells were seeded to the plates in desired dilutions considering cell density (mostly at the 1:5 ratio). (In certain situations, this centrifugation step was omitted, since serum (FBS) present in the growth media already inhibits the activity of trypsin, i.e. there might be no need for trypsin removal for these two cell lines. However, certain cell lines might be sensitive to the presence of trypsin at low concentrations in the growth media. If no centrifugation is performed, cell + tyrypsin + media mixture can directly be diluted to a new flask). Total media volume in a T75 flask were completed to around 20 ml. Cell confluency was checked continuously to avoid over confluency to avoid cell death. Usually, when cell confluency is around 90%, cells were passaged. If dead cell percentage is high (higher numbers of cells detached) or cell morphology is different than usual in the current cells in the flasks, a new stock of cells were thawed and used in the experiments.

Cell lines were regularly checked for the presence of any contamination. Passage numbers were kept at minimum for both cell lines.

Cells were frozen for further use by using freezing media (Biological Industries, Israel or media prepared at the lab) which include 10% DMSO, in 1.8 mL cryovials. Cryovials containing cells and freezing media were kept at –20 ºC for 1 hour, then at –80 ºC overnight and finally moved to liquid nitrogen (or kept at -80 ºC) (gradual decrease in temperature). In the thawing of frozen cell stocks, after quick thawing of freezing media + cells in cryovials by keeping the vial in a warm water bath for around 30 seconds, the contents of the vials were transferred using Pasteur pipettes into 10 ml

pre-warmed media in 50 ml canonical tubes and centrifuged at 2000 rpm for 5 minutes (or at 3000 rpm for 3 min) to remove DMSO present in freezing media. After removing the media and dissolving cell pellet with fresh media without DMSO (normal warmed fresh growth media (RPMI-1640)), all cells were seeded in T75 flasks. Next day, flasks were checked and media were changed to remove any artifacts from freezing media or to remove dead cells. Alternatively, thawed cells were directly (without centrifugation) transferred to a well in a 6-well plate in excess media (around the total volume of a well) to dilute the DMSO concentration (since DMSO is toxic to cells), and after cells are attached to the bottom of plate (around 4-5 hours later depending on the cell type and density), media was changed with pre-warmed fresh media to discard DMSO-containing media. When cell confluency is around 90%, cells were passaged to flasks with a larger surface area such as T75 flasks. We found that the second alternative is more suitable for cell stocks with a relatively higher percentage of dead cells, such as those with a high passage numbers or those not stored at liquid nitrogen.

In cell culture hood and cell culture room, UV light was turned on for approximately 30 min before and after any experiment performed in the cell culture. ESCO class II type A2 cell culture hood (Esco Lifesciences, Singapore) was used in all cell culture experiments. 70% ethanol and 10% bleach were used to clean surfaces in the cell culture hood. Over-passaging of cells was avoided, and cells were used in any experiment after at least one passage following the thawing of cell stocks stored in a liquid nitrogen tank / -80 C freezer. Cell culture room was periodically cleaned using 10% bleach prevent in water to prevent contamination.

2.3 Estrogen, Nigericin and Disulfiram Treatment

Cells were treated with different final concentrations of estrogen (17α-Estradiol, Cayman, Cat # 20776). Estrogen in crystalline solid form was dissolved in DMSO (Dimethyl sulfoxide, ultra-pure grade, Amresco, VWR) to prepare stock solutions. Estrogen in powder form and its solutions in DMSO were kept at -20 C. For RNA / protein isolation, 300.000 cells per well were seeded in 6-well plates. After 24 hours, estrogen was added to the media in wells. For control wells, an equal volume of DMSO was added. Cells were incubated with estrogen / DMSO for 48 hours before RNA / protein isolation. We minimized the volume of DMSO added to cells due to its toxicity.

Nigericin (Cayman, Cat # 11437) was used in the final concentration of 10 μM. Nigericin (sodium salt) in crystalline solid form was dissolved in DMSO to prepare stock solutions. Nigericin in

powder form and its solutions in DMSO were kept at -20 C. For ELISA experiments, cells were incubated with nigericin for 1 or 2 hours to induce pyroptosis and then media in the wells was collected to comparatively analyze pro-inflammatory molecule levels (such as IL-18, HMGB1) released from the cells. For microscopy experiments, cells were incubated with nigericin for 1-2 hours or around 24 hours, and then images were taken. For MTT experiments, cells were incubated with nigericin for around 24 hours and then the cell viability test was performed.

For MTT / microscopy experiments with disulfiram (N, N, N', N'-tetraethyl-thioperoxydicarbonic diamide; Cayman, Cat # 15303), we first added 50 μM disulfiram (dissolved in DMSO) to the cells seeded 24 h earlier (20.000 cells/well in 96-well plate), and after 1 h incubation, we added 10 μM nigericin. We performed MTT assay / microscopy experiments 24 hours later. Disulfiram inhibits pyroptosis by blocking gasdermin D pore formation (Hu et al., 2020). More specifically, at nM concentration, disulfiram covalently modifies human / mouse Cys191/Cys192 of GSDMD to inhibit pore formation (Hu et al., 2020). Disulfiram in powder form was kept at RT and at dark. Disulfiram stock solution dissolved in DMSO was kept at -20 C for further use.

2.4 Specific Caspase Inhibition

Caspase-1 inhibitor (Ac-YVAD-CHO; 10016) was purchased from Cayman Chemical Company (Michigan, USA). Caspase-4 inhibitor (sc-396109), caspase-6 inhibitor (sc-3080) and caspase-8 inhibitor (sc-3082) were purchased from Santa Cruz Biotechnology, Inc. (Dallas, USA). They all were dissolved in DMSO and stored at -20 C. Specific caspase inhibitors were used at a final concentration of 50 μM. For ELISA experiments, after 2 hours of incubation with specific caspase inhibitors, nigericin was applied and cells were further incubated for 1 h. For MTT Assay, cells were incubated with specific caspase inhibitors and nigericin for 24 hours.

Caspase-1 inhibitor (Ac-YVAD-CHO; 10016) (an inhibitor of caspase-1/interleukin-1β converting enzyme (ICE; Ki = 0.76 nM) and an acetylated form of the caspase-1 inhibitor YVAD-CHO) is selective for caspase-1 over caspase-4, -5, -8, -9, and -10 (Kis = 163-970 nM), as well as over caspase-2, -3, -6, and -7 (Kis = >10,000 nM for all) (Garcia-Calvo et al., 1998). Caspase-6 inhibitor

(Ac-VEID-FMK, sc-3080) is a cell-permeable, irreversible inhibitor of caspase-6,-8,-10. caspase-8 inhibitor (Ac-IETD-CHO, sc-3082) is an inhibitor of caspase-8 and granzyme B.

2.5 RNA Isolation

500.000 cells per well in 1 ml growth media were seeded in 6-well plates. Following day, certain treatments were performed (for instance, estrogen treatment, GSDMC overexpression / silencing, etc.; more details are given elsewhere in this section). 48 hours later, 1 ml ice-cold TRIzol (Invitrogen) / Hibrizol (Hibrigen, Turkey) was added to each well, mixed well by pipetting multiple times and incubated for 5 minutes at 15-30 C (or at RT) to permit complete dissociation of the nucleoproteins complex. Then, it was transferred to a clean (autoclaved and RNase-free) 1.5 ml microcentrifuge tube, and 200 µl ice-cold chloroform (for every 1 ml of TRIzol) was added, shaked for around 15 seconds by turning upside down and incubated at RT for 2-3 minutes. Samples were then centrifuged at 12000 rpm for 10 minutes at 4 C. Following the centrifugation step, upper colorless aqueous phase containing RNA was carefully transferred to a new clean 1.5 ml microcentrifuge tube labeled accordingly, and 500 µl isopropanol was added to this tube and mixed by turning the tube a few times. Later, the sample was incubated at 15-30 C (or at RT) for 10 min and then centrifuged at 12000 rpm for 10 min at 4 C. Supernatant was discarded, and 1 ml ice-cold 75% ethanol (prepared previously with RNase-free water) was added to RNA pellet to wash. The sample was just slowly mixed by turning the tube a few times. Centrifugation was performed at 12000 rpm at 4 C for 2 mins, and then ethanol was discarded. This washing step was repeated once more. At the end of the protocol, RNA pellet was air-dried in a cell culture hood (or in any sterile environment) and dissolved in ice-cold 50 µl RNase-free water and then kept at -20 C for shorter storage or at -80 C for longer periods (the volume of RNase-free water added to the RNA pellet can be changed based on the desired final concentration). RNA concentration was measured at 260 nm using a spectrophotometer (Thermo Scientific™ Multiskan™ GO Microplate Spectrophotometer). 1 µl RNA sample was loaded to each aperture on µDrop plate. Obtained absorbance value was multiplied by 40 after subtracting the absorbance value of RNase-free water to convert the absorbance value to ng/µl unit. Measurements were performed at least in duplicates, and average absorbance values were taken into account in concentration calculations. The quality of isolated RNA samples was determined with the ratio of A260/A280, and only high-quality RNA was used in the following experiments (i.e. qRT-PCR).

Isolated RNA samples were kept at -20 C (for short term storage) or –80 ºC (for long term storage) freezer before we use them in qRT-PCR experiments. Extensive freeze-thaw cycles of RNA samples were avoided in order not to decrease RNA quality. Before qRT-PCR, RNA concentrations for each experimental cases were diluted to the same concentration (considering the lowest concentration of RNA obtained from isolation experiments), and equal volume of RNA was used from these diluted RNA samples.

2.6 Quantitative Real Time Polymerase Chain Reaction (qRT-PCR)

For qRT-PCR, manufacturers' protocols were generally followed (One-Step BrightGreen qRT-PCR Kit, Applied Biological Materials, Inc. or Luna Universal One-Step RT-qPCR Kit, E3005X, New England BioLabs, Inc.). For each reaction, 10 ng RNA was used. In each 20 µl PCR reaction; 10 µl master mix, 0.4 µl enzyme mix, 1 µl forward and reverse primers (10 µM each) were used. Total volume was completed to 20 µl with nuclease-free water. 20 µl reaction mixture was transferred to a LightCycler™ capillary (Roche Diagnostics), and centrifuged at 4 C at 750 - 1000 rpm for 10 secs. Then, capillaries were placed in a LightCycler™ 1.5 qRT-PCR device (Roche Diagnostics). Reaction conditions were programmed as follows: 50 C for 25 min, 95 C for 15 min, (95 C for 15 sec, 55 C for 30 sec, 72 C for 35 sec) x 40 cycles, and 37 C for 30 sec. qRT-PCR experiments were performed in duplicates or triplicates in 3 independent experiments (i.e. minimum 6 data points for each condition). The relative gene expression was measured and normalized to GAPDH by the $2^{-\Delta\Delta Ct}$ method ($2^{-(Cp - GAPDH\_Cp)}$). Before combining data from different experiments prior to data analysis, all values were normalized to control values in each independent experiment. For instance, in each experiment, average (mean) of control cases were made equal to 100, and other values were multiplied by this factor (100 / average of control values) accordingly. This way, we could combine data from independent experiments and performed the analysis collectively.

2.6.1 Primers

Prepared primer stocks at 10 µM concentration were kept at -20 C. Original primer stocks were diluted to 10 µM using RNase-free water based on the volumes given on the label on the side of the tubes.

GSDMC - forward primer: 5′-CCCATCACCAAACCTGGAAGAC-3′
GSDMC - reverse primer: 5′-TCAACAGCCTCTGTCACCACGT-3′

GSDMD - forward primer: 5′-ATGAGGTGCCTCCACAACTTCC-3′
GSDMD - reverse primer: 5′-CCAGTTCCTTGGAGATGGTCTC-3′

GAPDH - forward primer: 5′-GTCTCCTCTGACTTCAACAGCG-3′
GAPDH - reverse primer: 5′- ACCACCCTGTTGCTGTAGCCAA-3′

2.7 ELISA for the Analysis of IL-8 and HMGB1 Levels Released from Cells upon Certain Treatments

For ELISA (Enzyme-linked immunosorbent assay) experiments, approximately 20.000 cells per well were seeded in 96-well plates. Next day, specific caspase inhibitors were added to wells at a final concentration of 50 μM. After 2 hours of incubation with caspase inhibitors, nigericin was applied and cells were further incubated for 1 h at 37 C incubator. Then, cell supernatants were collected to be used in ELISA experiments to measure the levels of IL-18 and HMGB1 released from cells. As control for caspase inhibitors and nigericin, an equal volume of DMSO was added to the wells since both caspase inhibitors and nigericin were previously prepared in DMSO. DMSO volume added to the cells in each case were kept at minimum since higher DMSO concentration is toxic to the cells. Ideally, to each well in 96-well plate, 1-3 μl DMSO was added depending on the experiment. Final DMSO volume in each well was equal between treated and control cells.

In ELISA experiments, cell culture supernatants transferred to microcentrifuge tubes were centrifuged at 3570 rpm (1000 g, with 7 cm radius of the rotor of the centrifuge) at 4 C to remove insoluble impurity and cell debris. The clear supernatants collected were then diluted with dilution buffer at 1:2 ratio to be used in the ELISA experiments.

In these experiments, following ELISA kits from FineTest (Wuhan, China) were used: Human IL-18(Interleukin 18) ELISA Kit (Cat # EH0011) and Human HMGB1(High mobility group protein B1) ELISA Kit (Cat # EH0884). ELISA kits were stored at 4 C. Manufacturer's protocol was followed in both experiments. Briefly, plates were washed 2 times with a wash buffer before the addition of samples. Then, 100 μl of properly diluted samples (supernatants from 96-well plates; diluted previously at 1:2 with sample dilution buffer provided with the kit, as indicated above) were added into wells of pre-coated plates, and plates were sealed with the cover and incubated at 37 C for 90 min. Later, the cover was removed and plate content was discarded. Plates were washed with

wash buffer 2 times, and 100 µl biotin-labeled antibody working solution was added at the bottom of each well. After covering the plate with the seal, plates were incubated for 60 min at 37 C. At the end of incubation period, cover was removed and plates were washed with wash buffer 3 times, by letting the wash buffer stay in the wells for at least 2 min each time. Then, 100 µl SABC (HRP-Streptavidin conjugate) working solution was added into each well, plates were covered and incubated for 30 min at 37 C. Afterwards, the cover was removed and plates were washed 5 times with wash buffer, again letting the wash buffer stay in the wells for at least 2 mins each time. Next, 90 µl TMB subtrate was added into each well, plates were covered and incubated at dark at 37 C for 20 min. Finally, 50 µl stop solution was added into each well, contents of the wells were mixed well by pipetting, and the absorbance was then read at 450 nm in a microplate reader (Thermo Scientific™ Multiskan™ GO Microplate Spectrophotometer).

2.8 Transfection for GSDMC and GSDMD Overexpression Using Pre-designed Overexpression Plasmids

For the transfection of ovarian cancer cell lines (A2780 and A2780-AD), 100.000 cells per well were seeded in a 24-well plate in 1 ml growth media for each well, the day before transfection. At the time of transfection, the confluency for adherent cells should be ideally 70-90%. 24 hours following the cell seeding, media was changed with 1 ml serum-free and also phenol red-free RPMI-1640 (pre-warmed). Around 0.5 µg plasmid DNA was diluted in 100 µl of serum-free RPMI-1640 growth media, and then 2 µl transfection reagent (TurboFect Transfection Reagent, Cat # R0532, Thermo Fisher Scientific) was added to the diluted DNA after briefly vortexing the transfection reagent, and then plasmid DNA : transfection reagent solution was mixed immediately by vortexing. The mixture was incubated for 15-20 min at RT. Later, 100 µl of the transfection reagent/DNA mixture was added drop-wise to each well and the plate was rocked gently to achieve even distribution of the complexes immediately after adding the transfection reagent. The plate was incubated at 37 °C in a CO_2 incubator for 48 hours, and then transgene expression was analyzed using qRT-PCR (at the mRNA level) and Western Blot (at the protein level).

When we performed the experiments in 6-well or 96-well plates, we changed the volumes of growth media, plasmid and transfection reagent, accordingly.

Overexpression plasmids (pPM-C-HA) for GSDMC (Accession number: BC035321) and GSDMD (Accession number: BC008904) were purchased from Applied Biological Materials Inc.

(Richmond, Canada). They contain kanamycin resistance genes for bacteria. Vector size of both plasmids are 4765 bp. Insert size for GSMDC plasmid is 1527 bp and for GSDMD plasmid is 1455 bp.

2.8.1 Bacterial transformation

To prepare LB broth, 25 grams of powder was dispersed in 1 L deionized water and swirled to completely dissolve on a magnetic stirrer. Later, it was sterilized by autoclaving at 121 C for 15 min, and stored at 4 C for further use. To prepare LB agar, 40 grams of powder was dispersed in 1 L deionized water and swirled to completely dissolve on a magnetic stirrer. Then, it was sterilized by autoclaving at 121 C for 15 min. After cooling to around 50 C, kanamycin stock solution was added to a final concentration of 50 µg/ml, and then poured into petri dishes near a lit Bunsen burner under sterile conditions, and allowed to set for a while. After cooling and solidifying, kanamycin containing petri dishes were transferred to a 4 C freezer with media containing side of the dish facing upside.

Competent cells were taken out of -80°C refrigerator and thawed on ice for approximately 20-30 mins. Agar plates (containing 50 µg/ml kanamycin) prepared previously (as detailed above) were removed from 4°C freezer, and warmed up to RT or 37 C. 5 µl plasmid DNA was added into 50 µl of competent cells in a microcentrifuge tube, and gently mixed by flicking the bottom of the tube a few times. The tube containing the competent cell: DNA mixture was incubated on ice for 30 mins. The tube was then placed into a 42°C water bath for 45 secs for heat shock, and put back on ice for 2 min. 1 ml LB media or SOC media (without kanamycin) was added to the tube containing bacteria, and the tubes were incubated in 37°C shaking incubator for at least 45 min. Tube's content were plated onto a 10 cm LB agar plate containing 50 µg/ml kanamycin near a lit Bunsen burner under sterile conditions. Plates were incubated at 37°C overnight, and the next day, the presence of any colonies were checked. If the formation of any colony is observed, plates were stored at 4 C for further use after covering the sides of plates with parafilm to avoid potential contamination.

2.8.2 Plasmid isolation

A single colony was selected from a plate containing 50 µg/mL kanamycin (see above) with a sterile micropipette tip near a Bunsen burner under sterile conditions, and grown overnight in 10 ml LB media without antibiotics at 37 C while shaking. Next day, plasmid isolation was performed as

follows (We used EZ-10 Spin Column Plasmid DNA Miniprep Kit from Bio Basic Inc., Markham ON, Canada; Cat # BS414): We used 5 – 10 ml overnight culture and added it in 1.5 ml portions to a microcentrifuge tube and centrifuged at 12,000 rpm for 2 minutes. We discarded the liquid completely and repeated the centrifuge step with another portion of culture in the same tube (Alternatively, we centrifuged bacteria cultures in 15 ml tubes at a lower rpm for a longer time, e.g. 4500 rpm for 10 min). Then, we added 200 µl of Solution I (to which RNase A was previously added) to the pellet, mixed well by pipetting several times and kept for 1 minute, and later added 400 µl of Solution II to the mixture, and mixed gently by inverting the tube few times (without vortexing) and kept at room temperature for 1 minute. Afterwards, we added 700 µl of Solution III, and mixed gently. We incubated the tubes at RT for 1 minute. After incubation, we centrifuged the tubes at 12,000 rpm for 5 minutes and transferred the half of the above supernatant to the EZ-10 column (for DNA) and let the column stand for 2 minutes. Then, we centrifuged the tubes at 10,000 rpm for 2 minutes and discarded the flow-through in the tube, and added the second half of the supernatant, centrifuged the tubes again at 10,000 rpm for 2 minutes. Later, we discarded the flow-through in the tube and added 750µl wash solution to the column, and centrifuged at 10,000 rpm for 2 minutes. We repeated this washing step. Afterwards, we discarded the flow-through in the collection tube and centrifuged at 10,000 rpm for an additional minute to remove any residual wash solution. Finally, we transferred the column to a clean 1.5 ml microcentrifuge tube and added 50 µl elution buffer (stored at RT) into the center part of the column and incubated at RT for 2 minutes and centrifuged at 10,000 rpm for 2 minutes. Plasmid DNAs were then stored at -20 C.

Plasmid DNA concentration was measured at 260 nm using a spectrophotometer (Thermo Scientific™ Multiskan™ GO Microplate Spectrophotometer). 1 µl plasmid DNA sample was loaded to each aperture on µDrop plate. Obtained absorbance value was multiplied by 50 (for RNA, it is 40) after subtracting the absorbance value of elution buffer to convert the absorbance value to ng/µl unit. Measurements were performed at least in duplicates.

2.9 Silencing Experiments

For silencing experiments, following siRNAs (small interfering RNAs) were used: Silencer pre-designed siRNAs (Invitrogen, Life Technologies Corp., CA, USA) (negative control: Cat # AS02K9RH; GSDMC: Cat #AS02KN42; GSDMD: Cat # AS0KN43). We prepared siRNA stocks as 5000 pmol (5 nmol) / 1.5 ml in RNase-free water. As transfection reagent, we used Lipofectamine 3000 (Invitrogen; Cat # L3000001) and followed manufacturer's protocol. Briefly,

we plated cells so they are 70-90% confluent at the time of transfection. Next day, we prepared siRNA-lipid complexes and added siRNA-lipid complexes to the cells. To prepare siRNA-lipid complexes, we first diluted Lipofectamine 3000 reagent in serum-free RPMI-1640 media. Similarly, we diluted siRNAs in serum-free RPMI-1640 media (For instance (for 6-well format), we diluted 75 pmol of siRNA (22.5 µl) in 125 µl media; 7.5 µl Lipofectamine 3000 in 125 µl media). Then, we added diluted siRNA to diluted transfection reagent at 1:1 ratio and incubated it for 10-15 minutes at RT. After adding siRNA-lipid complexes to the cells, we incubated cells for 2 days at 37 C. For 96-well format, we used 3 pmol siRNA and 0.3 µl Lipofectamine 3000 reagent. For 6-well format, we used 75 pmol siRNA and 7.5 µl Lipofectamine 3000 reagent.

We did not use P3000 reagent when diluting siRNAs as suggested in the product's protocol.

2.10 SDS-PAGE

2.10.1 Sample lysis

To prepare 1X lysis buffer, 10X RIPA buffer (ab156034, Abcam) was diluted to 1X with deonized water. For each 10 ml of lysis buffer, 1 tablet of cOmplete™, Mini, EDTA-free Protease Inhibitor Cocktail (PIC) (Cat # 11836170001, Roche) was added, and tablets were dissolved completely by vortexing. Lysis buffer containing protease inhibitors was stored at 4 C.

To prepare lysates from cells, to each well of a 6-well plate, after removing the media, 500 µl trypsin (pre-warmed to 37 C) was added. After all cells were detached from the bottom of the plate (checked under a microscope), they were collected to 1.5 ml tube and centrifuged at 3000 rpm for 3 min at 4 C. Trypsin was discarded, and 500 µl ice-cold PBS was added to cell pellet. The tube was centrifuged at 3000 rpm for 3 min at 4 C, and then PBS was discarded. Later, to cell pellet, 500 µl ice-cold lysis buffer (1X RIPA buffer containing protease inhibitor cocktail (PIC)) was added and shaked for 30 min at 4 C, and then centrifuged at 12000 rpm at 4 C for 20 min. Supernatant containing proteins was aspirated and kept at -20 C, and the pellet was discarded.

2.10.2 Determination of protein concentration by Bradford Assay

Protein concentration of samples was determined using Bradford Assay. In a 96-well plate, 5 ul of sample was added to a well, and 250 µl Bradford Reagent (Cat # 23200, Thermo Scientific) was

then added to the sample and mixed well. The plate was incubated at room temperature for at least 5 min, and absorbance values were measured at 595 nm in a spectrophotometer (Thermo Scientific™ Multiskan™ GO Microplate Spectrophotometer). Negative controls (samples containing no proteins) were also incorporated. Before using protein samples from different experimental cases (e.g. GSDMD-overexpressed vs not overexpressed) in further experiments, their concentrations were equalized to make the comparisons between cases posible.

2.10.3 Sample preparation

An equal volume of 2X Laemmli sample buffer (Cat # 1610737, BioRad) (65.8 mM Tris-HCl, pH 6.8, 2.1% SDS, 26.3% (w/v) glycerol, 0.01% bromophenol blue) was added to the protein sample. Thus, 2X concentration were diluted to 1X at the final solution. In order to prepare 2X sample buffer containing β-mercaptoethanol (BME), 950 µl of 2X Laemmli sample buffer was mixed with 50 µl of BME. Each cell lysate in sample buffer was boiled at 100°C for 5 min. Lysates were aliquoted and stored at -20°C for future use. B-mercaptoethanol was used to break disulfide bonds in the proteins to transform them from their 3D structure to 1D, together with SDS.

2.10.4 SDS-PAGE gel preparation

10% resolving / separating gels (for 10 ml) were prepared using the following volumes of the components: water (3.8 ml), 30% acrylamide (3.4 ml), 1.5 M Tris-HCl, pH 8.8 (2.6 ml), 10% SDS (sodium dodecyl sulfate) (100 µl), 10% APS (ammonium persulfate) (100 µl) and TEMED (Tetramethylethylenediamine) (10 µl). Stacking gel solutions were prepared using the following volumes (for 10 mL): Water (5.86 ml), 30% acrylamide (1.34 ml), 0.5 M Tris-HCl, pH 6.8 (2.6 ml), 10% SDS (100 µl), 10% APS (100 µl) and TEMED (10 µl). APS and TEMED were added just before pouring the gel mixtures into the space between spacer glasses, since they quickly catalyzes the polymerization reaction of acrylamide and make it solidified. After pouring the resolving gel solution in the plates assembled with spacers, to maintain an even and horizontal resolving gel surface, the surface was overlayed with isopropanol, and also to make it solidify faster. The gel was allowed to set for about 20-30 min (or less until it becomes solidified) at room temperature. Before, pouring the stacking gel, we discarded the overlayed isopropanol on the resolving gel by tilting the spacers. Then, we added the 5% stacking gel solution over the solidified resolving gel until it overflows (to remove the formation of any bubbles), and inserted the comb immediately ensuring no air bubbles are trapped in the gel or near the wells. Finally, we allowed the gel to set for about

20-30 min (or less until it becomes solidified) at room temperature. If not used immediately, prepared gels were stored at 4 C with combs still inserted into the gels, in plastic bags in order not to allow drying of the gels.

2.10.5 Loading and running the gel

Running buffer (Tris-Glycine/SDS) was prepared using 25 mM Tris base, 190 mM glycine, 0.1% SDS in distilled water. pH of the buffer was adjusted to 8.3 with NaOH and HCl solutions. Alternatively, at certain occasions, running buffer was prepared from 10X commercial running buffer solution.

Equal amounts of protein were loaded into the wells of the SDS-PAGE gel prepared previously (based on Bradford Assay), along with a molecular weight marker (Opti-Protein Marker, Cat # G252 Applied Biological Systems, Canada) (5 µl/lane) and electrophoresis was performed for 1–2 h at 100 V. Initially, a lower voltage (50V) was applied for around 5 min. When bromophenol blue present in the wells left the bottom of the gel, we stopped the electrophoresis.

2.11 Western Blot

2.11.1 Transfer to nitrocellulose membrane (Tank blotting, Electrophoretic Transfer)

Transfer buffer was prepared using 25 mM Tris base, 190 mM glycine, 20% methanol, and pH was adjusted to 8.3. The gel was immersed in transfer buffer for 10 to 15 minutes. Filter papers and nitrocellulose membrane (cut in similar size and shape to the gel) were soaked in transfer buffer for at least 30 seconds. The gel is then placed in the "transfer sandwich" (in the order of filter paper-gel-membrane-filter paper), cushioned by pads at both sides and pressed together by a support grid. Transfer was performed at 80 V for around 1.5 hours at cold (4 C).

2.11.2 Antibody staining

The membrane was blocked for 1 h at room temperature using blocking buffer (3–5% milk or BSA in TBST buffer). The membrane was incubated with appropriate dilutions of primary antibody (GSDMC, GSDMD or Beta-actin) in blocking buffer. The membrane was washed in three washes of TBST, 5 min each. Then, the membrane was incubated with the recommended dilution of

conjugated secondary antibody in blocking buffer at room temperature for 1 h and later washed in three washes of TBST, 5 min each. 1 liter of TBST (Tris-buffered saline, 0.1% Tween 20) was prepared using 100 ml of TBS 10x, 900 ml distilled water and 1 ml Tween 20. 1 liter of TBS (10X) (concentrated Tris-buffered saline) was prepared using: 24 g Tris base (formula weight: 121.1 g), 88 g NaCl (formula weight: 58.4 g). This mixture was dissolved in 900 ml distilled water and pH was adjusted to 7.6, and then distilled water was added to a final volume of 1 L.

For detection, SuperSignal® West Pico Chemiluminescent Substrate (Thermo Scientific, B2160636) was used. This is a highly sensitive enhanced substrate for detecting horseradish peroxidase (HRP) on immunoblots. Two substrate components were mixed at a 1:1 ratio to prepare the substrate Working Solution. The blot was incubated for 5 minutes in SuperSignal® West Substrate Working Solution and excess reagent was drained. Imaging was performed using ChemiDoc imaging system (Bio-Rad).

Following antibodies were used in these experiments: GSDMD Polyclonal Antibody (Elabscience, USA, Cat # E-AB-67333): reactivity: human, mouse, rabbit.; host: rabbit; isotype: IgG; MW: 53 kDa; dilution: WB 1500:2000. GSDMC Rabbit pAb (polyclonal antibody) (ELK Biotechnology Cat # ES2400): host species: rabbit; recommended dilutions: Western Blot 1/500 – 1/2000; observed band: 55 kDa.
Both antibodies were stored at -20 C upon delivery and repeated freeze / thaw cycles were avoided.

2.12 MTT Assay

For MTT assay, we first seeded cells at a density of 15.000-20.000 cells / well in 96-well plates. 24 hours later, we discarded the growth media from wells, and added 50 µl of serum-free RPMI-1640 (without phenol red) and 50 µl of MTT solution (Thiazolyl blue tetrazolium bromide (Bio Basic, Cat # 298-93-1), prepared as 5 mg/mL solution in PBS) into each well. Then, we incubated the plate at 37°C incubator for around 3 hours. After incubation, we added 150 µl DMSO as MTT solvent into each well and wrapped the plate in foil and shaked on an orbital shaker for around 15 minutes. Afterwards, we did pipetting of the liquid to fully dissolve the MTT formazan formed and finally read the absorbance at OD=590 nm in a microplate reader (Multiskan GO Microplate Spectrophotometer, Thermo Scientific). Bubble formation was avoided before reading. All the steps were performed at an environment without direct light.

In MTT Assay, metabolically active cells (i.e. live cells but not dead cells) reduce yellow tetrazolium MTT into purple formazan in part by the action of dehydrogenase enzymes. Therefore, the spectrophotometric signal from formazan correlates with the number of live cells present.

3 RESULTS[1]

[1] *A part of the data obtained in this thesis study have been published in journals given below:*

Berkel C, Cacan E. Differential Expression and Copy Number Variation of Gasdermin (GSDM) Family Members, Pore-Forming Proteins in Pyroptosis, in Normal and Malignant Serous Ovarian Tissue. Inflammation. 2021 Dec;44(6):2203-2216. doi: 10.1007/s10753-021-01493-0. PMID: 34091823.

Berkel C, Cacan E. Lower expression of NINJ1 (Ninjurin 1), a mediator of plasma membrane rupture, is associated with advanced disease and worse prognosis in serous ovarian cancer. Immunol Res. 2023 Feb;71(1):15-28. doi: 10.1007/s12026-022-09323-7. PMID: 36184655.

3. 1 Expression of Gasdermin D and Gasdermin C Is Upregulated in Serous Ovarian Cancer

Several studies have identified gasdermin D (GSDMD) as the sole executor of pyroptosis, a lytic pro-inflammatory type of programmed cell death (Kayagaki et al., 2015; Shi et al., 2015; He et al., 2015). However, more recent studies have proven that other members of the family are also capable

of executing pyroptotic cell death in different cell types and at various contexts. We found that GSDMD expression is increased at the mRNA level in serous ovarian cancer (OC) compared to normal (non-malignant) ovaries, in three independent gene expression datasets (Figure 3.1, GEO IDs for these transcriptomics datasets were given in figure captions). One of these datasets contains gene expression data for both early-stage and late-stage serous ovarian cancer samples (GSE12470; first panel); others contain data for samples from late-stage, high-grade serous ovarian cancer patients (HGSOC) (GSE18520, GSE26712; second and third panels). In all cases, gasdermin D shows elevated expression at the transcript level in ovarian tumors from serous ovarian cancer patients compared to normal ovaries from healthy controls (with no malignancy). In all comparisons, we found highly significant changes ($p \leq 0.001$) in the expression of GSDMD between ovarian tumor and normal samples (Figure 3.1). The fact that the same observations were made in all three independent datasets supports our inferences. Sample sizes (n) for these datasets were given in Materials and Methods section and in the figure legend.

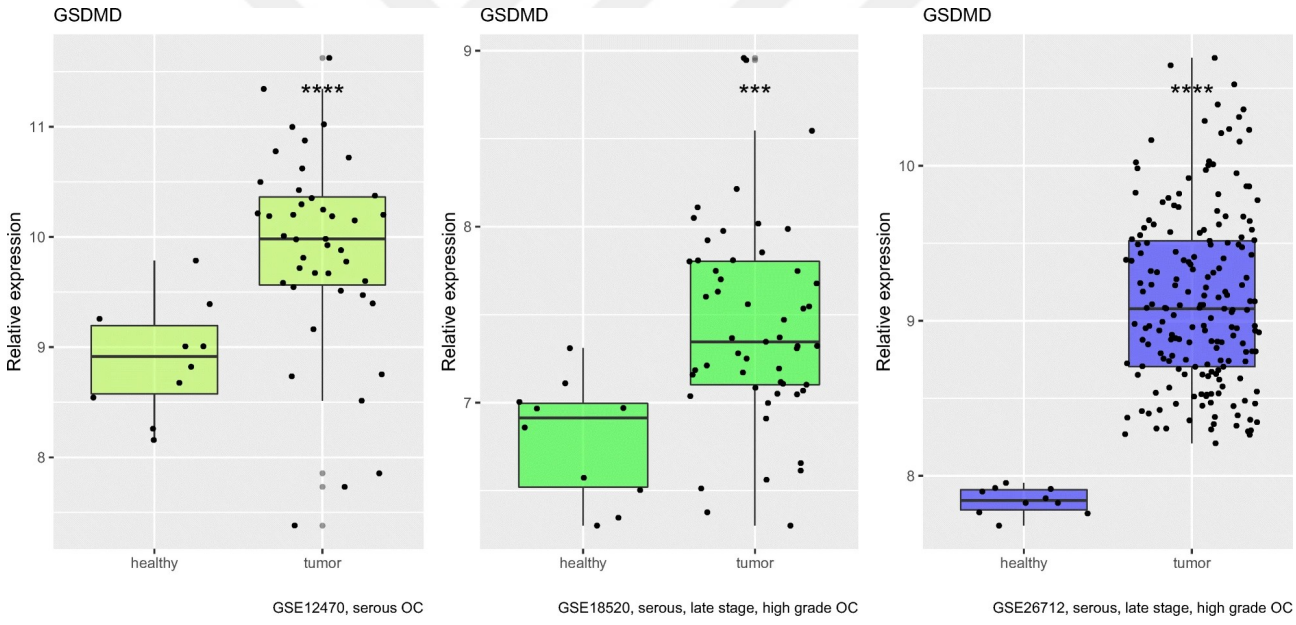

Figure 3.1. Expression of gasdermin D (GSDMD) is upregulated in serous ovarian cancer (tumor) compared to normal ovaries (healthy). Non-significant (ns): $p > 0.05$; *: $p \leq 0.05$; **: $p \leq 0.01$; ***: $p \leq 0.001$;****: $p \leq 0.0001$. OC: ovarian cancer. GSE12470 (n = 53), GSE18520 (n = 63), GSE26712 (n = 195). In the boxplots, the bottom and top sides of the box represent the lower and upper quartiles. The box covers the interquartile interval, where half of the data is found (i.e. half of the data points are inside the box area). The vertical line that split the box in two is the median

value of all the data points (here, the gene expression values). Different colors represent different datasets.

Similar to GSDMD, the expression of another member of gasdermin protein family, gasdermin C (GSDMC, MLZE), is also increased in serous ovarian cancer compared to healthy ovaries, in two independent datasets (Figure 3.2). The first plot in this figure shows data from serous ovarian cancer patients in general (all stages and grades combined), second plot shows data from late stage and high grade serous ovarian cancer patients (Figure 3.2). Please note that in the second plot, changes in the expression of GSDMC is more significant than that in the first plot, pointing to the possibility that during cancer progression (late stage or high grade), change in GSDMC expression at the mRNA level compared to non-malignant / healthy ovaries might be more dramatic. Sample sizes (n) of both datasets were given in Materials and Methods section and in the figure legend.

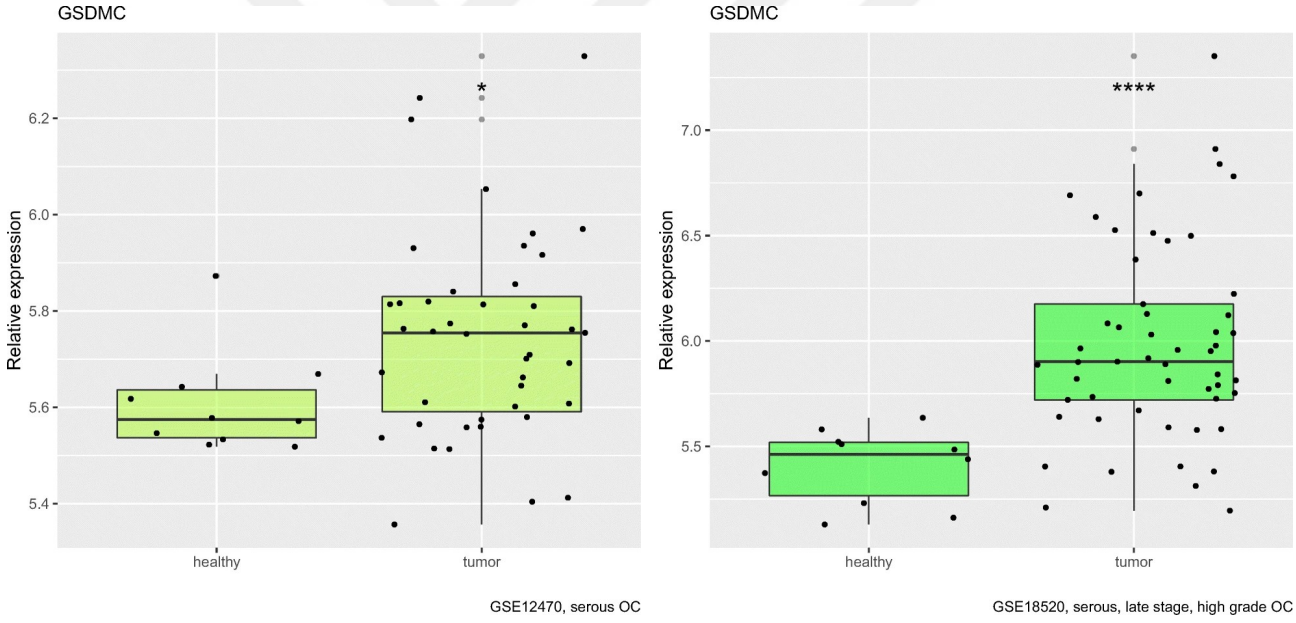

Figure 3.2. Expression of gasdermin C (GSDMC, MLZE) is upregulated / increased in serous ovarian cancer (tumor) compared to normal ovaries (healthy). Non-significant (ns): $p > 0.05$; *: $p \leq 0.05$; **: $p \leq 0.01$; ***: $p \leq 0.001$;****: $p \leq 0.0001$. OC: ovarian cancer. GSE12470 (n = 53), GSE18520 (n = 63). In the boxplots, the bottom and top sides of the box represent the lower and upper quartiles. The box covers the interquartile interval, where half of the data is found (i.e. half of the data points are inside the box area). The vertical line that split the box in two is the median

value of all the data points (here, the gene expression values). Different colors represent different datasets.

Since certain gasdermins should be cleaved within their linker regions between NT and CT domains by specific caspases to be active (membrane-targeting and pore-forming) in pyroptosis, we analyzed the expression profiles of caspases (caspase-1, -3, -4, -5, and -8, no data for caspase-11) in serous ovarian cancer (Figure 3.3). We found that expression of these caspases is mostly decreased at the mRNA level in serous ovarian cancer compared to ovarian tissue from healthy controls (Figure 3.3). Possibly, more than their expression levels, the activity and functionality of caspases should be taken into consideration in this context, since high caspase expression does not always lead to high caspase enzymatic activity and high gasdermin cleavage events.

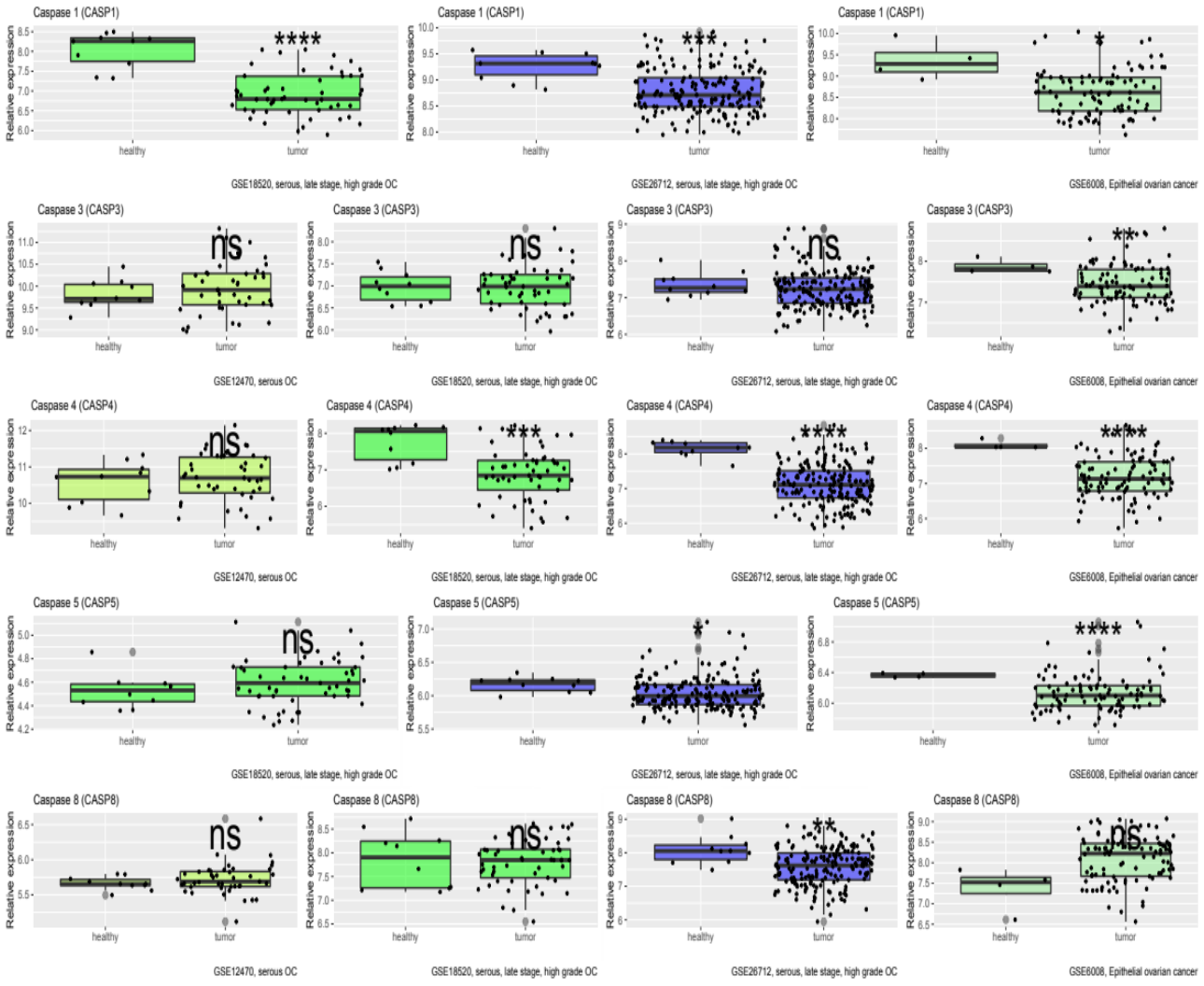

Figure 3.3. Expression profiles of caspases (caspase-1, -3, -4, -5, and -8, no data for caspas-11) in serous ovarian cancer compared to healthy ovaries.

In the boxplots, the bottom and top sides of the box represent the lower and upper quartiles. The box covers the interquartile interval, where half of the data is found (i.e. half of the data points are inside the box area). The vertical line that split the box in two is the median value of all the data points (here, the gene expression values). Different colors represent different datasets.

3.2 Expression of Gasdermin E and PJVK Is Downregulated in Serous Ovarian Cancer

In contrast to increased expression of GSDMD and GSDMC in serous ovarian cancer cells compared to normal ovarian cells, the expression of GSDME (DFNA5) decreases in serous ovarian cancer compared to normal ovaries in three independent gene expression datasets (Figure 3.4). The difference in the expression of GSDME between normal and tumor samples from ovaries is larger (more significant) in late-stage, high-grade serous ovarian cancer (second and third panels), compared to serous ovarian cancer (both early and late stages combined) (first panel). This may possibly indicate tumor stage- or tumor grade-dependent expression of GSDME in serous ovarian cancer. In other words, as cancer progresses to later stages or higher grades, the difference in terms of GSDME transcript levels between normal ovaries and ovarian tumors might be increasing, at least at the mRNA level.

Both GSDME (DFNA5) and PJVK (Pejvakin, DFNB59) belong to the deafness-associated genes (DFN). Protein sequences for GSDME and PJVK cluster closely together, distant from the other members of gasdermin family in humans (GSDMA-D) (Broz et al., 2020). In terms of evolution, GSDME and PJVK are the most ancient members of gasdermin family, and similar sequences can also be found in some lower vertebrates and in some invertebrates (Broz et al., 2020; Kersey et al., 2018; Zerbino et al., 2018; Jiang et al. 2020). Within the GSDME/PJVK clade, PJVK was a duplication from GSDME; however, it lost the last three exons which code for the CT auto-inhibitory domain in early vertebrates (Wang and Ruan, 2023). We found that, similar to GSDME, expression of PJVK is also decreased in serous ovarian cancer samples from patients compared to normal ovarian samples from healthy women (Figure 3.5). Expression data for PJVK is available in only one of the gene expression datasets analyzed in this study; and therefore, further research is needed to make stronger inferences on PJVK expression in ovarian cancer (Figure 3.5). Here, please note that PJVK is one of the least studied members of the family compared to other members of this protein family such as GSDMD.

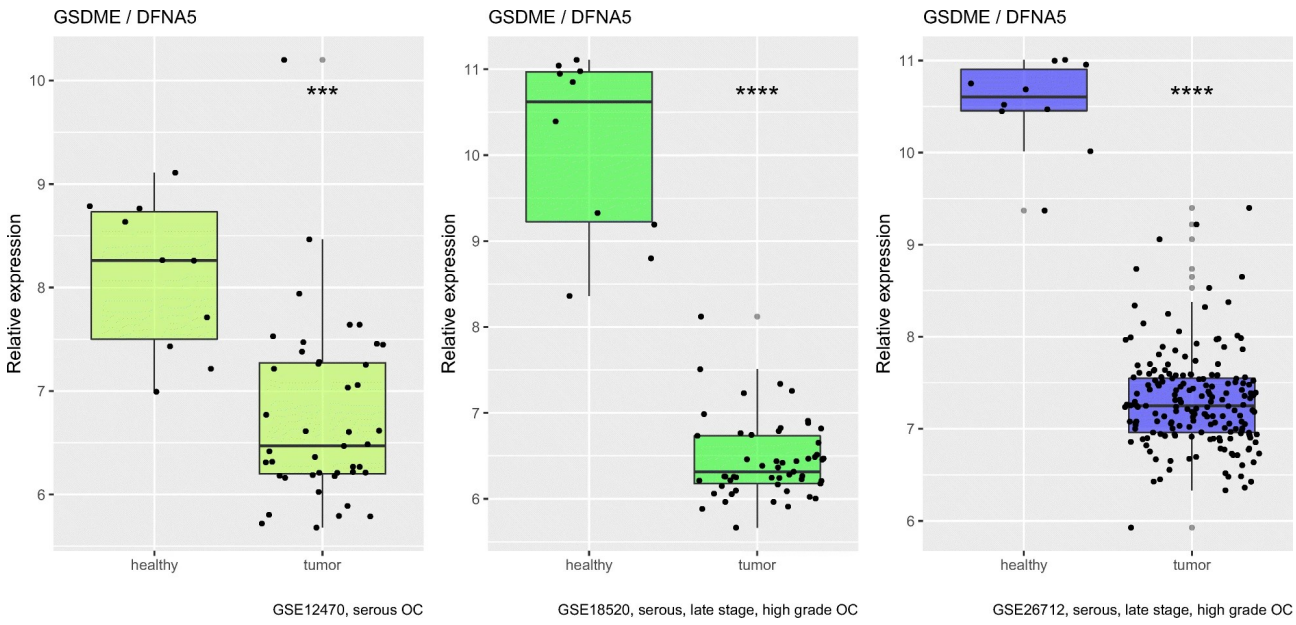

Figure 3.4. Expression of gasdermin E (GSDME) is downregulated / decreased in serous ovarian cancer compared to normal ovaries in three independent transcpriptomics datasets. Non-significant (ns): $p > 0.05$; *: $p \leq 0.05$; **: $p \leq 0.01$; ***: $p \leq 0.001$;****: $p \leq 0.0001$. *OC: Ovarian cancer*; DFNA5: Deafness, Autosomal Dominant 5. GSE12470 (n = 53), GSE18520 (n = 63), GSE26712 (n = 195). In the boxplots, the bottom and top sides of the box represent the lower and upper quartiles. The box covers the interquartile interval, where half of the data is found (i.e. half of the data points are inside the box area). The vertical line that split the box in two is the median value of all the data points (here, the gene expression values). Different colors represent different datasets.

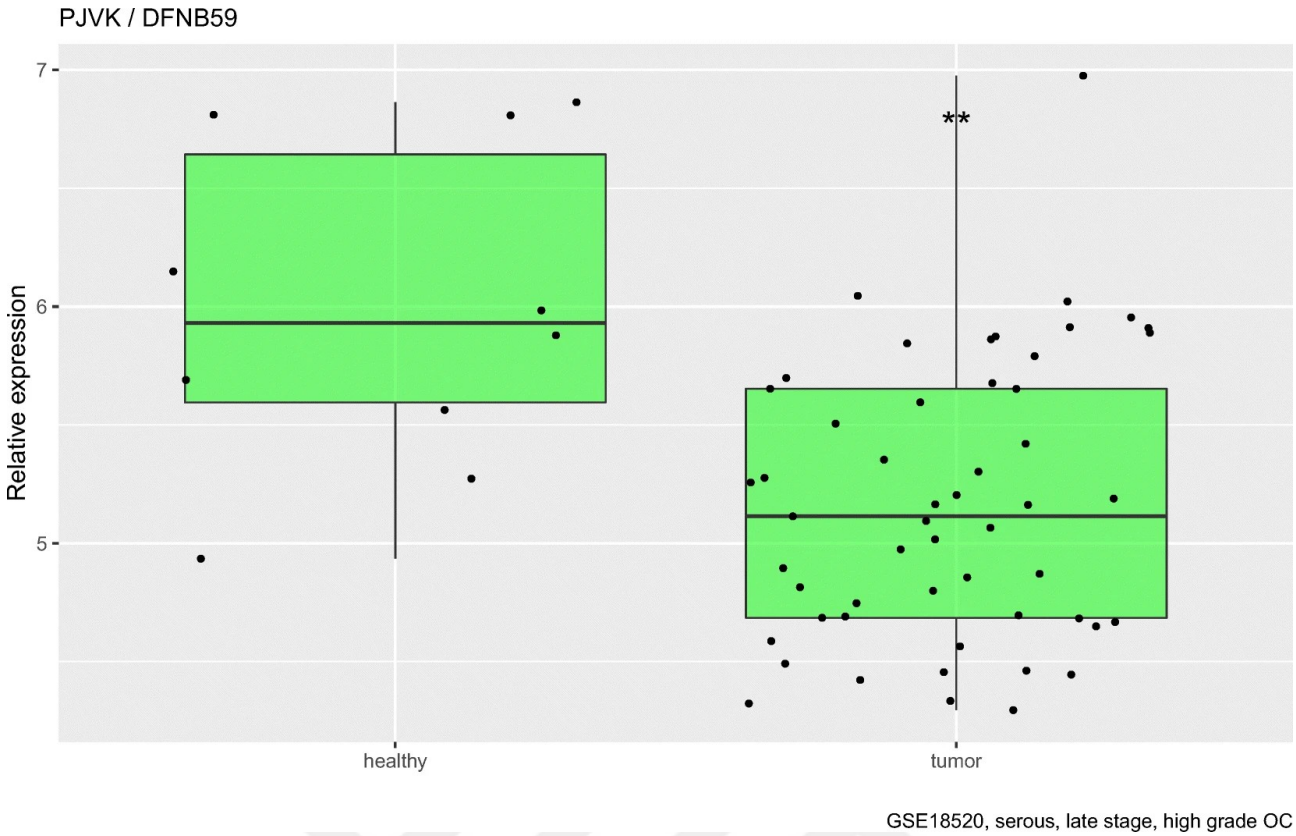

Figure 3.5. Expression of PJVK (Pejvakin, DFNB59) is downregulated in serous ovarian cancer compared to normal/healthy ovaries. Non-significant (ns): $p > 0.05$; *: $p \leq 0.05$; **: $p \leq 0.01$; ***: $p \leq 0.001$;****: $p \leq 0.0001$. *OC: Ovarian cancer*; DFNB59: Deafness, Autosomal Recessive 59. GSE18520 (n = 63). In the boxplots, the bottom and top sides of the box represent the lower and upper quartiles. The box covers the interquartile interval, where half of the data is found (i.e. half of the data points are inside the box area). The vertical line that split the box in two is the median value of all the data points (here, the gene expression values).

Furthermore, we observed that the expression of GSDMB is increased in serous ovarian cancer (both early and late stage combined) compared to normal ovaries, in one of the three datasets (Figure 3.6, first panel, top row), but remains unchanged in other two datasets (late-stage, high-grade serous ovarian cancer; second and third panels, top row, Figure 3.6). Unlike other members of gasdermin family, the expression of GSDMA at the transcript level does not change in serous ovarian cancer compared to normal non-malignant ovaries in two independent datasets ($p > 0.05$) (Figure 3.6, bottom row). Here, it can be proposed that these two members of the family might not be regulated at the transcription level unlike the other members in the ovarian cancer initiation or progression.

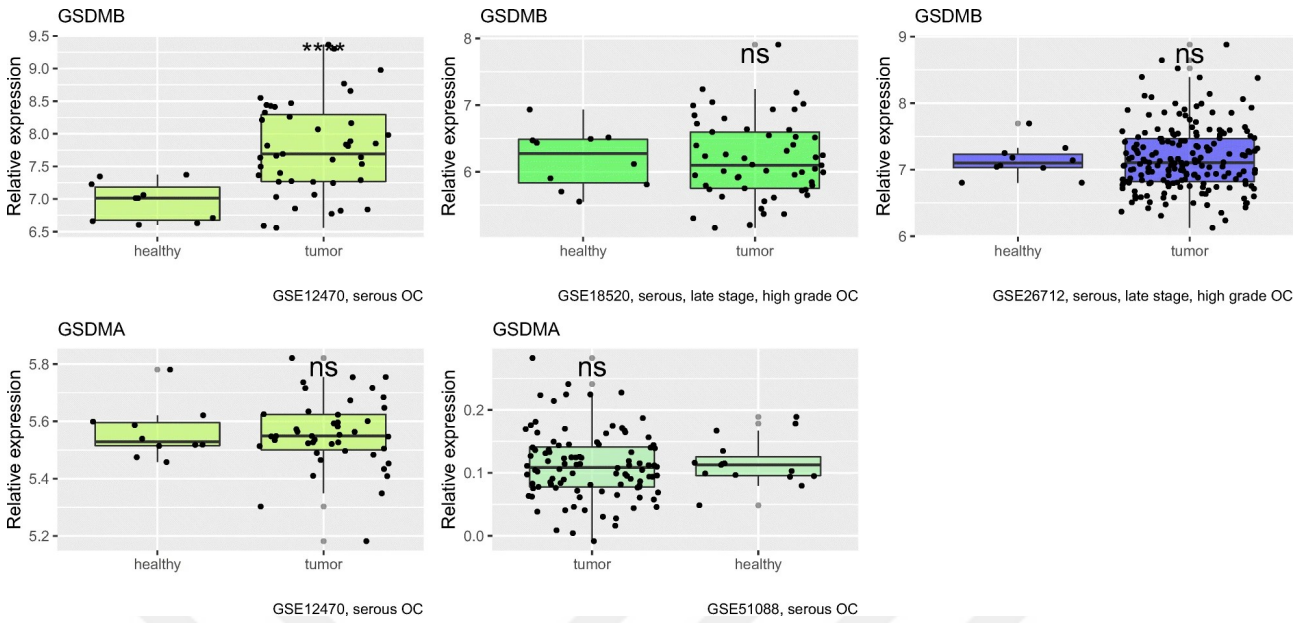

Figure 3.6. Expression of GSDMA and GSDMB in serous ovarian cancer compared to healthy ovaries. non-significant (ns): $p > 0.05$; *: $p \leq 0.05$; **: $p \leq 0.01$; ***: $p \leq 0.001$;****: $p \leq 0.0001$. *OC: Ovarian cancer*. GSE12470 (n = 53), GSE18520 (n = 63), GSE26712 (n = 195) and GSE51088 (n = 172). In the boxplots, the bottom and top sides of the box represent the lower and upper quartiles. The box covers the interquartile interval, where half of the data is found (i.e. half of the data points are inside the box area). The vertical line that split the box in two is the median value of all the data points (here, the gene expression values). Different colors represent different datasets.

Since we observed an increased expression in some gasdermins (GSDMD and GSDMC) and a decreased expression in others (GSDME and PJVK) (and no significant changes for the other members of the family (GSDMA, GSDMB)) in serous ovarian cancer at the transcript level, we analyzed the correlation of gasdermin expressions in four gene expression datasets, one of which is TCGA-OV (The Cancer Genome Atlas – Ovarian Cancer) dataset (Figure 3.7). We found that the expression of GSDME (DFNA5) is always negatively correlated with the expression of GSDMD (all negative values), though to varying extents in different datasets. More generally, it can be stated that GSDME (DFNA5) shows negative (or low) correlation with GSDMA-D, but positive correlation with PJVK (DFNB59), another DFN gene in the gasdermin family (please remember that GSDME and PJVK cluster more closely in terms of sequence homology) (Figure 3.7). In other words, more closely related proteins in terms of sequence homology / clustering, GSDME and

PJVK, might show parallel expression profiles in the context of ovarian cancer. Please note that expression of both of these genes similarly decrease at the mRNA level in ovarian tumors compared to healthy ovaries.

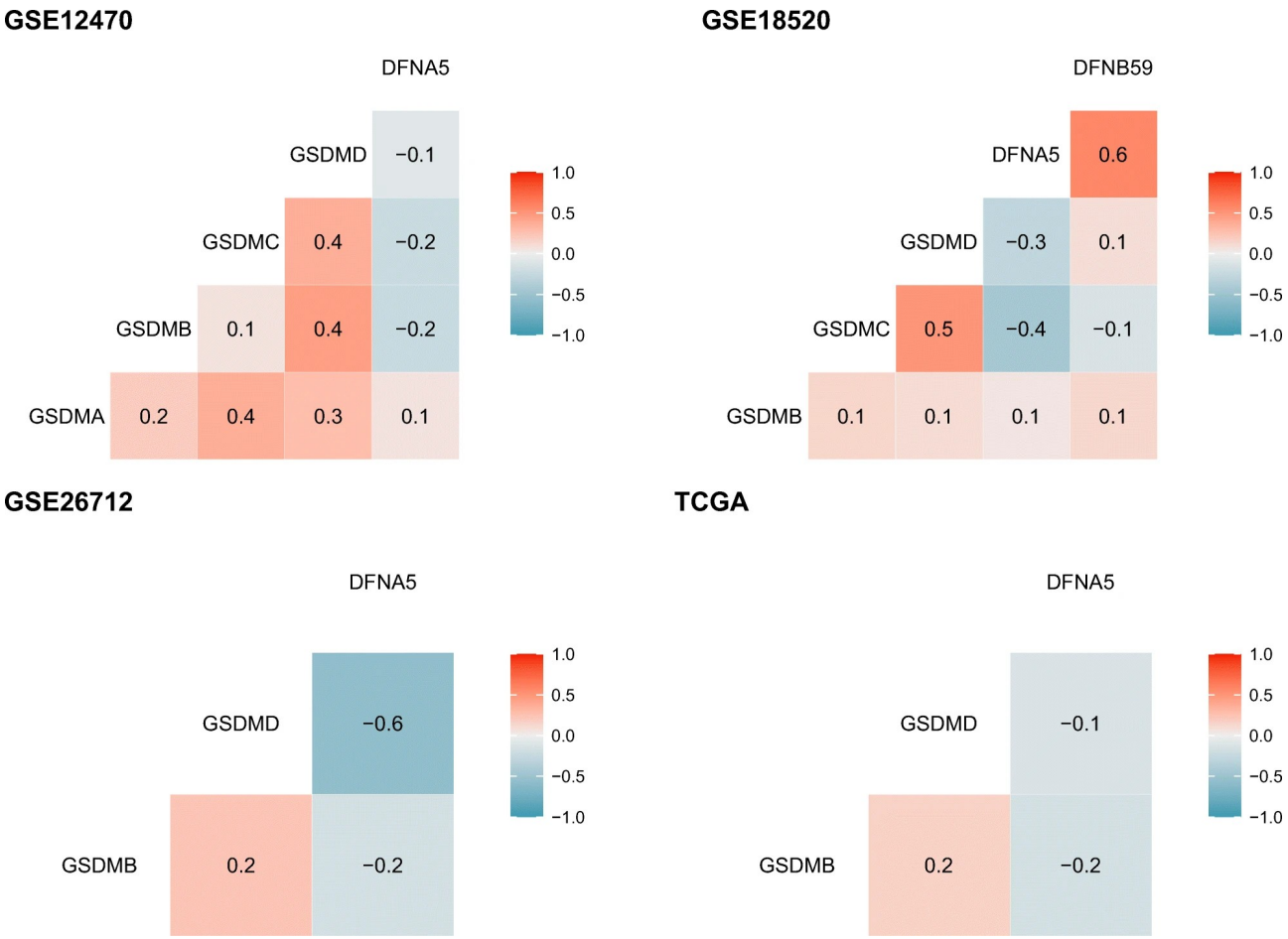

Figure 3.7. The correlation of gasdermin expressions in four gene expression datasets for serous ovarian cancer. Correlation of expression of different gasdermin family members in four different independent gene expression datasets. Red (or 1) indicates positive correlation and blue (or -1) indicates negative correlation between genes. GSE12470 (n = 53), GSE18520 (n = 63), GSE26712 (n = 195), TCGA-OV (n = 578).

A more recent study reported that cell-surface protein NINJ1 (Ninjurin 1) is essential for pyroptosis-related plasma membrane rupture (PMR). The formation of small pores in the plasma membrane by certain pore-forming gasdermin family members such as GSDMD is followed by subsequent plasma membrane rupture which was found to be mediated by NINJ1 (Kayagaki et al., 2021). However, the effect of NINJ1 is not specific to lytic cell death following pyroptosis, it also mediates

plasma membrane rupture following apoptosis (Kayagaki et al., 2021). We found that the expression of NINJ1 (Ninjurin 1) is increased in late-stage, high-grade serous ovarian cancer compared to that of healthy controls, similar to the changes in the expression of GSDMD and GSDMC in serous ovarian cancer (Figure 3.8). Here, data from two datasets were combined after normalization.

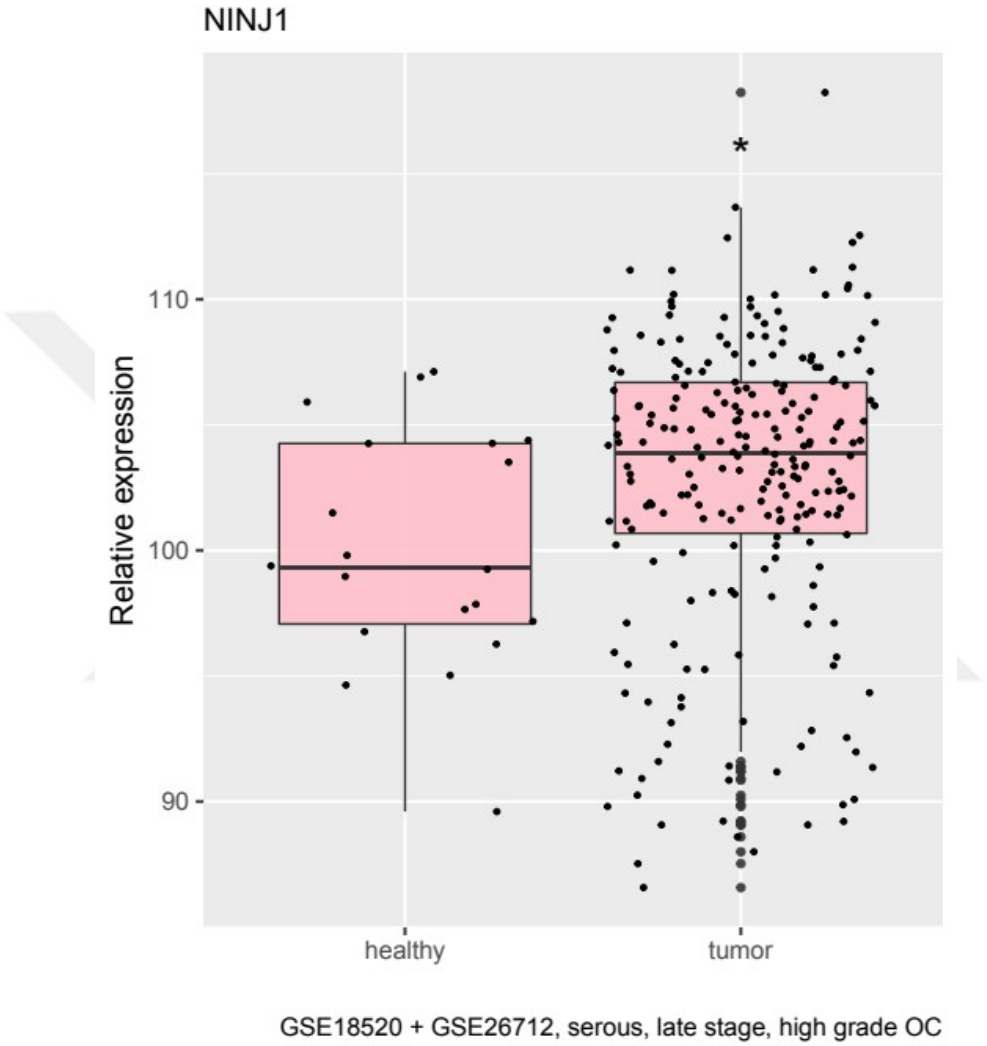

Figure 3.8. The expression of NINJ1 (Ninjurin 1) is increased in late-stage, high-grade serous ovarian cancer (tumor) compared to that of healthy controls. In the boxplots, the bottom and top sides of the box represent the lower and upper quartiles. The box covers the interquartile interval, where half of the data is found (i.e. half of the data points are inside the box area). The vertical line that split the box in two is the median value of all the data points (here, the gene expression values). Here, data from two datasets (GSE18520 and GSE26712) were combined after normalization.

3.3 GSDMB and GSDMD Expressions Show Differences Among Various Histotypes / Histological Subtypes of Epithelial Ovarian Cancer

Next, we analyzed the differential expression (DE) of gasdermins at the mRNA level among different histological subtypes of epithelial ovarian cancer (EOC), which is the most common and lethal of all types of ovarian cancers (OC) (Berkel and Cacan, 2021). For more detail on the histological subtypes of ovarian cancer, please see Introduction section. We found that the expression of GSDMB is increased in mucinous histotype compared to endometrioid (abbreviated as 'endo') and serous (abbreviated as 'ser') histotypes of epithelial ovarian cancer (Figure 3.9, first panel). The expression of GSDMD is elevated in clear cell and serous histotypes compared to endometrioid histotype (Figure 3.9, middle panel). Furthermore, GSDMD shows higher levels of expression at the transcript level in clear cell compared to mucinous histological type (Figure 3.9, middle panel). GSDME (DFNA5) expression is similar among different histotypes of EOC (Figure 3.9, last panel). This expression data points to the fact that certain gasdermins show histotype-dependent expression in epithelial ovarian cancer, and that studies on gasdermins in ovarian cancer should take this observation into account.

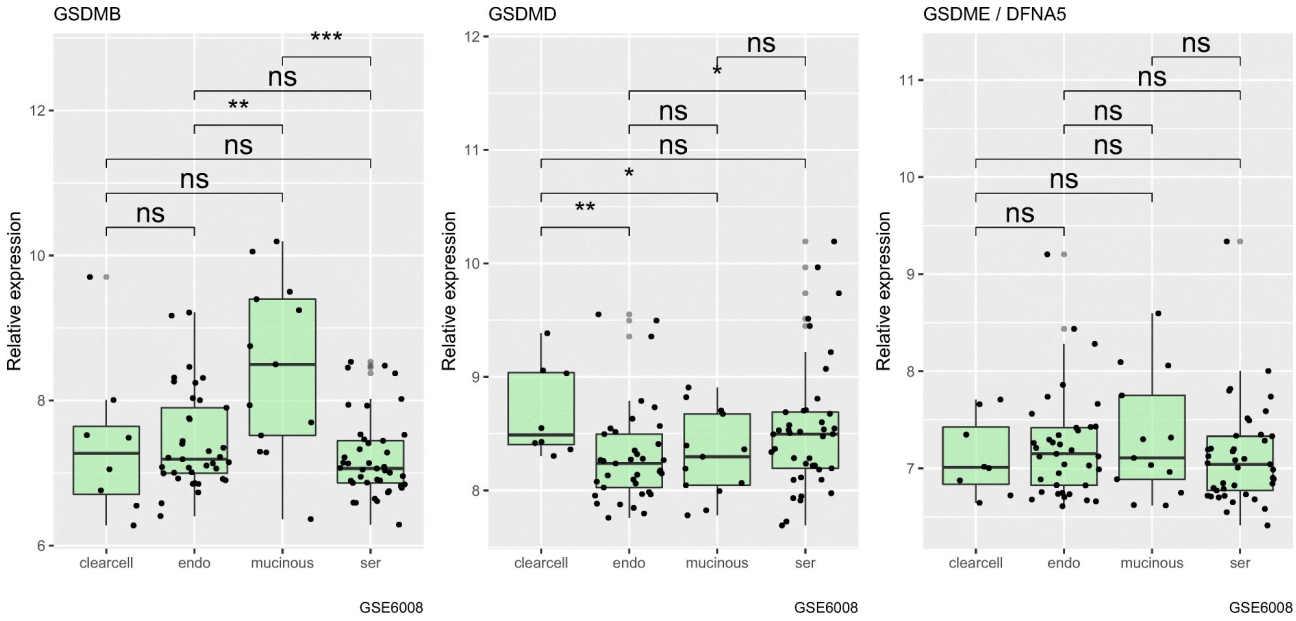

Figure 3.9. GSDMB and GSDMD expressions are different among various histotypes of epithelial ovarian cancer. Non-significant (ns): $p > 0.05$; *: $p \leq 0.05$; **: $p \leq 0.01$; ***: $p \leq 0.001$;****: $p \leq 0.0001$. OC: ovarian cancer; endo: endometrioid; ser: serous; DFNA5: Deafness, Autosomal Dominant 5. GSE6008 (n = 103). In the boxplots, the bottom and top sides of the box represent the lower and upper quartiles. The box covers the interquartile interval, where half of the data is found (i.e. half of the data points are inside the box area). The vertical line that split the box in two is the median value of all the data points (here, the gene expression values).

3.4 Copy Number Gains Are Highly Frequent in Genes Encoding GSDMC and GSDMD in Ovarian Cancer

Furthermore, we analyzed copy number variation (CNV) events (gains and losses) in genes encoding gasdermins in ovarian cancer (OV) using The Cancer Genome Atlas (TCGA)-Ovarian carcinoma dataset. We found that the percentage (%) of copy number gain events for GSDMC and GSDMD are around 54% and 48% in ovarian cancer patients, respectively, and the highest in ovarian cancer among other cancer types (Figure 3.10). In other words, approximately half of the women with ovarian cancer have GSDMC or GSDMD copy number gains. The total percentage of CNV events (both gain and loss) in genes encoding GSDMC, GSDMD, GSDME (DFNA5) and PJVK (DFNB59) is the highest in ovarian cancer among other cancer types in TCGA dataset, possibly highlighting the importance of these gasdermin members in ovarian cancer relative to other cancer types (Figure 3.10). Also, note that the percentage of CNV events and the order of top 5 cancers in which CNV events were more frequently observed are highly similar for GSDMA and GSDMB (Figure 3.10, first two panels). Here, please remember that these two genes also show similar changes in ovarian cancer in terms of expression. Based on this data showing that around 50% of ovarian cancer patients have copy number gains for GSDMC or GSDMD genes, we selected GSDMC and GSDMD for further *in vitro* study, as will be detailed in later sections. Above, we also found that expression of these two genes are increased in ovarian tumors compared to normal ovaries. Therefore, there might be some parallelity between higher percentage of copy number gain events and increased mRNA expression levels for these two genes in ovarian cancer.

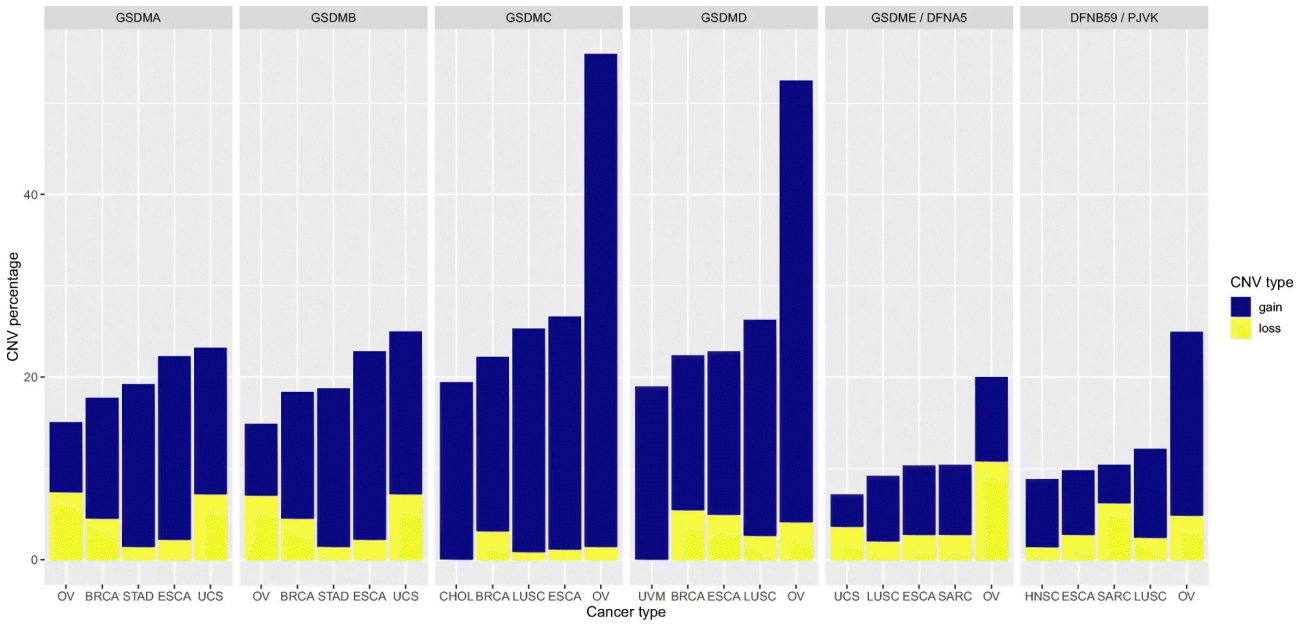

Figure 3.10. Copy number gains are highly frequent in genes encoding GSDMC and GSDMD in ovarian cancer. *CNV: copy number variation; gain: copy number gain; loss: copy number loss. OV: ovarian serous cystadenocarcinoma; BRCA: breast invasive carcinoma; STAD: stomach adenocarcinoma; ESCA: esophageal carcinoma; USC: uterine carcinosarcoma; CHOL: cholangio carcinoma; LUSC: lung squamous cell carcinoma; UVM: uveal melanoma; SARC: sarcoma; HNSC: head and neck squamous cell carcinoma.*

3.5 High Expression of GSDMD and GSDMC Is Associated with Shorter Progression-Free Survival (PFS) in TP53-Mutated Ovarian Cancer

We next asked if increased expression of GSDMD and GSDMC in serous ovarian cancer is associated with worse prognosis / shorter survival in these patients. We found that high expression of these two gasdermin family members, but not of others, is associated with decreased progression-free survival (PFS) in serous ovarian cancer patients with TP53 mutation (Figure 3.11), indicating that increased expression of either GSDMD and GSDMC observed in serous ovarian cancer might indeed contribute to higher mortality in patients with this disease, at least to a certain extent. Median progression-free survival for GSDMD low expression cohort is 20.47 months, whereas it is 15.77 months for high expression cohort. In a similar manner, median progression-free survival for GSDMC low expression cohort is 17.6 months, whereas it is 5.87 months for high expression cohort within patients with TP53-mutated serous ovarian cancer. Hazard ratio (HR) for GSDMD is

1.5 (logrank p = 0.00041), and for GSDMC, it is even higher (HR = 2.73, logrank p = 5.3e−06) (Figure 3.11, first two panels) (HRs of > 1 indicates worse prognosis for those genes).

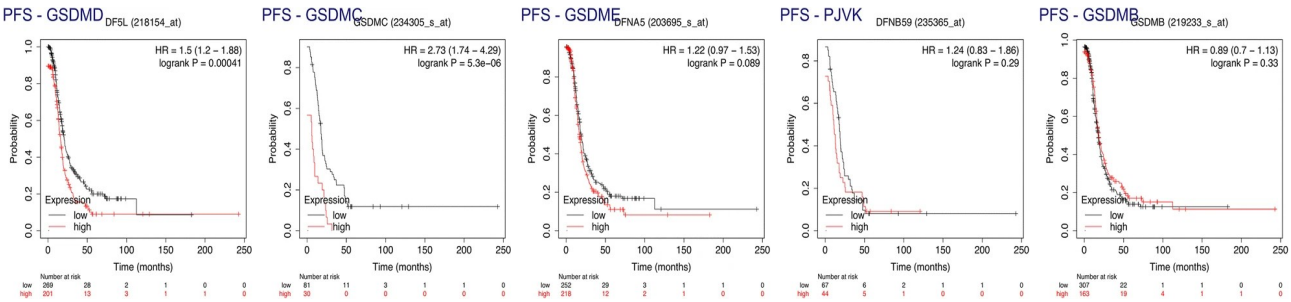

Figure 3.11. High expression of GSDMD and GSDMC is associated with shorter progression-free survival (PFS) in patients with TP53-mutated serous ovarian cancer. Kaplan-Meier (survival) plots showing the survival of TP53-mutated serous ovarian cancer patients with low (black lines) and high (red lines) expression of indicated gasdermin genes. *HR: hazard ratio. PFS: progression-free survival.*

3.6 Higher GSDMD and lower GSDME protein levels in ovarian tumors compared to surrounding/adjacent non-malignant stromal cells in the tumor microenvironment

Above, we showed that GSDMD is upregulated and GSDME is downregulated in ovarian cancer compared to normal ovaries, at the mRNA level (Berkel and Cacan, 2021). Using a publicly available proteomics dataset, we found that, similar to our findings at the mRNA level, GSDMD expression increases and GSDME expression decreases in ovarian tumors compared to surrounding normal / non-malignant stromal cells at the protein level (Figure 3.12). We did not observe any significant change in the protein levels of GSDMA between ovarian tumors and adjacent normal stromal cells in tumor microenvironment. This is in parallel to our previous observation that GSDMA mRNA levels do not change between ovarian tumors obtained from patients and healthy ovaries (Berkel and Cacan, 2021). Also note that, in addition to what was observed in ovaries, GSDME protein levels are lower in tumor cells relative to adjacent non-malignant stromal cells present in the omentum of HGSOC patients (Figure 3.12, middle plot).

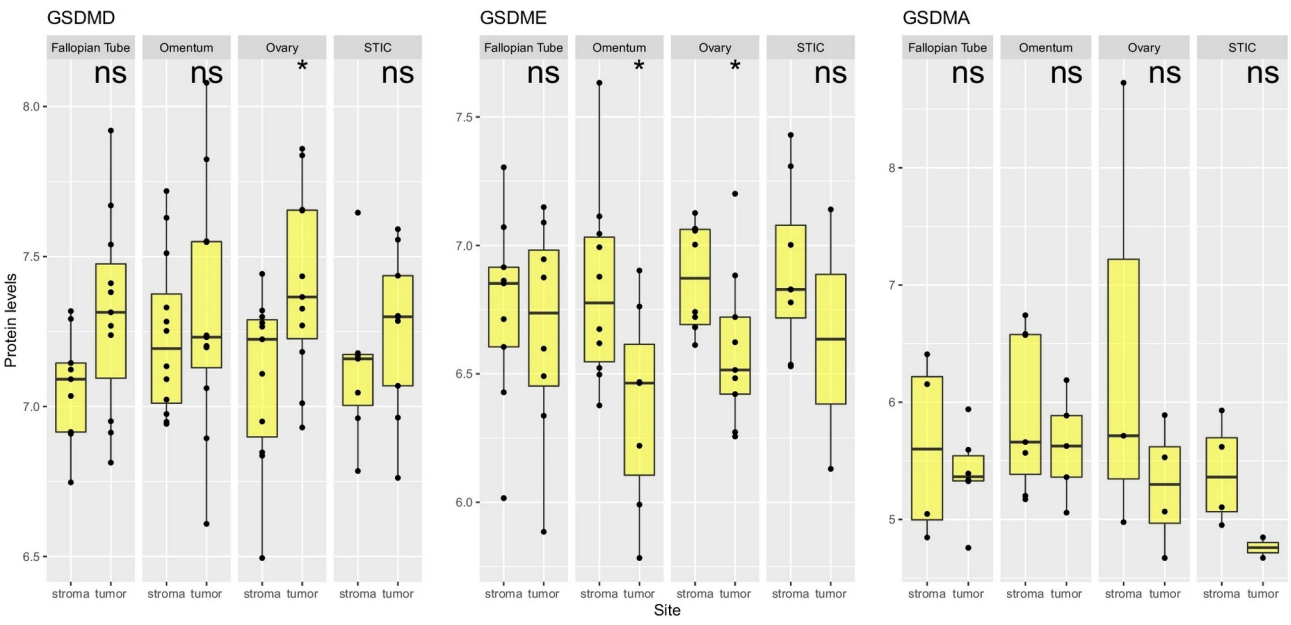

Figure 3.12. Higher GSDMD and lower GSDME protein levels in ovarian tumors compared to surrounding non-malignant stroma in ovarian cancer patients. Comparative protein levels of GSDMD (n = 94), GSDME (n = 73), and GSDMA (n = 46) in tumor and adjacent normal (non-malignant) stromal cells in four different anatomical locations in patients with high-grade serous ovarian cancer (HGSOC). Proteomics data is accessed from MaxQB — the MaxQuant DataBase of Max-Planck-Institut für Biochemie (http://maxqb.biochem.mpg.de/mxdb/project/show/9373012627500). Data for the other three members of the gasdermin family (GSDMB, GSDMC, and PJVK) is not available in this proteomic dataset. non-significant (ns): $p > 0.05$, *$p \leq 0.05$, **$p \leq 0.01$, ***$p \leq 0.001$, ****$p \leq 0.0001$. *STIC: serous tubal in situ carcinoma.* In the boxplots, the bottom and top sides of the box represent the lower and upper quartiles. The box covers the interquartile interval, where half of the data is found (i.e. half of the data points are inside the box area). The vertical line that split the box in two is the median value of all the data points (here, the gene expression values).

Data for the other three members of the gasdermin family (namely, GSDMB, GSDMC, and PJVK) is not available in this proteomics dataset; therefore, they could not be analyzed in this study. Further research is needed to determine how the expression of other gasdermins change at the protein level in ovarian tumors cells vs non-malignant stromal cells adjacent to ovarian tumor cells, in patients with ovarian cancer.

3.7 NINJ1 Expression Decreases from Early Stage to Late Stage in Serous Ovarian Cancer

A recent study showed that pores formed by gasdermins in the plasma membrane are not sufficient for the complete membrane rupture in pyroptosis, and NINJ1 mediates the final cataclysmic event in lytic cell death mechanisms including pyroptosis and apoptosis (Kayagaki et al., 2021; Wang and Shao, 2021). Authors of the mentioned study reported that cells lacking NINJ1 are unable to release various intracellular proteins with larger sizes such as LDH (lactate dehydrogenase; a standard measure of plasma membrane rupture) and HMGB1 (High mobility group box 1; a known damage-associated molecular pattern (DAMP)); however, they are able to release smaller molecules such as IL-18 and IL-1B through gasdermin pores (Kayagaki et al., 2021). They concluded that NINJ1is essential for pyroptosis-related plasma membrane rupture (Kayagaki et al., 2021).

Above, we showed that NINJ1 mRNA levels are higher in serous ovarian cancer compared to normal ovaries (Berkel and Cacan, 2021) ($p \leq 0.05$). This time, we analyzed changes in NINJ1 expression during cancer progression from early stage to late stage in patients with serous ovarian cancer, using patient transcriptome data from TCGA-OV project. We observed that NINJ1 expression is lower in late stage compared to early stage in serous ovarian cancer at the mRNA level ($p = 0.027$, sample size (n) = 578) (Figure 3.13A). Since cancer stage describes the size of a tumor and how far it has spread from its primary site, decreased NINJ1 levels might be contributing, at least to a certain extent, to increased tumor cell proliferation (i.e. size) and higher metastatic potential (i.e. spread) in serous ovarian cancer.

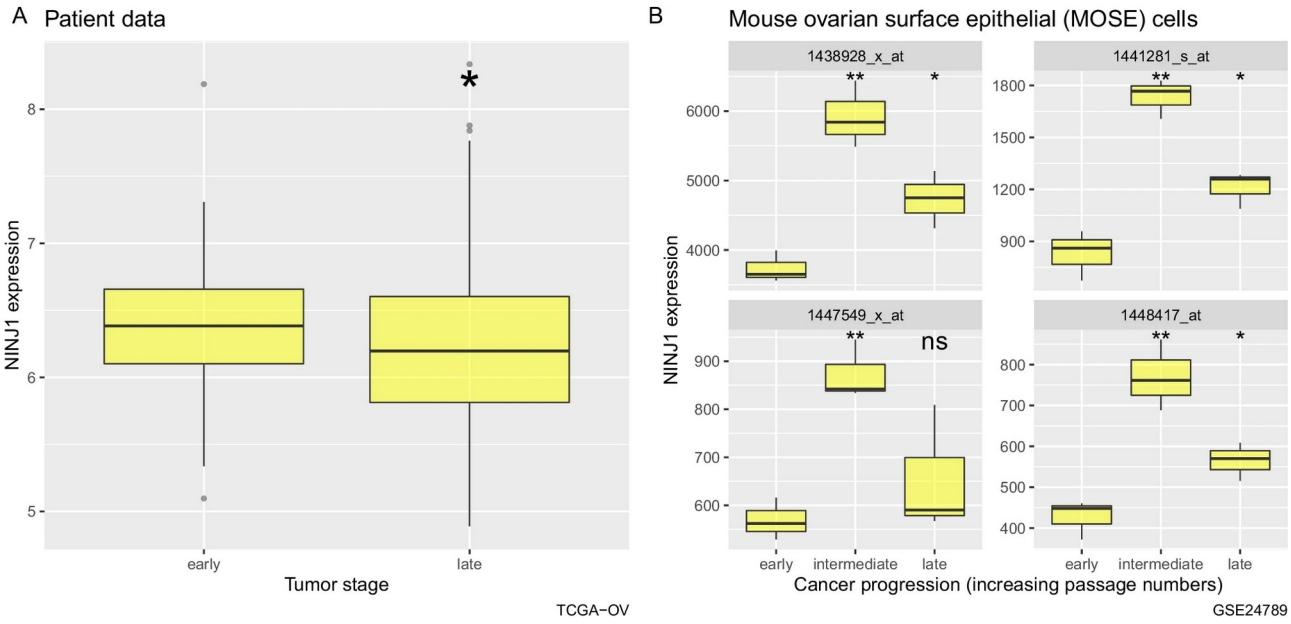

Figure 3.13. NINJ1 (Ninjurin 1) expression decreases from early to late stage in serous ovarian cancer. **A.** NINJ1 expression is lower in late stage serous ovarian cancer compared to early stage, at the mRNA level (n = 578: early stage (n = 43), late stage (n = 520), low grade (n = 75), and high grade (n = 480)). Data is obtained from TCGA-OV dataset and curatedOvarianData Bioconductor package. **B.** Differential NINJ1 mRNA levels between mouse ovarian surface epithelial (MOSE) cells at different stages of malignancy, as these cells transition from a pre-neoplastic to a malignant state (early cells: pre-neoplastic, non-malignant stage; intermediate cells: neoplastic, pre-invasive state; late cells: a malignant, invasive stage). Data is accessed from GSE24789 (n = 36). Panel titles represent different probes for NINJ1. non-significant (ns): $p > 0.05$, *$p \leq 0.05$, **$p \leq 0.01$, ***$p \leq 0.001$, ****$p \leq 0.0001$.

We also compared NINJ1 levels between mouse ovarian surface epithelial (MOSE) cells at different stages of malignancy, as these cells transition from a pre-neoplastic to a malignant state (early cells: pre-neoplastic, non-malignant stage; intermediate cells: neoplastic, pre-invasive state; late cells: a malignant, invasive stage). We found that NINJ1 expression at the mRNA level first increases from pre-neoplastic to neoplastic state (i.e. from early to intermediate cells), but then it decreases from neoplastic state to malignant and invasive state (i.e. from intermediate to late cells) (Figure 3.13B; each subplot shows data obtained using a different probe for NINJ1 whose IDs were indicated at the top of each subplot). This *in vitro* data is in line with our previous observation showing that NINJ1 levels are increased in ovarian cancer compared to normal ovaries (Berkel and Cacan, 2021), and also with data presented in Figure 3.13A showing that NINJ1 levels are decreased from early to late stage in ovarian cancer. In other words, NINJ1 mRNA levels seem to first increase during cancer development / initiation and then decrease during cancer progression (for instance, from early to late stage), pointing to possibility of highly dynamic regulation of its expression at the mRNA level during cancer initiation and progression. Changes in NINJ1 protein levels in the course of ovarian cancer initiation and progression should also be studied in detail to better understand the potential dynamic regulation of NINJ1 in ovarian cancer pathogenesis.

Furthermore, we showed that the correlation between GSDMD and NINJ1 expression at the mRNA level in ovarian tumors (R = 0.3; first subplot) is higher than that in healthy ovaries (R = 0.11; second subplot), although it is highly low at both contexts (Figure 3.14, top row). We also reported that these two proteins have not been found to interact based on currently available data in two independent protein–protein interaction databases, namely, BioGRID and STRING databases (Figure 3.14, bottom row).

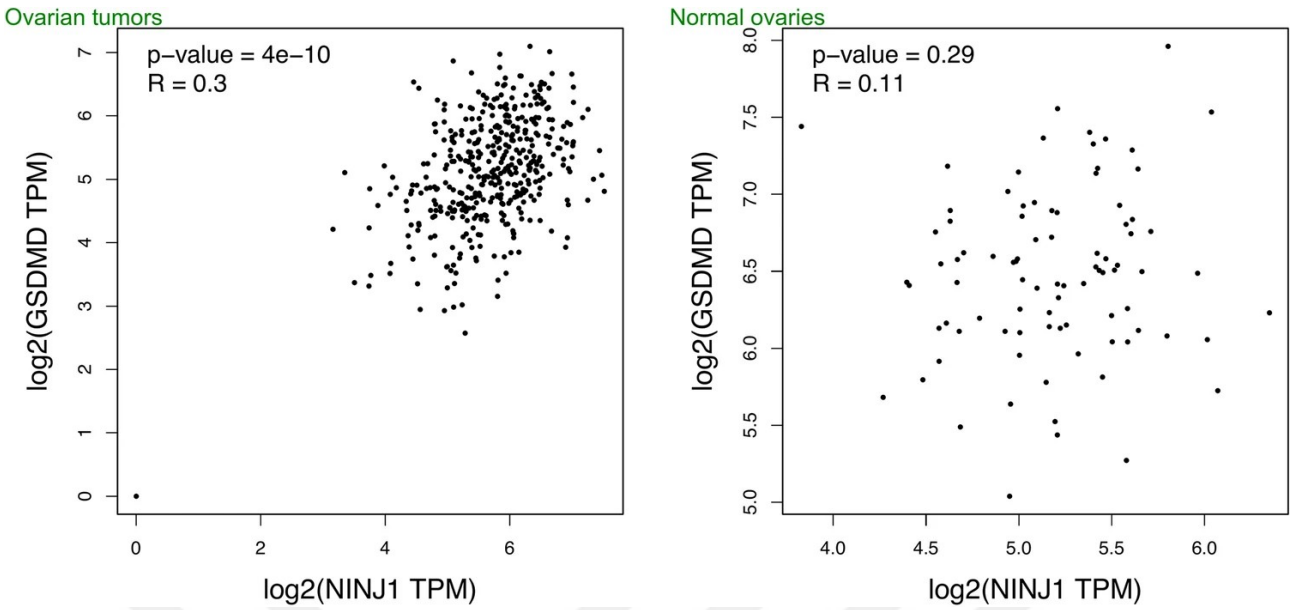

Figure 3.14. Top row: Correlation between GSDMD and NINJ1 expression in ovarian tumors and healthy ovaries. Correlation between GSDMD and NINJ1 expression at log2 scale in ovarian tumors (first subplot) and healthy ovaries (second subplot). The non-log scale was used for calculation and the log-scale axis was used for visualization. R: Pearson correlation coefficient, TPM: transcripts per million. Data from TCGA-OV and GTEx. **Bottom row:** Protein-protein interaction partners of NINJ1.

3.8 The Percentage of NINJ1 Copy Number Loss Events is the Highest in Ovarian Cancer among Other Cancers

Besides, we found that the percentage of NINJ1 copy number loss events (8.717%) is the highest in patients with ovarian cancer (OV) compared to those with other cancer types (Figure 3.15A). Surprisingly, the percentage of copy number gain events in NINJ1 gene in ovarian cancer (5.128%; third from top) is also among the highest within patients with cancer (Figure 3.15B). The percentage of NINJ1 copy number gain events is the highest in patients with SARC (sarcoma) followed by patients with ESCA (esophageal carcinoma) (Figure 3.15B). The fact that the percentage of both copy number losses and gains is high in ovarian cancer patients compared to patients with other cancers can possibly be explained by our two previous observations. We suggest that NINJ1 copy number increases might be responsible for the development / initiation of ovarian cancer in some patients; however, NINJ1 copy number losses might be responsible for the

progression of ovarian cancer in others. If this is the case, how NINJ1 might contribute to tumor initiation and how it might negatively regulate tumor progression in ovarian cancer is currently unknown and further research is needed.

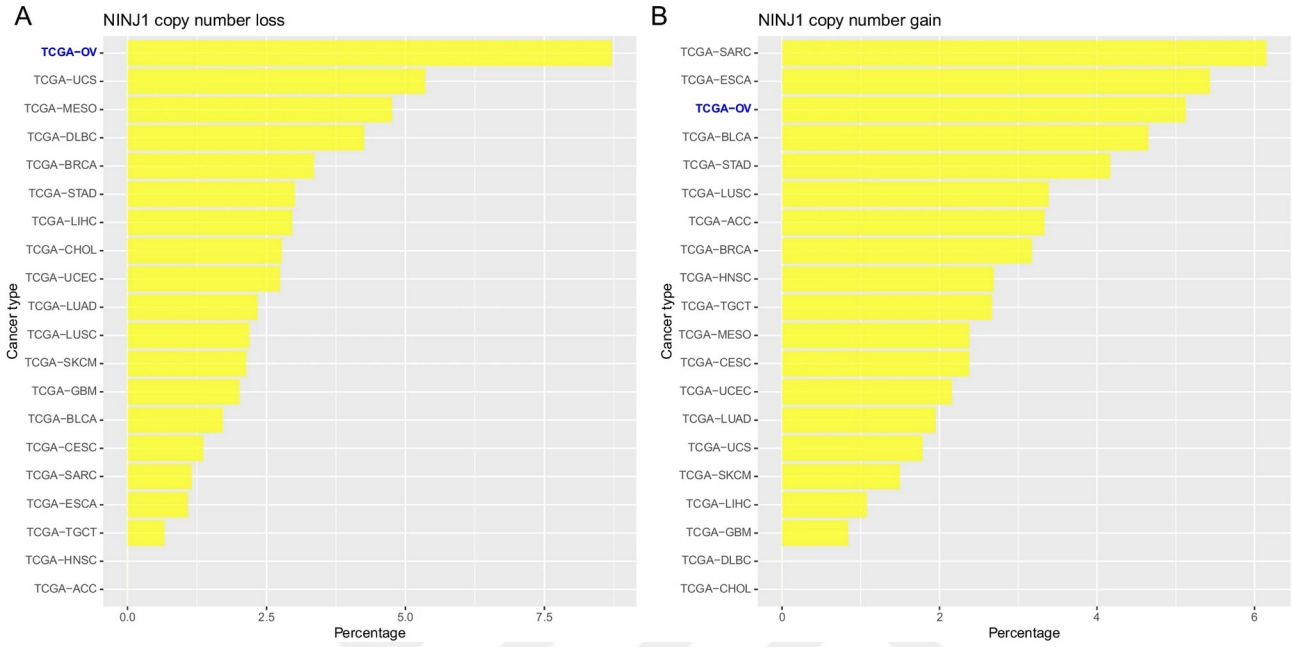

Figure 3.15. The percentage of NINJ1 copy number loss events is the highest in ovarian cancer among other cancers. Copy number variation (CNV) data for ovarian cancer patients was accessed from National Cancer Institute Genomic Data Commons Data Portal (https://portal.gdc.cancer.gov/) (Grossman et al., 2016; Huang et al., 2018; Berger et al., 2018). Cancer types were ordered based on the percentage of copy number gains (A) or losses (B) in NINJ1 gene from the highest to the lowest. ACC: adrenocortical carcinoma; BLCA: bladder urothelial carcinoma; BRCA: breast invasive carcinoma; CESC: cervical squamous cell carcinoma and endocervical adenocarcinoma; CHOL: cholangiocarcinoma; ESCA: esophageal carcinoma; GBM: glioblastoma multiforme; HNSC: head and neck squamous cell carcinoma; LIHC: liver hepatocellular carcinoma; LUAD: lung adenocarcinoma; LUSC: lung squamous cell carcinoma; DLBC: lymphoid neoplasm diffuse large B cell lymphoma; MESO: mesothelioma; OV: ovarian serous cystadenocarcinoma; SARC: sarcoma; SKCM: skin cutaneous melanoma; STAD: stomach adenocarcinoma; TGCT: testicular germ cell tumors; UCS: uterine carcinosarcoma; UCEC: uterine corpus endometrial carcinoma.

3.9 High Expression of NINJ1 is Associated with Better Overall Survival in Patients with Ovarian Cancer

Next, we compared overall survival (OS) of ovarian cancer patients with low or high expression of NINJ1. We found that high expression of NINJ1 is associated with better overall survival in ovarian cancer patients (all histotypes combined; Figure 3.16, first panel; logrank $p = 4e-06$, hazard ratio (HR) = 0.71) and in serous ovarian cancer patients (Figure 3.16, second panel; logrank $p = 0.0024$, HR = 0.78). In ovarian cancer patients (all histotypes combined), median overall survival of NINJ1 low expression cohort was 33.77 months, compared to 48 months in NINJ1 high-expression cohort (difference of 11.23 months) (Figure 3.16, third panel). Specifically in patients with serous histological type of ovarian cancer, median overall survival of NINJ1 low-expression cohort was 38.4 months, compared to 45.77 months in NINJ1 high-expression cohort (difference of 7.37 months) (Figure 3.16, third panel).

Furthermore, we analyzed the association of NINJ1 expression with overall survival in patients with ovarian cancer, after adjusting for the success of debulking surgery (debulking status defined as residual tumor smaller than 1 cm following cytoreduction surgery) and The International Federation of Gynecology and Obstetrics (FIGO) stage (FIGO staging is based on clinical staging, careful clinical examination before any definitive therapy has begun, with the exception of ovary, which includes surgical exploration), using 15 independent datasets with applicable expression and survival information, including TCGA data. The forest plot in Figure 3.16 (last panel) shows that overall hazard ratio (HR) for NINJ1 is significantly lower than 1 (0.87, $p = 4.885028e-07$). This indicates that ovarian cancer patients with high NINJ1 levels have better outcome / prognosis. Therefore, this analysis indicates that NINJ1 expression can be considered a prognostic of overall survival in patients with ovarian cancer (Figure 3.16).

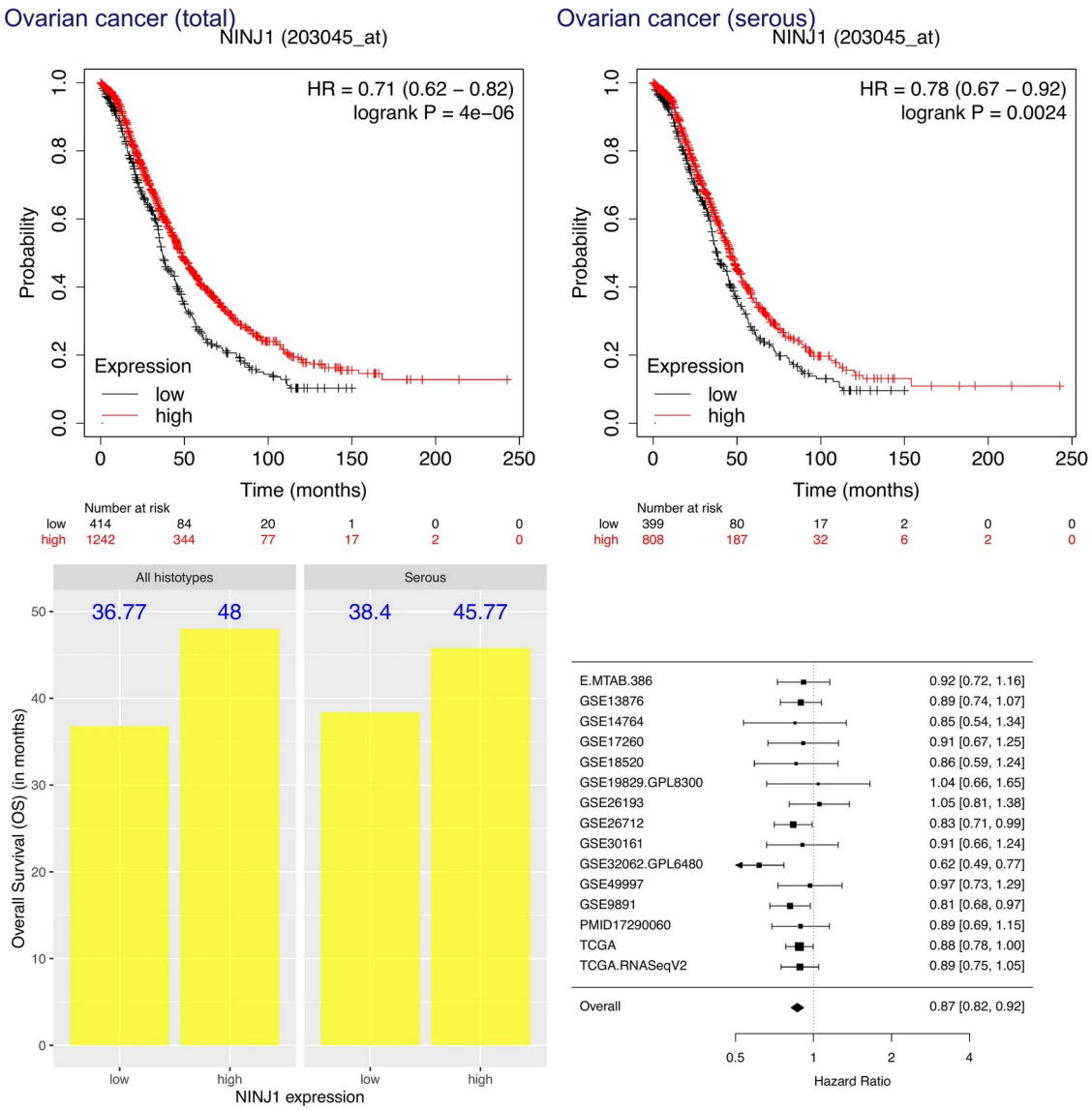

Figure 3.16. High expression of NINJ1 is associated with better overall survival in patients with ovarian cancer. Overall survival (OS) of ovarian cancer patients with low (black lines) or high (red lines) expression of NINJ1. First plot shows data for patients with all histological types (histotypes) of ovarian cancer, and second plots shows data only for patients with serous histotype of ovarian cancer. Third plot shows median overall survival of the indicated cohorts in months. First two plots were drawn using Kaplan–Meier Plotter tool (n = 1656) (http://kmplot.com/analysis/index.php?p=service&cancer=ovar). We did not restrict the analysis to disease subtypes and treatment groups, and used the default parameters in the tool. Last panel: A forest plot showing the association of NINJ1 expression with overall survival in patients with ovarian cancer after adjusting for the success of debulking surgery (debulking status defined as residual tumor smaller than 1 cm following cytoreduction surgery) and Federation of Gynecology and Obstetrics (FIGO) stage, using datasets with applicable expression and survival information (the names of the datasets were given in the left). *HR: hazard ratio.*

Since we observed that NINJ1 expression is lower in late stage compared early stage serous ovarian cancer (Figure 3.13), and that low NINJ1 expression is associated with worse survival in this patient group, we can speculate that low NINJ1 expression might contribute, at least to a certain extent, to shorter survival of patients with late stage ovarian cancer. Mechanistic studies are required to confirm these observations.

Similar to that observed in ovarian cancer patients, we found that lower expression of NINJ1 is also associated with poor prognosis in breast cancer, another cold tumor in women that is unlikely to trigger a strong immune response (Figure 3.17).

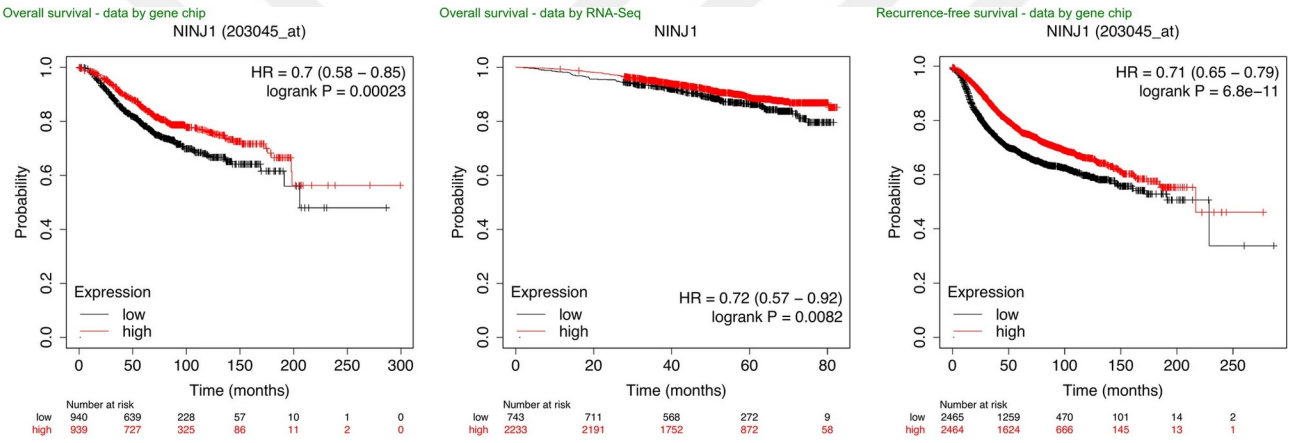

Figure 3.17. Lower expression of NINJ1 is associated with worse prognosis in breast cancer, another cold tumor in women. Kaplan–Meier plots showing the overall (first two subplots) and recurrence-free survival (last subplot) of breast cancer patients with low (shown in black) or high expression (shown in red) of NINJ1 (Nagy et al., 2021; Gyorffy et al., 2012). *HR: hazard ratio.*

3.10 NINJ1 mRNA Expression is Lower in Cisplatin-resistant Cells Compared to Cisplatin-Sensitive Ovarian Cancer Cells *in vitro*

Since we observed that NINJ1 mRNA levels are lower in late stage compared to early stage ovarian cancer, and that low NINJ1 expression is associated with shorter overall survival / worse prognosis of ovarian cancer patients, we wanted to see if lower NINJ1 expression is also associated with other parameters which contribute to worse prognosis in ovarian cancer, such as drug resistance. We

found that cisplatin-resistant A2780 ovarian cancer cells have decreased NINJ1 expression compared to cisplatin-sensitive A2780 cells (Figure 3.18; $p = 0.03$, $n = 10$). Thus, it can be inferred from this data that decreased NINJ1 expression might also contribute to resistance to chemotherapeutics such as cisplatin, a drug whose alternatives are used in the treatment of ovarian cancer; however, further *in vivo* studies are required. Lower survival rates observed in patients with low NINJ1 expression (thus increased resistance) might also be explained, at least in part, by their decreased response to drugs such cisplatin which is used in the standard treatment of ovarian cancer patients. However, further *in vivo* studies in animal models and clinical samples will be of high importance to confirm this *in vitro* observation.

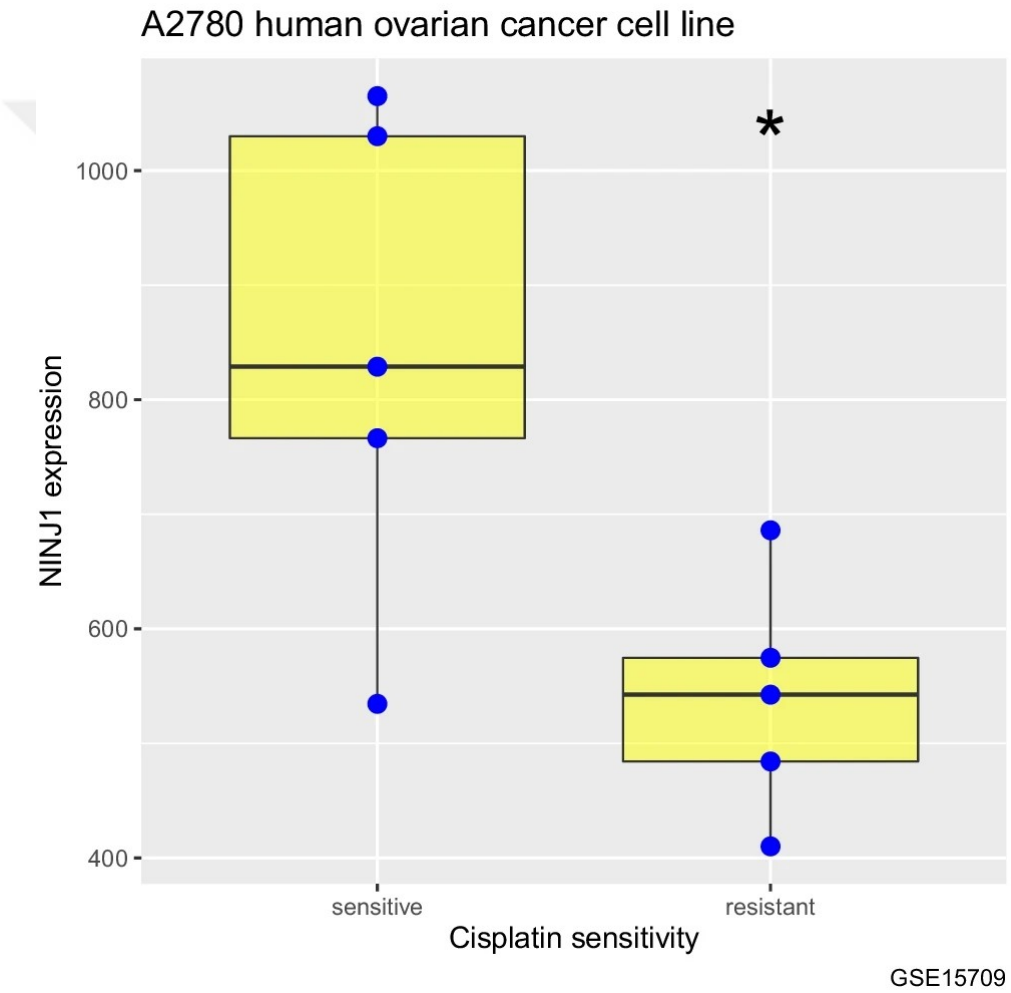

Figure 3.18. NINJ1 expression is lower in cisplatin-resistant cells compared to cisplatin-sensitive A2780 ovarian cancer cells *in vitro*. Data is obtained from Gene Expression Omnibus with the accession number GSE15709 ($n = 10$). non-significant (ns): $p > 0.05$, *$p \leq 0.05$, **$p \leq 0.01$, ***$p \leq 0.001$, ****$p \leq 0.0001$.

3.11 NINJ1 Expression is Positively Correlated with Immune Infiltration by Macrophages and Monocytes in Ovarian Cancer

Subsequently, we reported that NINJ1 mRNA levels are mostly positively correlated with the infiltration of ovarian tumors by macrophages and monocytes, using TIMER2.0 tool (Spearman's $p > 0$, $p < 0.05$) (Figure 3.19). This data points that lower expression of NINJ1 in advanced ovarian cancer might lead to decreased immune infiltration and thus might result in worse outcome due to lower anti-tumor immunity. In other words, NINJ1 might affect the immunogenicity of ovarian cancer, influencing survival rates in patients with this cold tumor. Also note that NINJ1 expression is positively correlated with the infiltration of tumors by these two immune cell types in most other cancer types, potentially showing that NINJ1 might have broader implications in cancer. Mechanistically, proinflammatory molecules such as LDH and HMGB1 released due to plasma membrane rupture mediated by NINJ1 might promote the infiltration of certain immune cells such as macrophages which are able to phagocytose dead cells, possibly leading to a decrease in tumor size; thus, high NINJ1 expression might contribute to better prognosis in ovarian cancer patients. In brief, this hypothetical cascade might be speculated to be active in the context of ovarian cancer: high NINJ1 levels → higher plasma membrane rupture events -> increased release of proinflammatory molecules → increased infiltration of immune cells to tumor site → efficient removal of dead cells by macrophages / phagocytes (efferocytosis?) → decrease in tumor size → better prognosis / survival of ovarian cancer patients with high NINJ1 levels. Mechanistic studies both in vitro and in vivo are required to test these hypothetical scenarios.

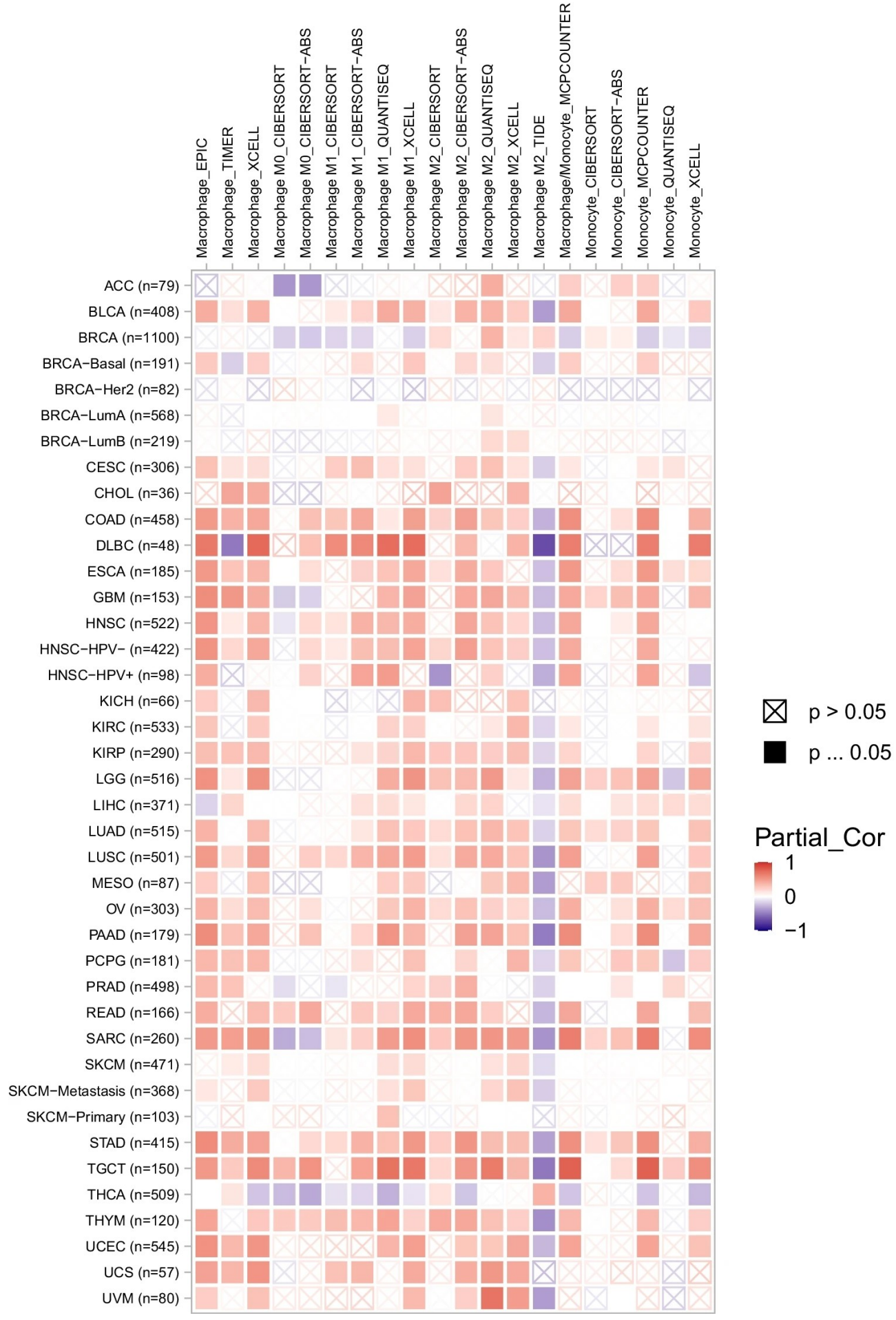
Macrophage_EPIC
Macrophage_TIMER
Macrophage_XCELL
Macrophage M0_CIBERSORT
Macrophage M0_CIBERSORT−ABS
Macrophage M1_CIBERSORT
Macrophage M1_CIBERSORT−ABS
Macrophage M1_QUANTISEQ
Macrophage M1_XCELL
Macrophage M2_CIBERSORT
Macrophage M2_CIBERSORT−ABS
Macrophage M2_QUANTISEQ
Macrophage M2_XCELL
Macrophage M2_TIDE
Macrophage/Monocyte_MCPCOUNTER
Monocyte_CIBERSORT
Monocyte_CIBERSORT−ABS
Monocyte_MCPCOUNTER
Monocyte_QUANTISEQ
Monocyte_XCELL
ACC (n=79)
BLCA (n=408)
BRCA (n=1100)
BRCA−Basal (n=191)
BRCA−Her2 (n=82)
BRCA−LumA (n=568)
BRCA−LumB (n=219)
CESC (n=306)
CHOL (n=36)
COAD (n=458)
DLBC (n=48)
ESCA (n=185)
GBM (n=153)
HNSC (n=522)
HNSC−HPV− (n=422)
HNSC−HPV+ (n=98)
KICH (n=66)
KIRC (n=533)
KIRP (n=290)
LGG (n=516)
LIHC (n=371)
LUAD (n=515)
LUSC (n=501)
MESO (n=87)
OV (n=303)
PAAD (n=179)
PCPG (n=181)
PRAD (n=498)
READ (n=166)
SARC (n=260)
SKCM (n=471)
SKCM−Metastasis (n=368)
SKCM−Primary (n=103)
STAD (n=415)
TGCT (n=150)
THCA (n=509)
THYM (n=120)
UCEC (n=545)
UCS (n=57)
UVM (n=80)
p > 0.05
p ... 0.05
Partial_Cor
1
0
−1

Figure 3.19. NINJ1 expression is positively correlated with immune infiltration by macrophages and monocytes in ovarian cancer (OV). NINJ1 mRNA levels are mostly positively correlated with the infiltration of ovarian tumors (OV) by macrophages and monocytes (Spearman's $p > 0$, $p < 0.05$). Analysis was performed using TIMER2.0 tool. The higher the redness, the more positive the correlation between NINJ1 expression and immune infiltration of tumors by macrophages or monocytes.

3.12 Estrogen Treatment Increases the Expression of GSDMC and GSDMD at the Transcript Level in Chemosensitive (A2780) but not in Chemoresistant (A2780-AD) Ovarian Cancer Cell Lines *in vitro*

We treated chemosensitive and chemoresistant ovarian cancer cell lines (A2780 and A2780-AD, respectively) with different concentrations of estrogen (E2, 32 and 128 nM) to see if it upregulates or downregulates the expression of GSDMC and GSDMD at the mRNA level by performing qRT-PCR. We performed these experiments since ovaries are the main source of estrogen in the body and they are also responsive to estrogen. We found that estrogen treatment at both concentrations increases both GSDMC and GSDMD expression in chemosensitive A2780 cell line (Figure 3.20, top row); but, not in chemoresistant A2780-AD cell line (Figure 3.20, bottom row). In A2780 cell line, estrogen treatment at a higher concentration (128 nM) increased GSDMC and GSDMD expression most significantly compared to estrogen treatment at a lower concentration (32 nM) (Figure 3.20, top row), pointing to the presence of a dose-dependent effect. We reported that estrogen treatment at these two concentrations does not change viability of both cell lines compared to untreated cells (Figure 3.21).

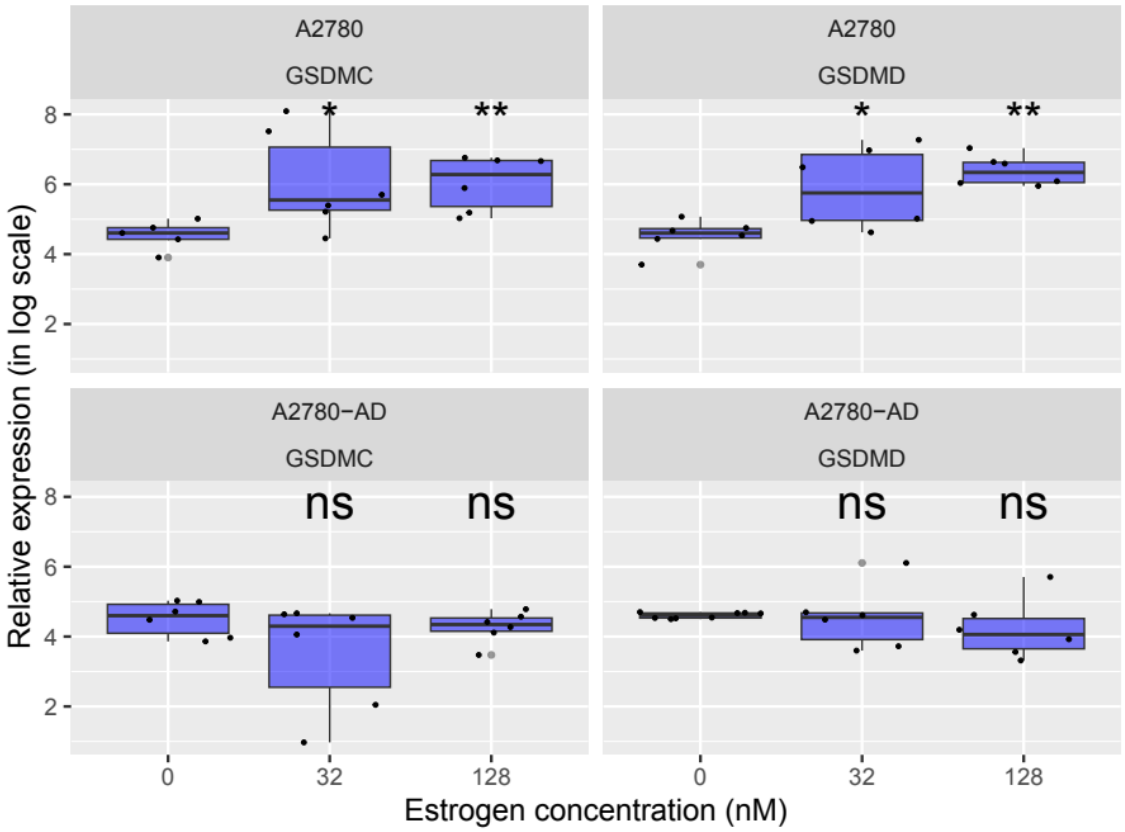

Figure 3.20. Estrogen treatment increases the expression of GSDMC and GSDMD in chemosensitive (A2780, top row) but not in chemoresistance (A2780-AD, bottom row) ovarian cancer cell lines *in vitro*.

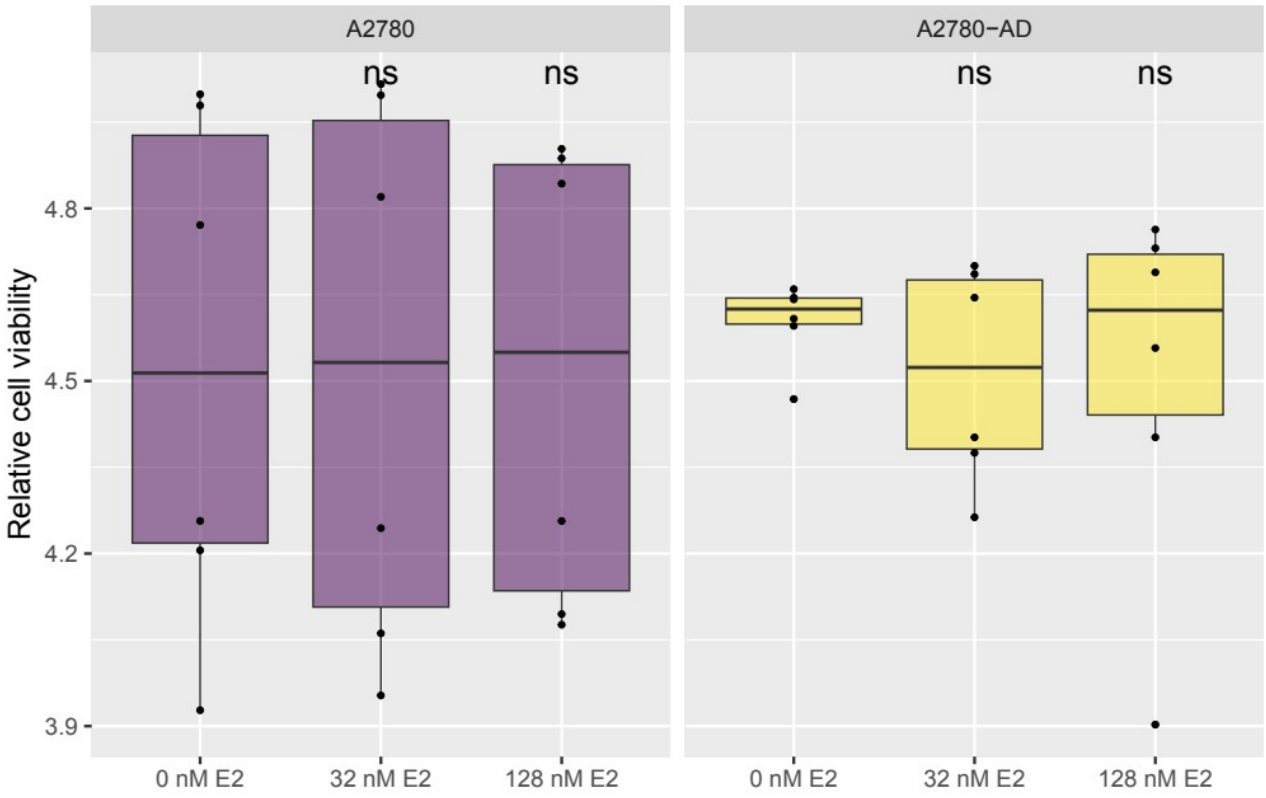

Figure 3.21. Estrogen treatment at both concentrations (32 and 128 nM) does not change viability of both ovarian cancer cell lines compared to untreated control cells.

3.13 Relative Viability of GSDMC- or GSDMD-overexpressing Ovarian Cancer Cell Lines in Response to Nigericin, a Pyroptosis Inducer, *in vitro*

Next, we overexpressed GSDMC and GSDMD genes in A2780 and A2780-AD ovarian cancer cell lines to see if it changes cell viability in response to treatment with nigericin, a potent microbial toxin that acts as a potassium ionophore and activator of NLRP3, which is used to induce pyroptosis. We first confirmed that transfection of both ovarian cancer cell lines with GSDMC or GSDMD overexpression plasmids leads to more than 10.000 fold increase in GSDMC and GSDMD gene expression as measured by qRT-PCR (Figure 3.22). We also performed Western Blot experiments to confirm overexpression experiments resulted in higher protein levels of both genes (data not shown). Interestingly, we found that GSDMC overexpression leads to a decrease in GSDMD mRNA levels in A2780 cell line, and to an increase in GSDMD mRNA levels in A2780-AD cell line (Figure 3.22). How GSDMC overexpression influences GSDMD expression and how

it does this differently in chemosensitive and chemoresistant ovarian cancer cell lines is currently unknown (Figure 3.22).

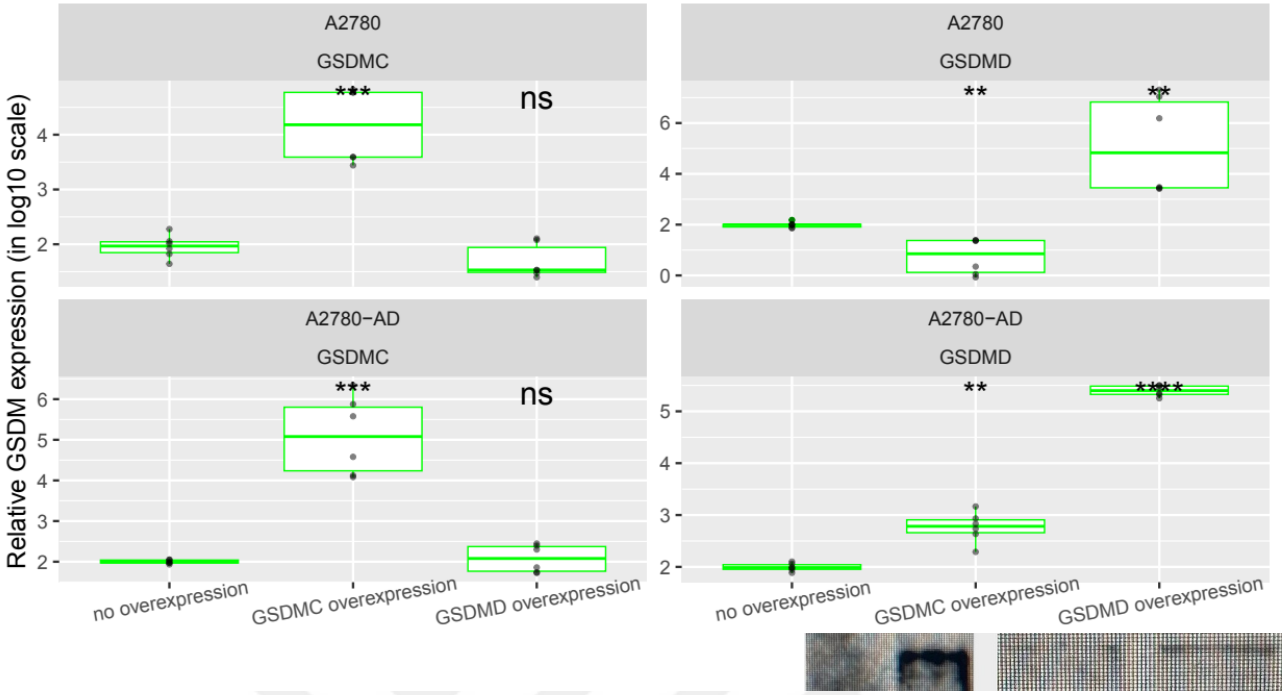

Figure 3.22. Transfection of both ovarian cancer cell lines (A2780 (top row) and A2780-AD (bottom row)) with GSDMC or GSDMD overexpression plasmids leads to more than 10.000 fold increase in GSDMC and GSDMD gene expression, respectively, as measured by qRT-PCR. WB images in order: no plasmid, GSDMD overexpression, no plasmid, GSMDC overexpression.

After confirming that overexpression experiments work in both ovarian cancer cell lines, we studied how overexpression of GSDMC or GSDMD influences cell viability in response to nigericin, a toxin which is used to induce pyroptosis experimentally. We found that upon GSDMC overexpression, the decrease in cell viability in nigericin-treated A2780-AD cells (compared to DMSO-treated control cells, shown as "none") reduced to a less significant level (from ** to *) compared to that in A2780-AD negative control cells (Figure 3.23, bottom row). This might be due to the possibility that GSDMC overexpressing cells might respond more efficiently to nigericin-induced inflammasome formation, limiting their death due to pyroptosis. This is also somehow parallel to our previous observation that ovarian tumors (which are often more resistant to cell death) have higher levels of GSDMC mRNA levels compared normal ovaries which are non-malignant. In other words, we can speculate that increased levels of GSDMC (both *in vitro* and *in vivo*) might enable ovarian cells to be more resistant to cell death upon certain stimuli, such as nigericin (a pyroptosis inducer). Please also note that we observed this GSDMC overexpression-

mediated resistance to nigericin-induced cell death only in chemoresistant ovarian cancer cell lines (A2780-AD), but not in chemosensitive ovarian cancer cell lines (A2780) (Figure 3.23). We also found that GSDMD overexpression does not lead to any resistance / sensitivity to nigericin-induced cell death (i.e. pyroptotic cell death) in both ovarian cancer cell lines *in vitro* (Figure 3.23). We also need to point that nigericin, unexpectedly, did not induce cell death (or decrease in cell viability) in A2780 cell lines in this experimental setup; however, this was not the case in other experimental setups (please see below figures).

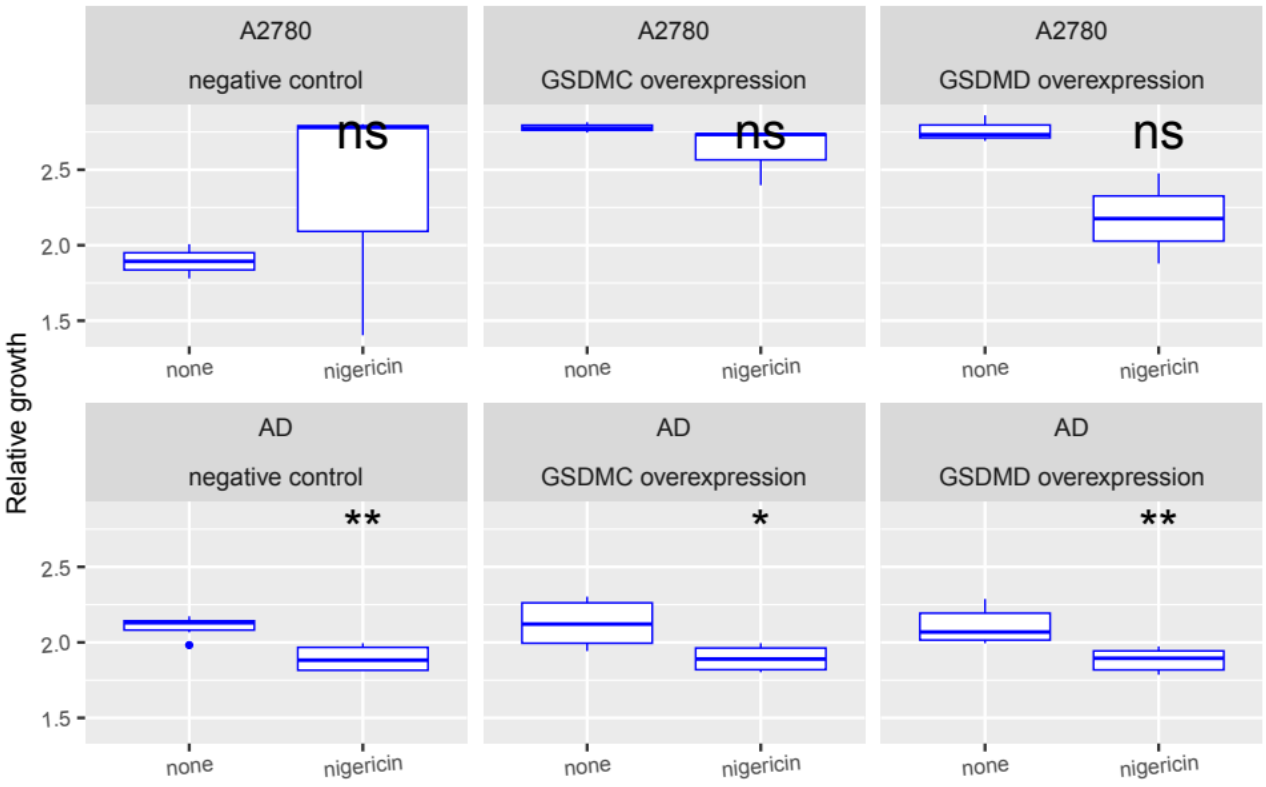

Figure 3.23. The influence of GSDMC or GSDMD overexpression on cell viability in response to nigericin, a pyroptosis inducer toxin, in chemosensitive (A2780, upper row) and chemoresistant (A2780-AD) ovarian cancer cell lines *in vitro*.

Moreover, we found that GSDMC or GSDMD overexpression increases cell viability in untreated (without nigericin treatment) A2780 cells (Figure 3.24). However, this was not the case for A2780 cells treated with nigericin or for the treated or untreated A2780-AD cells (Figure 3.24). This also show some parallelity to our previous data that ovarian cancer cells have increased expression of

GSDMC and GSDMD at the mRNA level. In other words, we provided data showing that overexpression of either GSDMC or GSDMD increases cell viability significantly in chemosensitive (A2780) ovarian cancer cell lines but not in chemoresistant (A2780-AD) ovarian cancer cell lines (Figure 3.24). Besides, this GSDMC or GSDMD overexpression-induced cell growth in A2780 cell line is lost when cells are treated with nigericin (i.e. in the case of induction of pyroptosis). Therefore, we can speculate that, at the absence of pyroptotic stimuli, both GSDMC and GSDMD promotes cell proliferation in certain groups of ovarian cancer cells (in our case, in those with chemosensitive profile) (Figure 3.24).

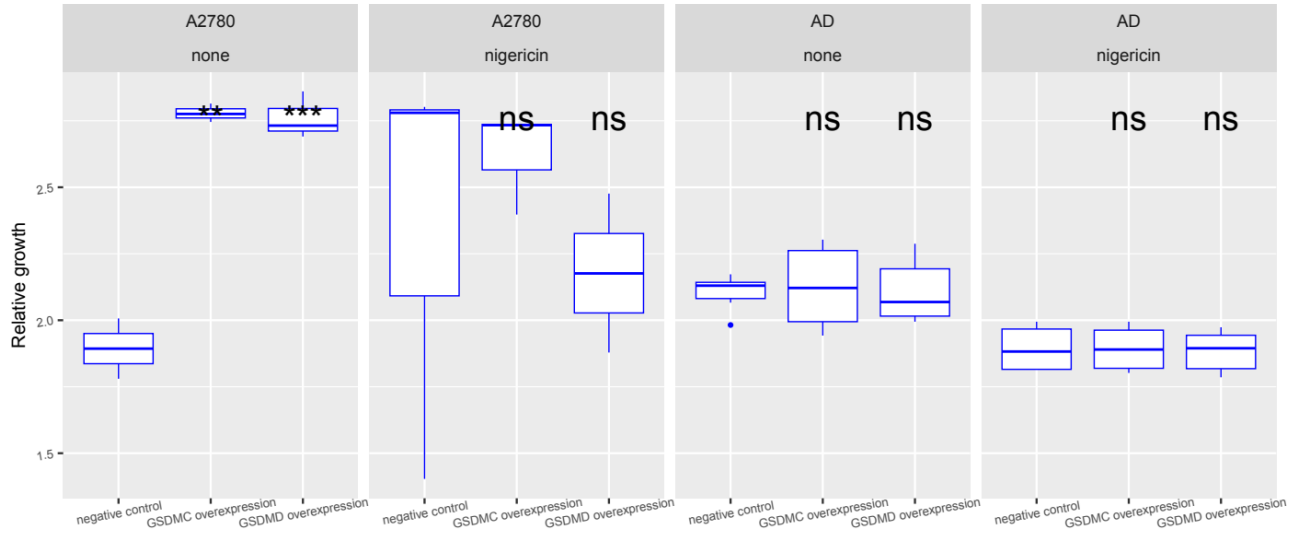

Figure 3.24. GSDMC or GSDMD overexpression increases cell viability in untreated chemosensitive A2780 ovarian cancer cells (first plot). This GSDMC or GSDMD overexpression-induced cell growth in A2780 cell line is lost when cells are treated with nigericin, a pyroptosis inducing bacterial toxin (second plot). GSDMC or GSDMD overexpression does not effect cell viability in untreated (third plot) or nigericin-treated (last plot) chemoresistant A2780-AD ovarian cancer cells.

3.14 GSDMD Silencing Decreases the Change in Cell Viability between Untreated and Nigericin-treated A2780 Cells

Later, we performed silencing experiments using siRNAs (small interfering RNAs) against GSDMC and GSDMD genes to see how the silencing of these gasdermin genes affects cell viability

in response to nigericin treatment. We found that when GSDMD gene is silenced in A2780 cells, the decrease in cell viability in response to nigericin is reduced to a less significant level compared to that in negative siRNA-transfected A2780 cells (Figure 3.25, top row, compared last and first panels). In other words, nigericin normally decreases cell viability significantly in A2780 cells by possibly promoting pyroptotic cell death; however, when GSDMD gene is silenced using specific siRNAs, the effect of nigericin on cell viability is decreased to a less significant level in A2780 cells. This might point that GSDMD might be an important mediator of cell death in response to nigericin in A2780 cells, since its inhibition leads to a decreased response to nigericin-induced decreases in cell viability (Figure 3.25, top row). Please note that silencing of GSDMD does not completely block nigericin-induced decrease in cell viability in A2780 cells, i.e its silencing itself is not sufficient to eliminate the effect of nigericin on cell death in these cells (Figure 3.25, top row).

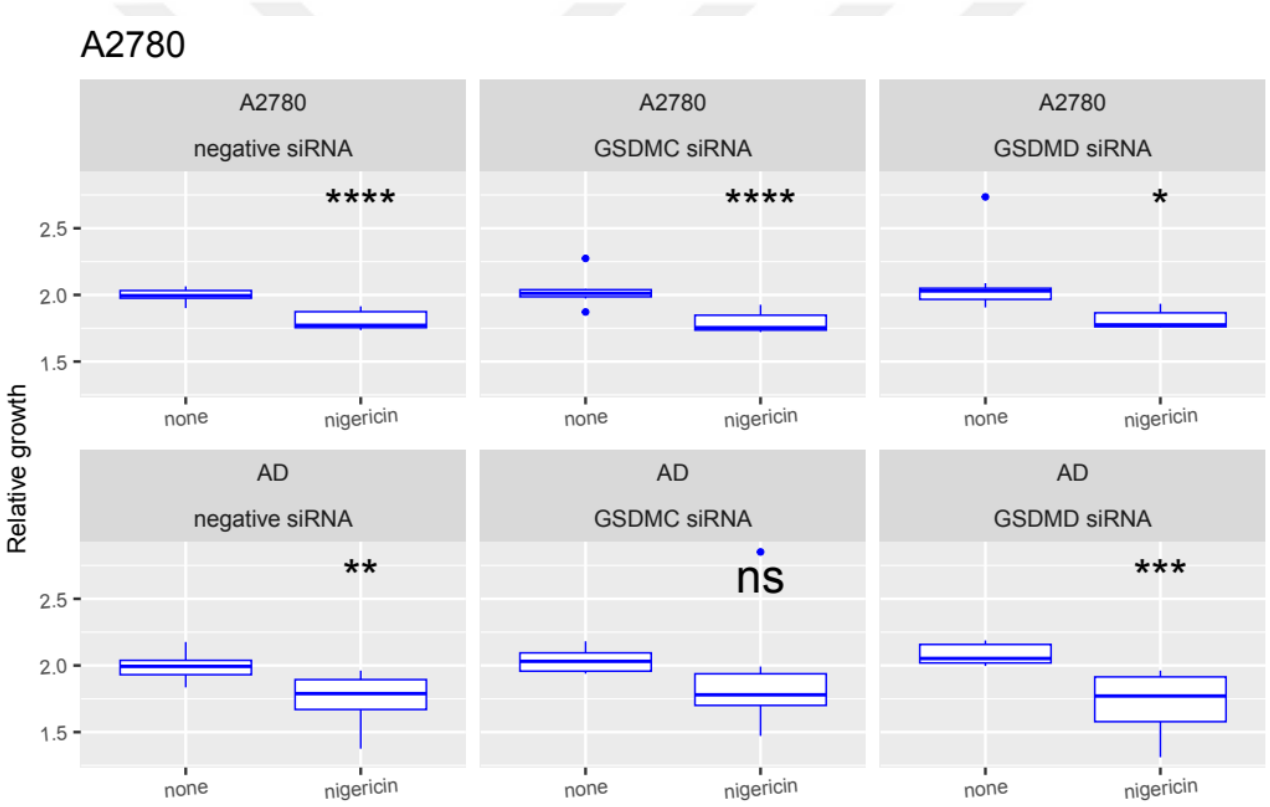

Figure 3.25. GSDMD silencing decreases the change in cell viability between untreated and nigericin-treated A2780 cells, and GSDMC silencing decreases the change in cell viability between untreated and nigericin-treated A2780-AD cells.

3.15 GSDMC Silencing Decreases the Change in Cell Viability between Untreated and Nigericin-treated A2780-AD Cells

Next, we found that when GSDMC gene is silenced in A2780-AD cells, the decrease in cell viability in response to nigericin is reduced to a non-significant (ns) level compared to that in negative siRNA-transfected A2780-AD cells (Figure 3.25, bottom row). In other words, nigericin normally decreases cell viability significantly in A2780-AD cells as expected, possibly by promoting pyroptotic cell death; however, when GSDMC gene is silenced using siRNAs targeted to GSDMC, the effect of nigericin on cell viability is lost in A2780-AD cells. In contrast, when GSDMD gene is silenced in this cell line, the decrease in cell viability in response to nigericin is increased (Figure 3.25, bottom row). We can speculate that inhibition of GSDMC alone is sufficient to block nigericin-induced cell death in chemoresistant A2780-AD ovarian cancer cells (Figure 3.25, bottom row).

3.16 The Effect of Specific Caspase Inhibitors on Cell Viability in Response to Nigericin in Chemosensitive and Chemoresistant Ovarian Cancer Cell Lines *in vitro*

To identify caspases responsible for pyroptosis in ovarian cancer cells, we used specific caspase inhibitors: caspase-1 inhibitor, caspase-4 inhibitor, caspase-6 inhibitor and caspase-8 inhibitor. In A2780 cell line, we found that inhibition of any these caspases results in the loss of nigericin-induced decreases in cell viability (Figure 3.26, top row). This might mean that inhibition of any these caspases is sufficient to block nigericin-induced cell death in these chemosensitive cells. In other words, we can speculate that all of these caspases might be participating in nigericin-induced cell death (i.e. pyroptotic cell death) to certain extents, since the inhibition of any of them results in the loss of nigericin-induced decreases in cell viability (Figure 3.26, top row). In contrast, the inhibition of only caspase-1, but not of any other caspases studied, led to a loss of nigericin-induced decreases in cell viability in chemoresistant A2780-AD cell line (Figure 3.26, bottom row). For caspases-4, -6 and -8, the inhibition of caspase activity did not result in the loss of nigericin-induced decreases in cell viability (Figure 3.26, bottom row). Therefore, we can state that caspases responsible for pyroptotic cell death in chemosensitive and chemoresistant ovarian cancer cells might be different or they might be functional at varying degrees between these ovarian cancer cells with different chemosensitivity profiles (Figure 3.26). Please also note that we used a single concentration for specific caspase inhibitors (see Materials and Methods); therefore, at different

concentrations, they might show different effects on pyroptotic cell death depending on the concentrations used or on even the incubation periods studied.

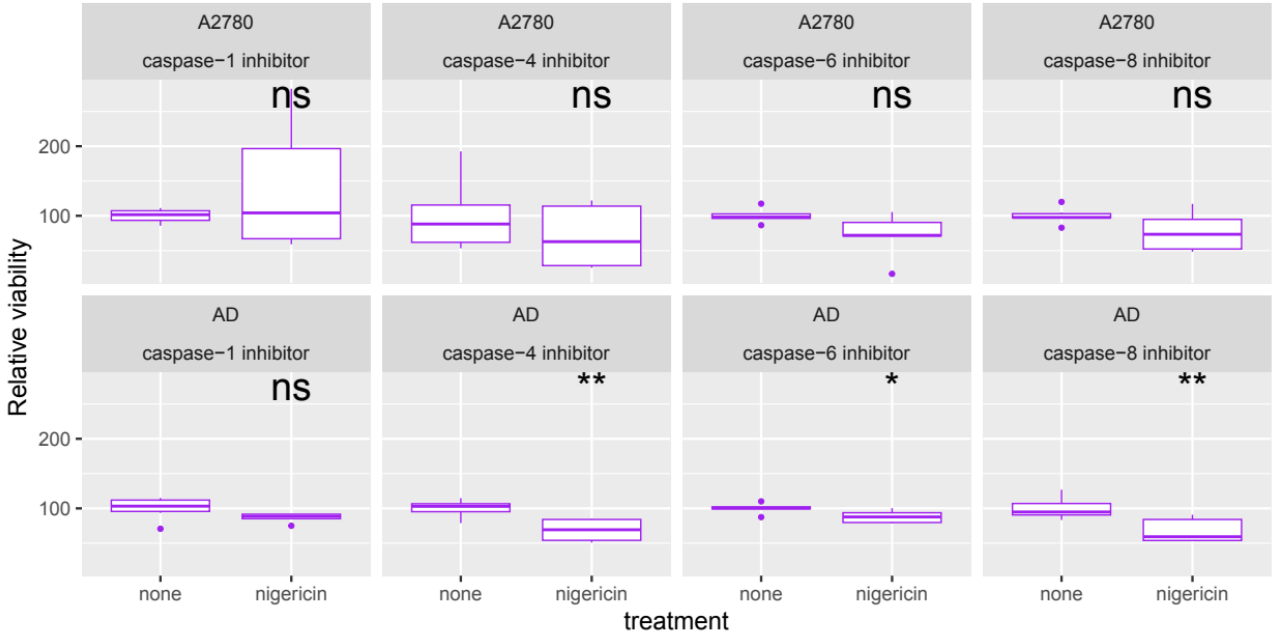

Figure 3.26. The effect of specific caspase inhibitors on cell viability in response to nigericin in chemosensitive (A2780, upper row) and chemoresistant (A2780-AD, bottom row) ovarian cancer cell lines *in vitro*.

We also compared the effect of specific caspase inhibitors on cell viability between themselves in nigericin-treated A2780 and A2780-AD cell lines (Figure 3.27). We found that although the inhibition of these four caspases alone affects cell viability similarly in A2780 cell line treated with nigericin (Figure 3.26, 3.27), the inhibition of these caspases alone leads to some differences in cell viability between different caspases inhibitors in its chemoresistant subline, A2780-AD, again treated with nigericin (Figure 3.27). This might point to the fact that different caspases might have varying functionalities in terms of pyroptotic cell death in chemoresistant ovarian cancer cells, as shown in our experimental setup (Figure 3.27)

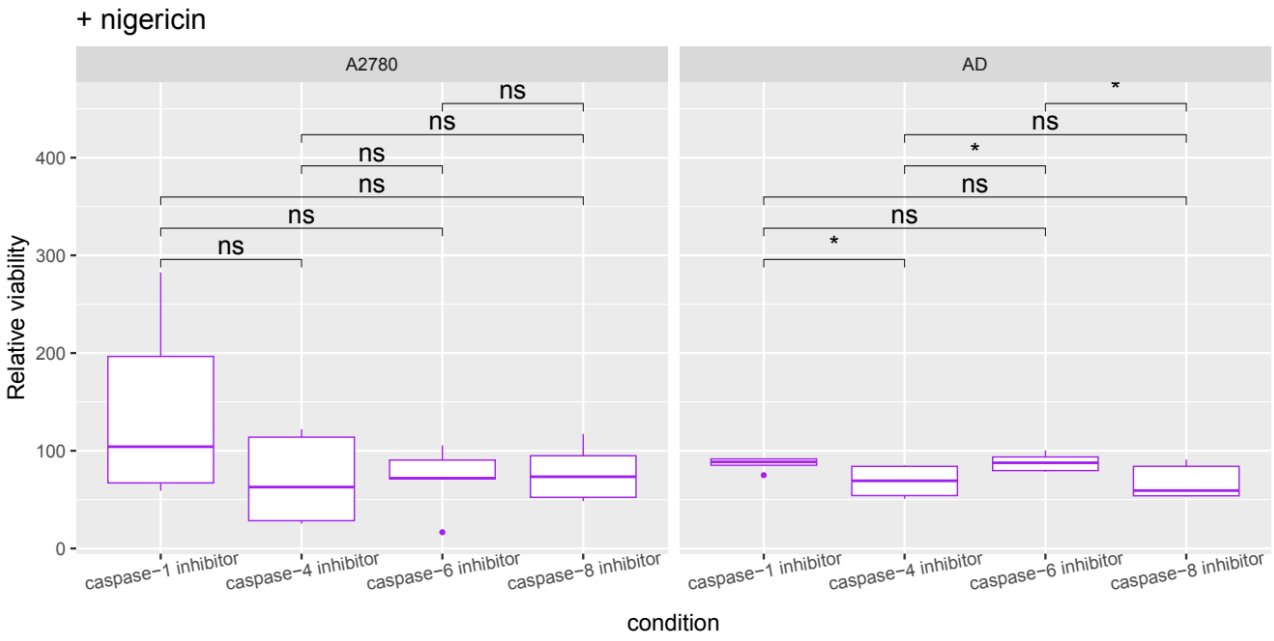

Figure 3.27. The comparison of the effect of specific caspase inhibitors on cell viability between themselves in nigericin-treated A2780 and A2780-AD cell lines.

Besides, we compared the released HMGB1 and IL-18 levels in ovarian cancer cell lines treated with nigericin and specific caspase inhibitors (Figure 3.28). Although non-significant, we found that upon inhibition of caspase-1, -4 or -8, the levels of released IL-18 from A2780 cells treated with nigericin slightly decreased compared to A2780 cells treated only with nigericin but not with any of the specific caspase inhibitors (Figure 3.28, second plot). The inhibition of caspase-1 and -6 slightly lowered the released IL-18 levels from A2780-AD cells treated with nigericin compared to A2780-AD cells treated only with nigericin but not with any of the specific caspase inhibitors (Figure 3.28, last plot). However, the inhibition of any of these caspases did not lead to an observable change in the levels of HMGB1 released from A2780 and A2780-AD cells treated with nigericin (Figure 3.28, first and third plot). Here, note that IL-18 is a smaller molecule than HMGB1, and that the release of HMGB1 might require the formation of even larger pores, such as those formed after NINJ1-mediated plasma membrane rupture following the formation of gasdermin pores. Inhibition of certain caspases might lead to lowered numbers of gasdermin pores through which small proinflammatory molecules such as IL-18 are released into the extracellular space; however, since HMGB1 is larger in size than gasdermin pores, levels of its release are not directly effected by the formation of gasdermin pores in the context of ovarian cancer. Therefore, the inhibition of certain caspases might limit the release of IL-18 from both chemosensitive and chemoresistant ovarian

cancer cells treated with nigericin, due to formation of decreased number of gasdermin pores, their inhibition might not significantly effect the release of larger proinflammatory molecules such as LDH and HMGB1, as proposed previously in other studies performed in other cell types and contexts.

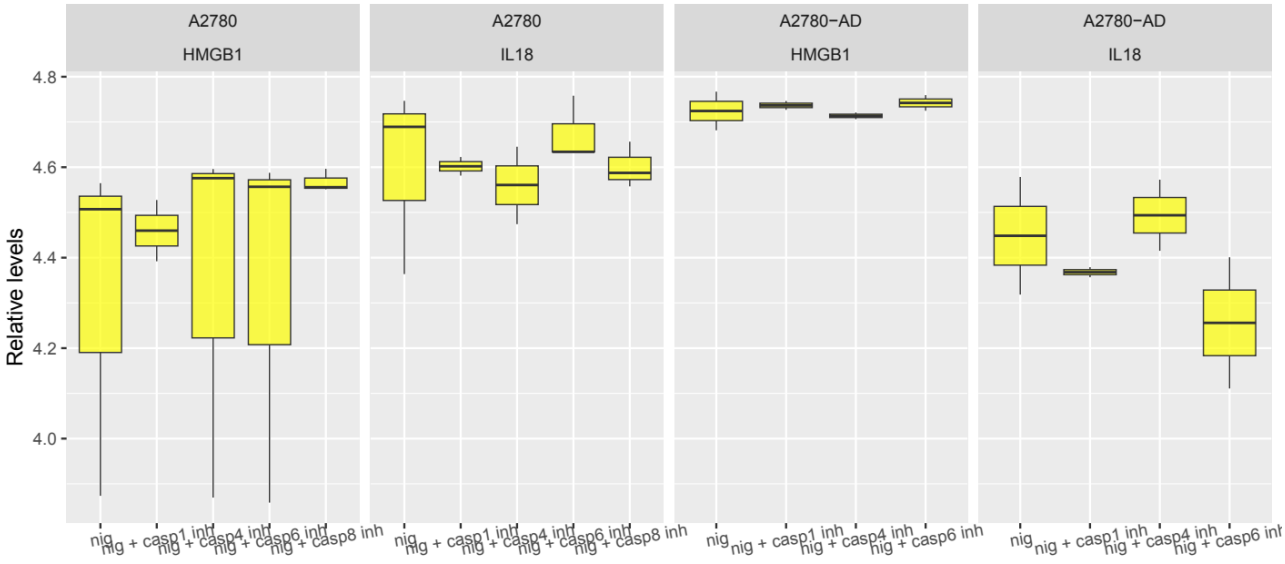

Figure 3.28. The levels of released HMGB1 and IL-18 from ovarian cancer cell lines treated with nigericin and specific caspase inhibitors. Nig: nigericin. Casp: caspase.

3.17 Treatment with Disulfiram to Inhibit GSDMD Pore Formation

Next, we treated both ovarian cancer cell lines with nigericin (10 μM) or disulfiram (50 μM) or their combination (Figure 3.29) and compared the cell viability. At nM concentration, disulfiram is able to covalently modify human/mouse Cys191/Cys192 in GSDMD to block GSDMD-mediated pore formation (Hu et al., 2020). This drug still allows IL-1β and GSDMD processing, but inhibits pore formation, thereby preventing IL-1β release and ultimate pyroptosis (Hu et al., 2020). In A2780 cell line, we found that cell viability is similar for all three cases, namely, nigericin, disulfiram or their combination. However, in A2780-AD cell line, we observed that their combination (disulfiram + nigericin) leads to a decreased viability compared to nigericin alone or disulfiram alone. In both cell lines, unexpectedly, disulfiram decreased viability to the similar levels observed with nigericin. This might point that the inhibition of GSDMD pore formation can result in cell death in cell lines. If GSDMD would be the main pyroptosis mediator in these cell lines, we would expect that when used in combination with nigericin, it would limit nigericin's effect on

pyroptotic cell death to a certain extent. However, this is not the case for both cell lines, potentially showing that gasdermins other than GSDMD might be relatively more important in pyroptotic cell death in these cells. This data also supports our previous observations that in ovarian cancer cells, GSDMC and GSDMD expression is increased and that GSDMC or GSDMD overexpression leads to increased cell growth in untreated A2780 cells. Here, the blockade of GSDMD pore formation decreases cell viability in both cell lines, pointing that GSDMD might contribute to malignancy (increased survival) in ovarian cancer cells. This is also in parallel to the survival data. We above showed that ovarian cancer patients with high GSDMC or GSDMD expression have lower survival rates compared to ovarian cancer patients with high GSDMC or GSDMD expression, respectively. In summary, increased GSDMD levels might lead to worse prognosis / decreases survival possibly by promoting or contributing to enhanced ovarian tumor growth. However, further mechanistic studies are required to delineate molecular and physiological events directly connecting increased GSDMD levels to unfavorable prognosis in patients with ovarian cancer.

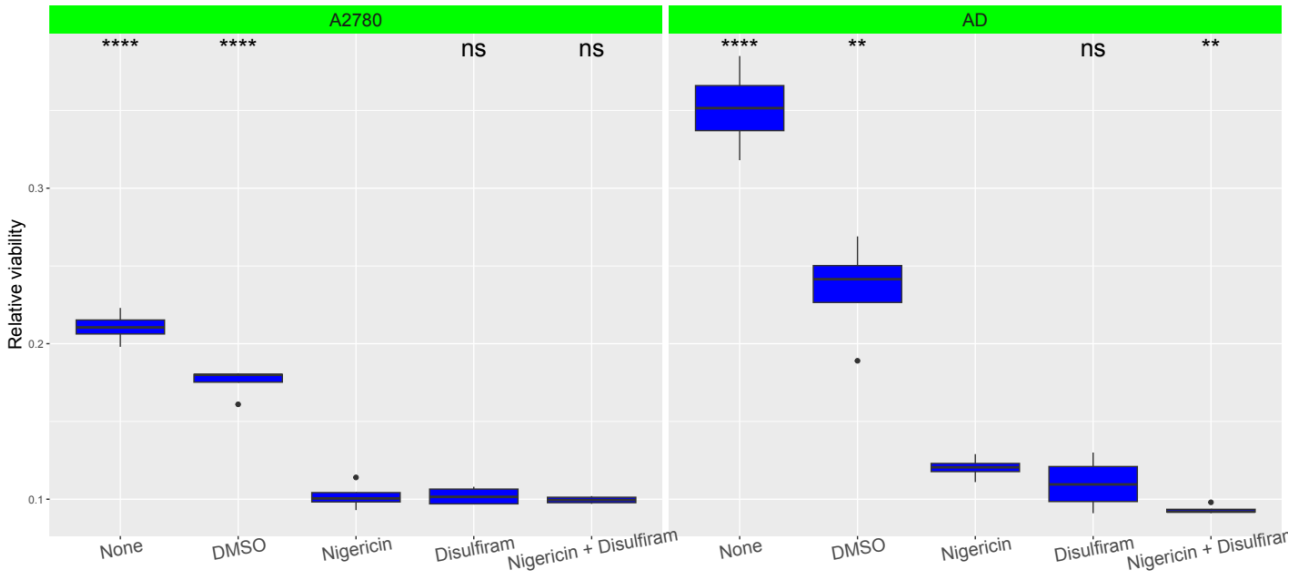

Figure 3.29. Treatment with disulfiram to inhibit GSDMD pore formation and its influence on cell viability in chemosensitive (A2780) and chemoresistant (A2780-AD) ovarian cancer cell lines *in vitro*.

Below (Figure 3.30-3.33), representative microscopy images showing the effect of nigericin, a pyroptotis inducer bacterial toxin, on cell morphology and cell viability of chemosensitive (A2780) and chemoresistant (A2780-AD) ovarian cancer cells are given.

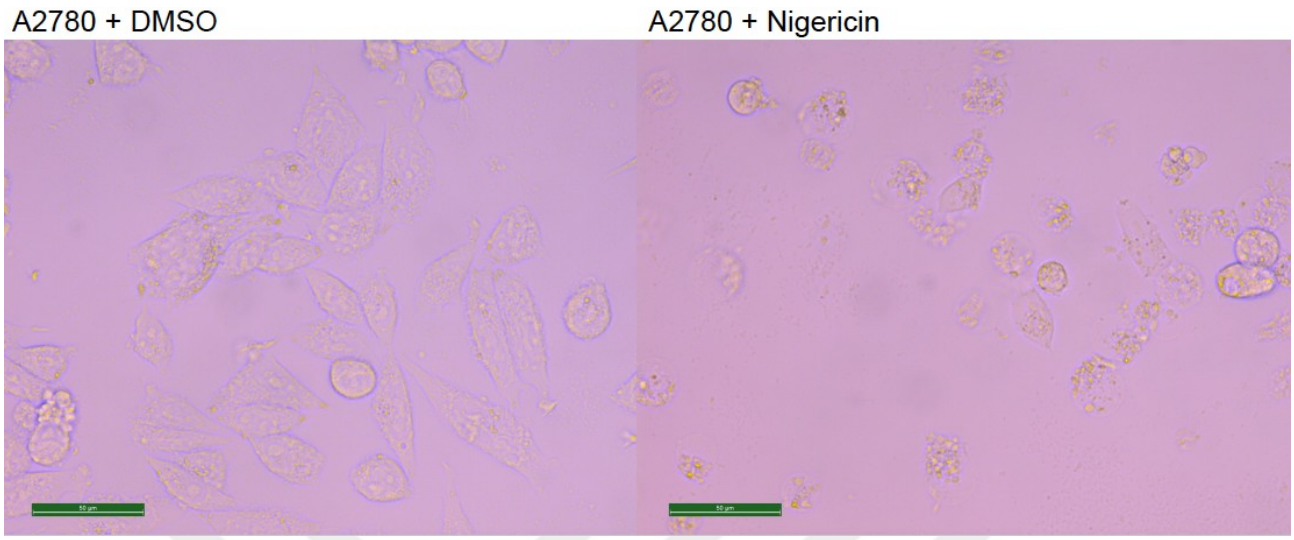

Figure 3.30. Microscopy images of chemosensitive A2780 ovarian cancer cell lines treated with DMSO or nigericin

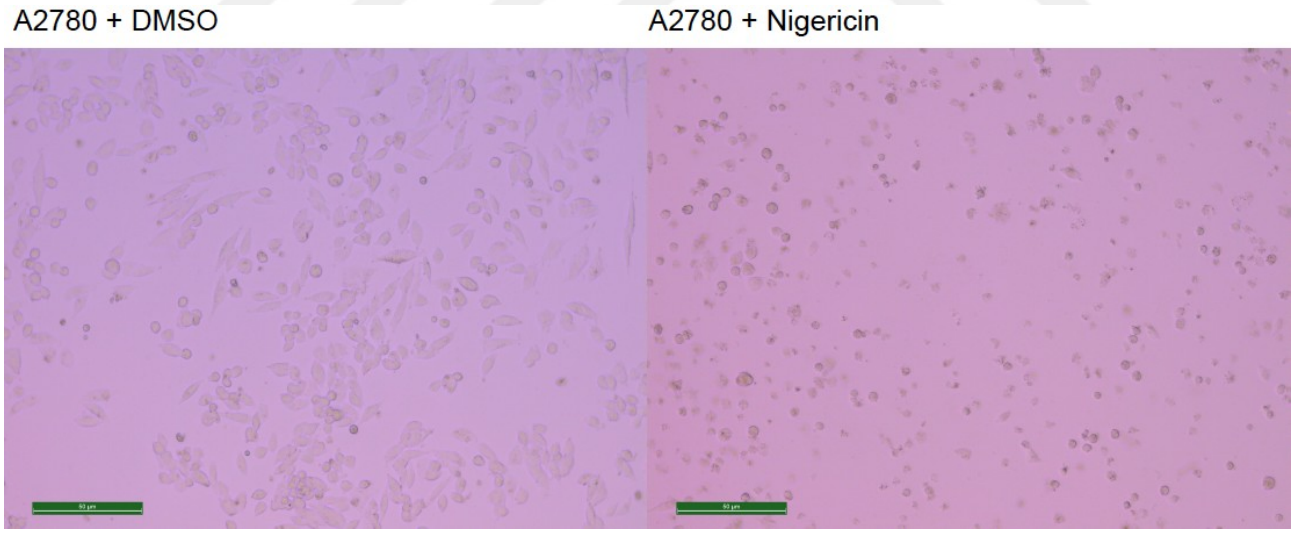

Figure 3.31. Microscopy images of chemosensitive A2780 ovarian cancer cell lines treated with DMSO or nigericin

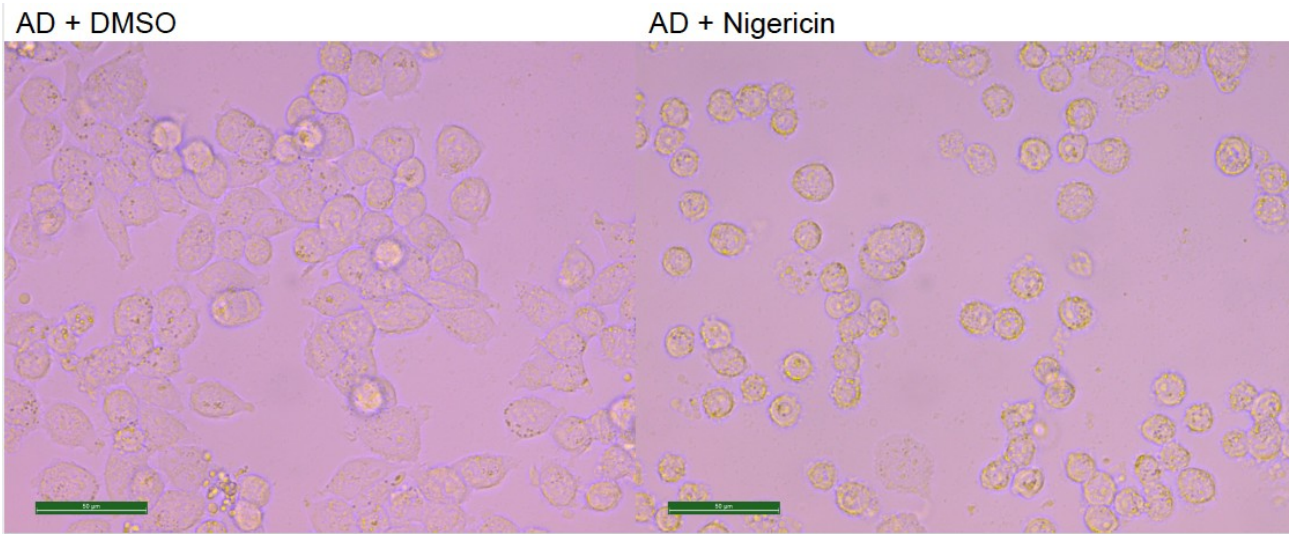

Figure 3.32. Microscopy images of chemoresistant A2780-AD ovarian cancer cell lines treated with DMSO or nigericin

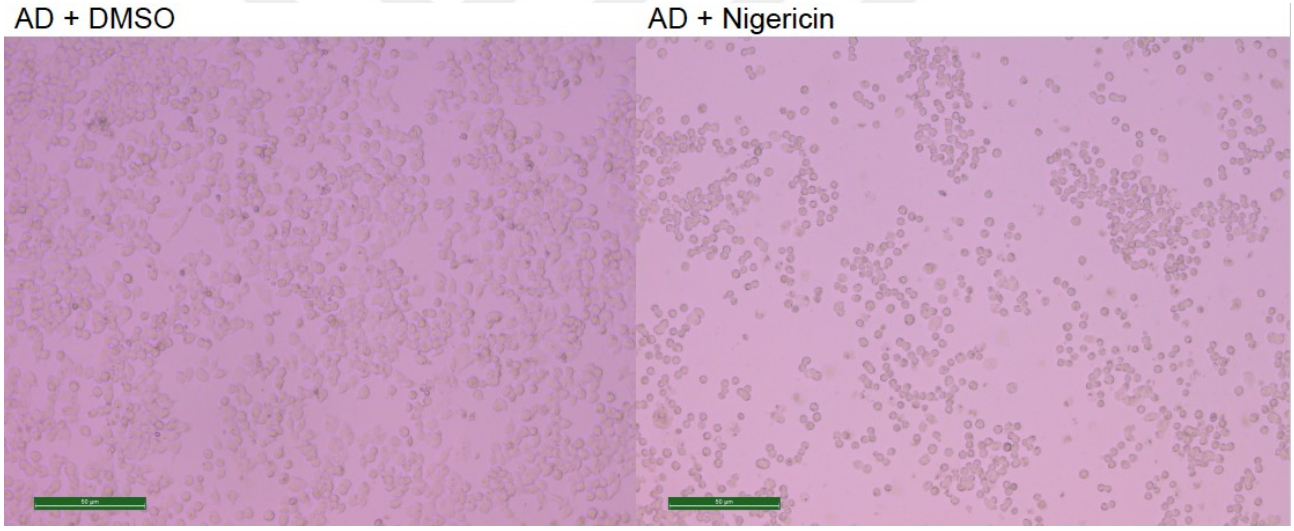

Figure 3.33. Microscopy images of chemoresistant A2780-AD ovarian cancer cell lines treated with DMSO or nigericin

4 DISCUSSION

Pyroptosis, a type of pro-inflammatory programmed cell death, is mediated by the members of gasdermin (GSDM) protein family, accompanied by several inflammatory and immune responses. Certain signals such as pathogen-associated molecular patterns (PAMPs), endogenous danger signals, or alterations to cellular homeostasis result in the activation of pro-inflammatory caspases (such as caspase-1, caspase-4, caspase-5, caspase-11 and caspase-12) within the inflammasome complex (Broz et al., 2020; Broz and Dixit, 2016; Martinon and Tschopp, 2007). For instance, activated caspases such as caspase 1 and caspase 4/5/11 cleave GSDMD within its central linker region and thereby release the repressor activity of its C-terminal region on its N-terminal pore-forming activity (Kayagaki et al., 2015; Shi et al., 2015; He et al., 2015; Broz et al., 2020). Following the permeabilization of the plasma membrane (PM) by pores created by GSDMD, cells undergo pyroptosis that promotes the release of mature IL-1β and IL-18 (Broz et al., 2020).

Since gasdermins have not been previously studied in detail in serous ovarian cancer, we analyzed differential expression of gasdermin family members in patients with serous ovarian cancer in comparison to ovarian samples from healthy women. We found that GSDMD and GSDMC have higher expression at the mRNA level in serous ovarian cancer compared to normal (non-malignant) ovaries, by analyzing several independent transcriptomics datasets in R programming environment. In support of these findings, we showed that copy number gain events (CNV gain) in these two gasdermins are around 50% in patients with ovarian cancer, quite higher than that of other members of gasdermin family (Gao et al., 2018). In other words, approximately half of the patients with ovarian cancer have copy number gains in GSDMD or GSDMD genes. Similarly, Gao et al. reported that GSDMD protein levels were significantly higher in non-small cell lung cancer (NSCLC) and lung adenocarcinoma, compared to adjacent non-malignant tissues (Gao et al., 2018). Authors also reported that knockdown of GSDMD attenuates tumor proliferation in NSCLC, showing that high GSDMD levels may contribute to tumor growth in NSCLC (Gao et al., 2018). Another study showed that GSDMC is highly expressed in metastatic melanoma cells, and its levels are upregulated during the course of acquisition of metastatic potential in these cells (Watabe et al., 2001). Similarly, this points that high GSDMC levels might be associated with more advanced and deadly disease in the context of melanoma (Watabe et al., 2001). Miguchi et al. suggested that GSDMC functions as an oncogene, promoting cell proliferation in colorectal carcinogenesis, since they found that the silencing of GSDMC results in a significant reduction in the proliferation and tumorigenesis of colorectal cancer cell lines, whereas its overexpression enhances cell proliferation

(2016). Combined, above studies demonstrate that certain gasdermin protein family members such as GSDMC and GSDMD might promote tumor initiation or progression, at least to a certain extent, in different cancer types. Although studies mentioned above highlighted the pro-tumorigenic role of both GSDMD and GSDMC in several cancer types similar to our findings in serous ovarian cancer, one study suggested that GSDMC might act as a tumor suppressor gene in esophageal squamous cell carcinomas, since its expression is decreased in this cancer (Saeki et al., 2009). Thus, it can be proposed that these two gasdermin family members may contribute to the development and progression of cancer in a cancer type–specific manner. In other words, gasdermin proteins may have opposite roles in cancer development and progression depending on the cancer type or even on cancer subtype.

Several previous studies reported that GSDMD can be inactivated by apoptotic caspases including caspase-3 and caspase-7 by cleaving the protein at a distinct site from the cleavage site of the inflammatory caspases such as caspase-1 and caspase-11 (Chen et al., 2019; Taabazuing et al., 2017). These studies demonstrate that GSDMD-dependent pore formation and subsequent cell lysis is suppressed in the course of apoptosis, and that there is a bidirectional crosstalk between apoptotic and pyroptotic cell death in certain cell types (Chen et al., 2019; Taabazuing et al., 2017). Therefore, increased expression of GSDMD in serous ovarian cancer, in theory, might be counteracted by the increased activity of apoptotic caspases. Although we found that the expression of caspase-3 does not increase at the mRNA level in serous ovarian cancer, its expression at the protein level or its activity might be higher, and thus block or limit the GSDMD-mediated pyroptosis in serous ovarian cancer cells. We also showed that the expression of certain inflammatory caspases such as caspase-1, caspase-4, and caspase-5 are decreased at the transcript level in serous ovarian cancer. Therefore, although the expression of, e.g., GSDMD is increased in serous ovarian cancer at the mRNA level, its pore-forming activity might not be increased in parallel due to the lower levels of caspases that cleave GSDMD to activate it or due to the absence or decreased levels of upstream events leading to pyroptotic cell death such as inflammasome activation. Please note that decreased expression of certain caspases at the mRNA level might not indicate decreased protein levels or lower activities. Future research is required to test these scenarios to determine if increased or decreased expression of certain gasdermins indeed lead to increased or decreased pore formation and subsequent lytic cell death events, respectively.

In contrast to GSDMD and GSDMC, we found that the expression of GSDME (DFNA5) and PJVK (DFNB59) are downregulated / decreased in serous ovarian cancer samples compared to samples

from healthy controls, at the transcript level. These two proteins belong to the deafness-associated genes (DFN), and their protein sequences cluster closely together, distant from the other members of gasdermin family in humans (GSDMA-D) (Broz et al., 2020). Decreased expression of both DFN genes of gasdermin family may reflect their similar functional importance in serous ovarian cancer. GSDME is an executioner of pore formation in caspase-3-mediated pyroptotic cell death, and it is frequently silenced at the epigenetic level by methylation, in various cancer types including gastric, breast, and colorectal cancer, pointing the function of GSDME as a tumor suppressor (Rogers et al., 2017; Akino et al., 2007; Croes et al., 2018; Croes et al., 2017; Kim et al., 2008; Ibrahim et al. 2019; Yokomizo et al., 2012; Kim et al., 2008). A recent study showed that GSMDE limits tumor growth by increasing anti-tumor immunity through the enhancement of the phagocytosis of tumor cells by tumor-associated macrophages and of the number and functions of tumor-infiltrating natural-killer and CD8+ T lymphocytes (Zhang et al., 2020). Our findings which show the downregulation of GSDME in serous ovarian cancer compared to healthy ovaries are in line with these previous studies which suggest the role of GSDME as a tumor suppressor. In other words, the decrease in the mRNA expression of tumor suppressor GSMDE might support / contribute to pro-tumorigenic mechanisms in ovarian cancer. Further research is needed to understand how GSDME is regulated by epigenetic mechanisms and in which contexts in serous ovarian cancer. Here, it should also be noted that the protein levels and pyroptotic activity of GSDME can also be regulated post-transcriptionally or post-translationally. Moreover, Wang et al. showed that certain chemotherapy drugs can induce pyroptosis through caspase-3 cleavage of gasdermin E, providing a link with cancer chemotherapy and the activity of gasdermins and ultimate proinflammatory cell death (Wang et al., 2007). To our knowledge, PJVK (Pejvakin, DFNB59) has not been previously studied in the context of cancer research; thus, this is the first study pointing to the potential role of PVJK similar to GSDME, the other DFN gene of gasdermin family, in cancer. Since both genes show similar expression profiles in ovarian cancer based on our data, we can propose that PJVK similar to GSDME might have some tumor suppressor functions in ovarian cancer; however, further in vitro and in vivo mechanistic research is needed.

We showed that the expression of GSDMB is increased in serous ovarian cancer samples compared to samples from healthy controls. However, when we compared the expression of GSDMB between ovarian samples from healthy individuals and ovarian samples from women with late-stage and high-grade serous ovarian cancer, we did not observe any significant difference at the mRNA level. This discrepancy might be due to tumor stage- and grade-dependent expression of GSDMB in serous ovarian cancer. Since a recent report showed the importance of GSDMB in the enhancement

of anti-tumor immunity in another cancer type, further research is needed to better understand the changes in the expression of GSDMB in serous ovarian cancer initiation and progression and its role in ovarian cancer (Zhou et al., 2020).

Furthermore, we found that the expression of GSDMD is generally negatively correlated with the expression of GSDME (DFNA5) in ovarian samples, though, to varying extents in different transcriptomics datasets. This finding may reflect their opposite functions of these genes (for instance, tumor suppressor vs oncogenic roles) in this tissue; however, experimental data is required to uncover underlying mechanisms regulated by both genes in the context of ovarian cancer, in the future. To our knowledge, this is the first study showing the differential expression and copy number variation (CNV) events of gasdermin family members in serous ovarian cancer. Since our findings are mostly parallel to that have been previously observed in other cancer types, therapeutic targeting (either inhibition or activation of the function, depending on the gasdermin family member) of some gasdermins might show promise in the clinic in the treatment of various cancer types. Besides, considering that ovarian cancer is mostly known for its highly immunosuppressive microenvironment, a better understanding of this proinflammatory cell death in ovarian cancer may guide the development of novel immunotherapy strategies with favorable response rates in this cancer type (Chardin and Leary, 2021). Moreover, a better understanding of epigenetic regulation of and also posttranscriptional / posttranslational regulation of some gasdermin family members in serous ovarian cancer initiation and progression may be valuable in the early detection and disease follow-up of this deadly cancer.

In the second part of this study, we showed that both GSDMD and GSDME expressions at the protein level differ between ovarian tumors and adjacent normal / non-malignant stromal cells in the tumor microenvironment of ovarian cancer patients. We found that GSDMD protein levels are higher in ovarian tumors, whereas GSDME protein levels are lower, compared to adjacent non-malignant cells. This is in line with our previous observations performed at the mRNA level as reported at the first part of this thesis (Berkel and Cacan, 2021). We also formerly showed that GSDMD copy number gains are present in almost half of the patients with ovarian cancer, and that more than 50% of total CNV events in GSDME gene are copy number losses (CNV loss) (Berkel and Cacan, 2021). Therefore, we speculate that GSDMD and GSDME might have opposite functions / roles (for instance, pro- and anti-tumor) in ovarian cancer. Increased expression of GSDMD might contribute, at least in part, to the development of ovarian cancer (also supported by our survival analysis reported at the first part); however, higher expression of GSDME might negatively regulate ovarian cancer initiation. Also, in parallel to our findings on gene expression

changes of gasdermin genes between ovarian tumor and healthy ovary samples at the mRNA level (Berkel and Cacan, 2021), GSMDA protein levels seem to not change between normal (non-malignant stromal cells adjacent to ovarian tumors) and malignant ovary cells. This indicates that not all gasdermin family members are necessarily of equal importance in the context of ovarian cancer, and that some gasdermin protein family members might have relatively higher functionality in upstream events leading to the development or progression of ovarian cancer, or in general in cancer.

Since NINJ1 has been recently identified as a protein responsible for complete plasma membrane rupture (PMR) in pyroptosis in addition to other cell death pathways such as apoptosis (Kayagaki et al., 2021; Wang and Shao, 2021), we studied its expression in the course of cancer progression in serous ovarian cancer. We found that its expression is decreased in late stage compared to early stage in serous ovarian cancer. In the late stage, tumor size is relatively larger and it has already spread from where it originated (primary site to secondary sites) (Berkel and Cacan, 2021). In parallel, we showed that its low expression is associated with worse overall survival / prognosis of women with ovarian cancer (in addition to patients with breast cancer, another cold tumor in women), and that NINJ1 can be considered a prognostic marker for better outcome / prognosis in patients with ovarian cancer. In support of these observations, we observed that cisplatin-resistant ovarian cancer cells (A2780 cell line) have lower NINJ1 expression *in vitro*, compared to cisplatin-sensitive cells, and NINJ1 expression is positively correlated with immune infiltration of ovarian tumors by macrophages and monocytes, possibly explaining why its lower expression is associated with worse prognosis. In other words, ovarian tumors with high NINJ1 expression may respond better to chemotherapies and may have high immune cell infiltration levels, ultimately leading to favorable prognosis. All these data presented above points that ovarian cancer cells might acquire the ability to enhance proliferation or inhibit cell death, to promote metastasis, and to develop resistance to cisplatin by decreasing NINJ1 levels, thus possibly blocking or limiting complete plasma membrane rupture and ultimately limiting anti-tumor immunity which otherwise might be induced by the released proinflammatory cytoplasmic contents such as LDH and HMGB1. How NINJ1 mechanistically contributes to worse prognosis in this patient group remains unknown and further research is needed to be able to develop novel treatment strategies to promote NINJ1-mediated lytic cell death specifically in tumor cells of ovarian cancer patients.

Besides, we found that the correlation between gasdermin D (GSDMD) and NINJ1 mRNA expression is higher in ovarian tumors compared to that in healthy ovaries, possibly indicating their

coordinated or regulated involvement in ovarian cancer initiation or progression. Since NINJ1 functions downstream of gasdermin pore formation by using its evolutionarily conserved extracellular domain for oligomerization to promote subsequent plasma membrane rupture in the lytic phase (Kayagaki et al., 2021; Wang and Shao, 2021), cooperative and sequential mechanisms of these two proteins in cell death might require the coordinated regulation of their expression. First, the formation of gasdermin pores might lead to the release of small pro-inflammatory molecules such as IL-18, but this can be reversed (i.e. gasdermin pores can be removed without ultimate cell death). However, if gasdermin pore formation is followed by the activity of NINJ1, plasma membrane rupture might lead to the release of pro-inflammatory molecules which are larger in size and possibly higher in concentration, leading to the ultimate lytic cell death which is irreversible in contrast to pore formation following gasdermin activity. Further research is needed to understand whether expression of GSDMD and NINJ1 is regulated by the same upstream proteins and how the formation of gasdermin pores vs NINJ1-mediated PMR is controlled in the context of ovarian cancer.

Furthermore, in the previous part, we found that NINJ1 mRNA expression is higher in ovarian tumors obtained from patients compared to normal ovaries from women with no malignant disease (Berkel and Cacan, 2021). Therefore, it seems that NINJ1 might contribute differently to tumor initiation and tumor progression. In support of this, we showed in this part of the study that NINJ1 expression first increases from pre-neoplastic to neoplastic state, but ultimately it decreases from neoplastic state to malignant and invasive state, in mouse ovarian surface epithelial (MOSE) cells at different stages of malignancy (Creekmore et al., 2011). This observation suggests that NINJ1 transcript levels might be highly dynamic from initiation to progression of tumor. We propose that during cancer progression from early to late stage, ovarian cancer cells might attempt to suppress plasma membrane rupture (and therefore lytic cell death) by negatively regulating the expression of NINJ1 to a certain threshold to be able better survive in blood and new sites in the body during the process of metastasis. In late stage, they can also acquire the ability to partially inhibit / limit plasma membrane rupture upon treatment with certain chemotherapeutics used in the treatment of ovarian cancer. In other words, during ovarian cancer initiation and progression, the expression of NINJ1 might be dynamic and highly regulated at the mRNA level. A better understanding of NINJ1-related lytic mechanisms in tumor initiation, progression and drug resistance in ovarian cancer is needed for cancer researchers to be able to develop novel treatment modalities.

Finally, we observed that the percentage of NINJ1 copy number loss events (CNV loss) is the highest in ovarian cancer patients among those with other cancers. This group of patients may represent ovarian cancer patients with advanced disease. The percentage of NINJ1 copy number gain events is also high in ovarian cancer patients (top third among all cancer types), and this group of patients may represent patients with early stage disease. A complete study with a larger sample size on NINJ1 CNV events based on tumor stage and grade is required to confirm these observations.

In summary, certain members of gasdermin (GSDM) family and NINJ1 might be important players in tumor initiation and progression in serous ovarian cancer. These proteins participating in different steps of pyroptotic cell death might have complementary functions in this highly lethal malignancy in women. A complete picture of how pyroptosis and ultimate plasma membrane rupture mediated by NINJ1 are involved in ovarian cancer will be of high importance in order to identify potential therapeutic targets within this recently identified group of pyroptotic and cell lysis-promoting proteins. We suggest that certain proteins in this pro-inflammatory cell death mechanism and subsequent plasma membrane rupture may represent actionable therapeutic vulnerabilities in the treatment of ovarian cancer patients.

5. NOTE

Some of the data obtained during this thesis study were published in two different journals (Berkel and Cacan, 2021; Berkel and Cacan; 2023) given below. Another paper mostly reporting data from *in vitro* experiments will be published soon.

Berkel C, Cacan E. Differential Expression and Copy Number Variation of Gasdermin (GSDM) Family Members, Pore-Forming Proteins in Pyroptosis, in Normal and Malignant Serous Ovarian Tissue. Inflammation. 2021 Dec;44(6):2203-2216. doi: 10.1007/s10753-021-01493-0. Epub 2021 Jun 6. PMID: 34091823.

Berkel C, Cacan E. Lower expression of NINJ1 (Ninjurin 1), a mediator of plasma membrane rupture, is associated with advanced disease and worse prognosis in serous ovarian cancer. Immunol Res. 2023 Feb;71(1):15-28. doi: 10.1007/s12026-022-09323-7. Epub 2022 Oct 3. PMID: 36184655.

6. REFERENCES

Acheson N, Chan KK. Epithelial ovarian cancer. In: Shafi MI, Luesley DM, Jordan JA, editors. Handbook of Gynaecological Oncology. London: Churchill Livingstone; 2001. pp. 231–41.

Aglietti, R.A., A. Estevez, A. Gupta, M.G. Ramirez, P.S. Liu, N. Kayagaki, C. Ciferri, V.M. Dixit, and E.C. Dueber. 2016. GsdmD p30 elicited by caspase-11 during pyroptosis forms pores in membranes. Proc Natl Acad Sci U S A 113 (28): 7858–7863. https://doi.org/10.1073/pnas.1607769113 Epub 2016 Jun 23. PMID: 27339137; PMCID: PMC4948338.

Agostini, L. et al. NALP3 forms an IL-1β-processing inflammasome with increased activity in Muckle-Wells autoinflammatory disorder. Immunity 20, 319–325 (2004).

Akino, K., M. Toyota, H. Suzuki, T. Imai, R. Maruyama, M. Kusano, N. Nishikawa, Y. Watanabe, Y. Sasaki, T. Abe, E. Yamamoto, I. Tarasawa, T. Sonoda,M.Mori, K. Imai, Y. Shinomura, and T. Tokino. 2007 Jan. Identification of DFNA5 as a target of epigenetic inactivation in gastric cancer. Cancer Sci. 98 (1): 88–95. https://doi.org/10.1111/j.1349-7006.2006.00351.x.

Alboukadel Kassambara (2020). ggpubr: 'ggplot2' Based Publication Ready Plots. R package version 0.4.0. https://CRAN.Rproject. org/

Ali, M. W., Cacan, E., Liu, Y., Pierce, J. Y., Creasman, W. T., Murph, M. M., Govindarajan, R., Eblen, S. T., Greer, S. F., & Hooks, S. B. (2013). Transcriptional suppression, DNA methylation, and histone deacetylation of the regulator of G-protein signaling 10 (RGS10) gene in ovarian cancer cells. PloS one, 8(3), e60185. https://doi.org/10.1371/journal.pone.0060185

Angosto-Bazarra, D. et al. Evolutionary analyses of the gasdermin family suggest conserved roles in infection response despite loss of pore-forming functionality. BMC Biol. 20, 9 (2022).

Armstrong D, Alvarez R, Bakkum-Gamez J, Barroilhet L, Behbakht K, Berchuck A, et al. NCCN guidelines insights: ovarian cancer, version 1.2019. J Natl Compr Cancer Netw. 2019;17:896–909.

Armstrong DK. Relapsed ovarian cancer: challenges and management strategies for a chronic disease. Oncologist. 2002;7:20–28. doi: 10.1634/theoncologist.7-suppl_5-20.

Auguie B (2017). _gridExtra: Miscellaneous Functions for "Grid" Graphics_. R package version 2.3, <https://CRAN.R-project.org/package=gridExtra>.

Baptiste Auguie (2017). gridExtra: miscellaneous functions for “Grid” graphics. R package version 2.3. https://CRAN.Rproject. org/package=gridExtra

Barber E, Matei D. Immunotherapy in ovarian cancer: We are not there yet. Lancet Oncol. 2021;22:903–5.

Barrett T, Wilhite SE, Ledoux P, Evangelista C, Kim IF, Tomashevsky M, Marshall KA, Phillippy KH, Sherman PM, Holko M, Yefanov A, Lee H, Zhang N, Robertson CL, Serova N, Davis S, Soboleva A. NCBI GEO: archive for functional genomics data sets—update. Nucleic Acids Res. 2013 Jan;41(Database issue):D991-5.

Beaufort CM, Helmijr JC, Piskorz AM, Hoogstraat M, Ruigrok-Ritstier K, Besselink N, Murtaza M, van IJcken WF, Heine AA, Smid M, Koudijs MJ, Brenton JD, Berns EM, Helleman J. Ovarian cancer cell line panel (OCCP): clinical importance of in vitro morphological subtypes. PLoS One. 2014 Sep 17;9(9):e103988. doi: 10.1371/journal.pone.0103988. Erratum in: PLoS One. 2015;10(3):e0122284. PMID: 25230021; PMCID: PMC4167545.

Berkel C, Cacan E. Differential Expression and Copy Number Variation of Gasdermin (GSDM) Family Members, Pore-Forming Proteins in Pyroptosis, in Normal and Malignant Serous Ovarian Tissue. Inflammation. 2021 Dec;44(6):2203-2216. doi: 10.1007/s10753-021-01493-0. Epub 2021 Jun 6. PMID: 34091823.

Berkel C, Cacan E. GAB2 and GAB3 are expressed in a tumor stage-, grade- and histotype-dependent manner and are associated with shorter progression-free survival in ovarian cancer. J Cell Commun Signal. 2021 Mar;15(1):57-70. https://doi.org/10.1007/ s12079-020-00582-3. Epub 2020 Sep 4.PMID: 32888136; PMCID: PMC7904992.

Berkel C, Cacan E. Lower expression of NINJ1 (Ninjurin 1), a mediator of plasma membrane rupture, is associated with advanced disease and worse prognosis in serous ovarian cancer. Immunol Res. 2023 Feb;71(1):15-28. doi: 10.1007/s12026-022-09323-7. Epub 2022 Oct 3. PMID: 36184655.

Berkel, C., and E. Cacan. 2021. Transcriptomic analysis reveals tumor stage- or grade-dependent expression of miRNAs in serous ovarian cancer. Hum Cell. 34: 862–877. https://doi.org/10.1007/ s13577-021-00486-3.

Bommer GT, Feng Y, Iura A, Giordano TJ et al. IRS1 regulation by Wnt/beta-catenin signaling and varied contribution of IRS1 to the neoplastic phenotype. J Biol Chem 2010 Jan 15;285(3):1928-38. PMID: 19843521

Bonome T, Levine DA, Shih J, Randonovich M et al. A gene signature predicting for survival in suboptimally debulked patients with ovarian cancer. Cancer Res 2008 Jul 1;68(13):5478-86. PMID: 18593951

Bonome T, Levine DA, Shih J, Randonovich M, Pise-Masison CA, Bogomolniy F, Ozbun L, Brady J, Barrett JC, Boyd J, Birrer MJ. A gene signature predicting for survival in suboptimally debulked patients with ovarian cancer. Cancer Res. 2008 Jul 1;68(13):5478- 86. doi: https://doi.org/10.1158/0008-5472.CAN-07-6595. PMID: 18593951; PMCID: PMC7039050.

Bray F, Ferlay J, Soerjomataram I, Siegel RL, Torre LA, Jemal A. Global cancer statistics 2018: GLOBOCAN estimates of incidence and mortality worldwide for 36 cancers in 185 countries. CA Cancer J Clin. 2018;68(6):394–424.

Brennan, M. A. & Cookson, B. T. Salmonella induces macrophage death by caspase-1-dependent necrosis. Mol. Microbiol. 38, 31–40 (2000).

Bristow, R.E., R.S. Tomacruz, D.K. Armstrong, E.L. Trimble, and F.J. Montz. 2002 Mar 1. Survival effect of maximal cytoreductive surgery for advanced ovarian carcinoma during the platinum era: a meta-analysis. J Clin Oncol. 20 (5): 1248–1259. https://doi.org/ 10.1200/JCO.2002.20.5.1248.

Broz, P., and V.M. Dixit. 2016 Jul. Inflammasomes: mechanism of assembly, regulation and signalling. Nat Rev Immunol. 16 (7): 407– 420. https://doi.org/10.1038/nri.2016.58.

Broz, P., P. Pelegrín, and F. Shao. 2020 Mar. The gasdermins, a protein family executing cell death and inflammation. Nat Rev Immunol. 20 (3): 143–157. https://doi.org/10.1038/s41577-019-0228-2.

Cacan, E., Ali, M. W., Boyd, N. H., Hooks, S. B., & Greer, S. F. (2014). Inhibition of HDAC1 and DNMT1 modulate RGS10 expression and decrease ovarian cancer chemoresistance. PloS one, 9(1), e87455. https://doi.org/10.1371/journal.pone.0087455

Cancer Genome Atlas Research Network. Integrated genomic analyses of ovarian carcinoma. Nature. 2011 Jun 29;474(7353):609-15. doi: https://doi.org/10.1038/nature10166. Erratum in: Nature. 2012 Oct 11;490(7419):298. PMID: 21720365; PMCID: PMC3163504.

Carl-McGrath, S., R. Schneider-Stock, M. Ebert, and C. Röcken. 2008 Jan. Differential expression and localisation of gasdermin-like (GSDML), a novel member of the cancer-associated

GSDMDC protein family, in neoplastic and non-neoplastic gastric, hepatic, and colon tissues. Pathology. 40 (1): 13–24. https://doi.org/ 10.1080/00313020701716250.

Chai Q, Yu S, Zhong Y, Lu Z, Qiu C, Yu Y, Zhang X, Zhang Y, Lei Z, Qiang L, Li BX, Pang Y, Qiu XB, Wang J, Liu CH. A bacterial phospholipid phosphatase inhibits host pyroptosis by hijacking ubiquitin. Science. 2022 Oct 14;378(6616):eabq0132. doi: 10.1126/science.abq0132. Epub 2022 Oct 14. PMID: 36227980.

Chan K. Reducing Delays in Referrals. Cancer Services Collaborative Service Improvement Guide: Ovarian Cancer. London: NHS Modernisation Agency; 2001.

Chardin L, Leary A. Immunotherapy in Ovarian Cancer: Thinking Beyond PD-1/PD-L1. Front Oncol. 2021 Dec 13;11:795547. doi: 10.3389/fonc.2021.795547. PMID: 34966689; PMCID: PMC8710491.

Chen KW, Demarco B, Heilig R, Shkarina K, Boettcher A, Farady CJ, Pelczar P, Broz P. Extrinsic and intrinsic apoptosis activate pannexin-1 to drive NLRP3 inflammasome assembly. EMBO J. 2019 May 15;38(10):e101638. doi: https://doi.org/10.15252/ embj.2019101638. Epub 2019 Mar 22. PMID: 30902848; PMCID: PMC6517827.

Chen W, Zheng R, Baade PD, Zhang S, Zeng H, Bray F, et al. Cancer statistics in China, 2015. CA Cancer J Clin. 2016;66:115–32.

Chen, X. et al. Pyroptosis is driven by non-selective gasdermin-D pore and its morphology is different from MLKL channel-mediated necroptosis. Cell Res. 26, 1007–1020 (2016).

Chen, Y. & Du, H. The promising PARP inhibitors in ovarian cancer therapy: from Olaparib to others. Biomed. Pharmacother. 99, 552–560 (2018).

Coleman RL, Oza AM, Lorusso D, Aghajanian C, Oaknin A, Dean A, et al. Rucaparib maintenance treatment for recurrent ovarian carcinoma after response to platinum therapy (ARIEL3): a randomised, double-blind, placebo-controlled, phase 3 trial. Lancet. 2017;390:1949–1961.

Cookson, B. T. & Brennan, M. A. Pro-inflammatory programmed cell death. Trends Microbiol. 9, 113–114 (2001).

Core Team, R. 2020. R: a language and environment for statistical computing. In R Foundation for Statistical Computing. Vienna: Austria. URL https://www.R-project.org/.

Coukos, G., J. Tanyi, and L.E. Kandalaft. 2016. Opportunities in immunotherapy of ovarian cancer. Ann Oncol (Suppl 1): i11–i15. https://doi.org/10.1093/annonc/mdw084 PMID: 27141063; PMCID: PMC4852275.

Croes L, Beyens M, Fransen E, Ibrahim J, Vanden Berghe W, Suls A, PeetersM, Pauwels P, Van Camp G, Opde Beeck K. Large-scale analysis of DFNA5 methylation reveals its potential as biomarker for breast cancer. Clin Epigenetics. 2018 Apr 11;10:51. https://doi.org/10.1186/s13148-018-0479-y. PMID: 29682089; PMCID: PMC5896072.

Croes L, de Beeck KO, Pauwels P, Vanden Berghe W, Peeters M, Fransen E, Van Camp G. DFNA5 promoter methylation a marker for breast tumorigenesis. Oncotarget. 2017 May 9;8(19):31948- 31958. https://doi.org/10.18632/oncotarget.16654. PMID: 28404884; PMCID: PMC5458261.

de Beeck KO, Van Laer L & Van Camp G DFNA5, a gene involved in hearing loss and cancer: a review. Ann. Otol. Rhinol. Laryngol 121, 197–207 (2012).

Degen M, Santos JC, Pluhackova K, Cebrero G, Ramos S, Jankevicius G, Hartenian E, Guillerm U, Mari SA, Kohl B, Müller DJ, Schanda P, Maier T, Perez C, Sieben C, Broz P, Hiller S. Structural basis of NINJ1-mediated plasma membrane rupture in cell death. Nature. 2023 May 17. doi: 10.1038/s41586-023-05991-z. Epub ahead of print. PMID: 37198476.

Demarco B, Grayczyk JP, Bjanes E, Le Roy D, Tonnus W, Assenmacher CA, Radaelli E, Fettrelet T, Mack V, Linkermann A, Roger T, Brodsky IE, Chen KW, Broz P. Caspase-8-dependent gasdermin D cleavage promotes antimicrobial defense but confers susceptibility to TNF-induced lethality. Sci Adv. 2020 Nov 18;6(47):eabc3465. doi: https://doi.org/10.1126/sciadv.abc3465. PMID: 33208362; PMCID: PMC7673803.

Ding, J., K. Wang, W. Liu, Y. She, Q. Sun, J. Shi, H. Sun, D.C. Wang, and F. Shao. 2016. Pore-forming activity and structural autoinhibition of the gasdermin family. Nature 535 (7610): 111– 116. https://doi.org/10.1038/nature18590 Epub 2016 Jun 8. Erratum in: Nature. 2016 Dec 1;540(7631):150.

Don, M. M. et al. Death of cells by apoptosis following attachment of specifically allergized lymphocytes in vitro. Aust. J. Exp. Biol. Med. Sci. 55, 407–417 (1977).

Drake, C.G., E.J. Lipson, and J.R. Brahmer. 2014. Breathing new life into immunotherapy: review of melanoma, lung and kidney cancer. Nat Rev Clin Oncol (1): 24–37. https://doi.org/10.1038/nrclinonc.2013.208 Epub 2013 Nov 19. PMID: 24247168; PMCID: PMC4086654.

E. Pujade-Lauraine, P. Combe Recurrent ovarian cancer Ann Oncol, 27 (Suppl 1) (2016), pp. I63-i65

Eckert MA, Coscia F, Chryplewicz A, Chang JW, Hernandez KM, Pan S, Tienda SM, Nahotko DA, Li G, Blaženović I, Lastra RR, Curtis M, Yamada SD, Perets R, McGregor SM, Andrade J, Fiehn O, Moellering RE, Mann M, Lengyel E (2019) Proteomics reveals NNMT as a master metabolic regulator of cancer-associated fibroblasts. Nature 569(7758):723–728. https://doi.org/10.1038/s41586-019-1173-8

Elias EE, Lyons B, Muruve DA. Gasdermins and pyroptosis in the kidney. Nat Rev Nephrol. 2023 May;19(5):337-350. doi: 10.1038/s41581-022-00662-0. Epub 2023 Jan 3. PMID: 36596918.

Ferlay, J., I. Soerjomataram, R. Dikshit, S. Eser, C. Mathers, M. Rebelo, D.M. Parkin, D. Forman, and F. Bray. 2015 Mar 1. Cancer incidence and mortality worldwide: sources, methods and major patterns in GLOBOCAN 2012. Int J Cancer. 136 (5): E359–E386. https://doi.org/10.1002/ijc.29210.

Fink, S. L. & Cookson, B. T. Caspase-1-dependent pore formation during pyroptosis leads to osmotic lysis of infected host macrophages. Cell Microbiol. 8, 1812–1825 (2006).

Fitch M, Deane K, Howell D, Gray RE. Women's experiences with ovarian cancer: reflections on being diagnosed. Can Oncol Nurs J. 2002;12:152–68.

Galluzzi, L. et al. Molecular mechanisms of cell death: recommendations of the Nomenclature Committee on Cell Death 2018. Cell Death Differ. 25, 486–541 (2018).

Ganzfried BF, Riester M, Haibe-Kains B, Risch T, Tyekucheva S, Jazic I, Wang XV, Ahmadifar M, Birrer MJ, Parmigiani G, Huttenhower C, Waldron L. curatedOvarianData: clinically annotated data for the ovarian cancer transcriptome. Database (Oxford). 2013 Apr 2;2013:bat013. doi: https://doi.org/10.1093/database/ bat013. PMID: 23550061; PMCID: PMC3625954.

Gao J, Qiu X, Xi G, Liu H, Zhang F, Lv T, Song Y. Downregulation of GSDMD attenuates tumor proliferation via the intrinsic mitochondrial apoptotic pathway and inhibition of EGFR/Akt signaling and predicts a good prognosis in non-small cell lung cancer. Oncol Rep. 2018 Oct;40(4):1971-1984. https://doi.org/10.3892/ or.2018.6634. Epub 2018 Aug 7. PMID: 30106450; PMCID: PMC6111570.

Garcia-Calvo, M., Peterson, E.P., Leiting, B., et al. Inhibition of human caspases by peptide-based and macromolecular inhibitors. J. Biol. Chem. 273(49), 32608-32613 (1998).

Gentleman RC, Carey VJ, Bates DM, Bolstad B, Dettling M, Dudoit S, Ellis B, Gautier L, Ge Y, Gentry J, Hornik K, Hothorn T, Huber W, Iacus S, Irizarry R, Leisch F, Li C, Maechler M,

Rossini AJ, Sawitzki G, Smith C, Smyth G, Tierney L, Yang JY, Zhang J. Bioconductor: open software development for computational biology and bioinformatics. Genome Biol. 2004;5(10):R80. doi: 10.1186/gb-2004-5-10-r80. Epub 2004 Sep 15. PMID: 15461798; PMCID: PMC545600.

Goff B.A., Mandel L.S., Drescher C.W. Development of an ovarian cancer symptom index: possibilities for earlier detection. Cancer. 2007;109(2):221–227.

Goff B.A., Mandel L.S., Melancon C.H., Muntz H.G. Frequency of symptoms of ovarian cancer in women presenting to primary care clinics. J. Am. Med. Assoc. 2004;291(22):2705–2712.

Goff BA, Mandel L, Muntz HG, Melancon CH. Ovarian carcinoma diagnosis: results of a national ovarian cancer survey. Cancer. 2000;89:2068–75.

Grossman RL, Heath AP, Ferretti V, Varmus HE, Lowy DR, Kibbe WA, Staudt LM. Toward a shared vision for cancer genomic data. N Engl J Med. 2016 Sep 22;375(12):1109-12. doi: https://doi.org/ 10.1056/NEJMp1607591. PMID: 27653561; PMCID: PMC6309165.

Guo C, Song C, Zhang J, Gao Y, Qi Y, Zhao Z, Yuan C. Revisiting chemoresistance in ovarian cancer: Mechanism, biomarkers, and precision medicine. Genes Dis. 2020 Dec 1;9(3):668-681. doi: 10.1016/j.gendis.2020.11.017. PMID: 35782973; PMCID: PMC9243319.

Gyorffy B: Discovery and ranking of the most robust prognostic biomarkers in serous ovarian cancer, Geroscience, 2023, doi: 10.1007/s11357-023-00742-4.

Gyorffy, B., A. Lánczky, and Z. Szállási. 2012 Apr 10. Implementing an online tool for genome-wide validation of survival-associated biomarkers in ovarian-cancer using microarray data from 1287 patients. Endocr Relat Cancer. 19 (2): 197–208. https://doi.org/10.1530/ERC-11-0329.

Hadley Wickham and Jennifer Bryan (2019) readxl: Read Excel Files. R package version 1.3.1. https://CRAN.R-project.org/

He, W.T., H. Wan, L. Hu, P. Chen, X. Wang, Z. Huang, Z.H. Yang, C.Q. Zhong, and J. Han. 2015. Gasdermin D is an executor of pyroptosis and required for interleukin-1β secretion. *Cell Res* (12): 1285–1298. https://doi.org/10.1038/cr.2015.139 Epub 2015 Nov 27. PMID: 26611636; PMCID: PMC4670995.

Hendrix, N.D., R. Wu, R. Kuick, D.R. Schwartz, E.R. Fearon, and K.R. Cho. 2006 Feb 1. Fibroblast growth factor 9 has oncogenic activity and is a downstream target of Wnt signaling in

ovarian endometrioid adenocarcinomas. Cancer Res. 66 (3): 1354–1362. https://doi.org/10.1158/0008-5472.CAN-05-3694.

Hergueta-Redondo M, Sarrió D, Molina-Crespo Á, Megias D, Mota A, Rojo-Sebastian A, García-Sanz P, Morales S, Abril S, Cano A, Peinado H, Moreno-Bueno G. Gasdermin-B promotes invasion and metastasis in breast cancer cells. PLoS One. 2014 Mar 27;9(3):e90099. doi: https://doi.org/10.1371/journal.pone.0090099. PMID: 24675552; PMCID: PMC3967990.

Hester J, Bryan J (2022). _glue: Interpreted String Literals_. R package version 1.6.2, <https://CRAN.R-project.org/package=glue>.

Hoppenot, C., Eckert, M. A., Tienda, S. M. & Lengyel, E. Who are the long-term survivors of high grade serous ovarian cancer? Gynecol. Oncol. 148, 204–212 (2018).

Hou J, Zhao R, Xia W, Chang CW, You Y, Hsu JM, Nie L, Chen Y, Wang YC, Liu C, Wang WJ, Wu Y, Ke B, Hsu JL, Huang K, Ye Z, Yang Y, Xia X, Li Y, Li CW, Shao B, Tainer JA, Hung MC. PD-L1-mediated gasdermin C expression switches apoptosis to pyroptosis in cancer cells and facilitates tumour necrosis. Nat Cell Biol. 2020 Oct;22(10):1264-1275. doi: https://doi.org/10.1038/s41556-020-0575-z. Epub 2020 Sep 14. Erratum in: Nat Cell Biol. 2020 Nov;22(11):1396. PMID: 32929201; PMCID: PMC7653546.

Hu JJ, Liu X, Xia S, Zhang Z, Zhang Y, Zhao J, Ruan J, Luo X, Lou X, Bai Y, Wang J, Hollingsworth LR, Magupalli VG, Zhao L, Luo HR, Kim J, Lieberman J, Wu H. FDA-approved disulfiram inhibits pyroptosis by blocking gasdermin D pore formation. Nat Immunol. 2020 Jul;21(7):736-745. doi: 10.1038/s41590-020-0669-6. Epub 2020 May 4. PMID: 32367036; PMCID: PMC7316630.

Huang J, Chan WC, Ngai CH, Lok V, Zhang L, Lucero-Prisno DE 3rd, Xu W, Zheng ZJ, Elcarte E, Withers M, Wong MCS, On Behalf Of Ncd Global Health Research Group Of Association Of Pacific Rim Universities Apru. Worldwide Burden, Risk Factors, and Temporal Trends of Ovarian Cancer: A Global Study. Cancers (Basel). 2022 Apr 29;14(9):2230. doi: 10.3390/cancers14092230. PMID: 35565359; PMCID: PMC9102475.

Huber W, Carey VJ, Gentleman R, Anders S, Carlson M, Carvalho BS, Bravo HC, Davis S, Gatto L, Girke T, Gottardo R, Hahne F, Hansen KD, Irizarry RA, Lawrence M, Love MI, MacDonald J, Obenchain V, Oleś AK, Pagès H, Reyes A, Shannon P, Smyth GK, Tenenbaum D, Waldron L, Morgan M. Orchestrating high-throughput genomic analysis with

Bioconductor. Nat Methods. 2015 Feb;12(2):115-21. doi: https://doi.org/10.1038/nmeth.3252. PMID: 25633503; PMCID: PMC4509590.

Huxham IM, Barlow AL, Lewis AD, Plumb J, Mairs RJ, Gaze MN, Workman P. Differential intracellular processing of the anthracycline drug ME2303 in doxorubicin-sensitive (A2780) and -resistant (A2780AD) human ovarian cancer cells as studied with confocal laser scanning microscopy and image analysis. Int J Cancer. 1994 Oct 1;59(1):94-102. doi: 10.1002/ijc.2910590118. PMID: 7927910.

Ibrahim J, Opde Beeck K, Fransen E, Croes L, Beyens M, Suls A, Vanden Berghe W, Peeters M, Van Camp G. Methylation analysis of Gasdermin E shows great promise as a biomarker for colorectal cancer. Cancer Med. 2019 May;8(5):2133-2145. https://doi.org/ 10.1002/cam4.2103. Epub 2019 Apr 16. PMID: 30993897; PMCID: PMC6536921.

IJ Jacobs, U Menon, A Ryan, et al. Ovarian cancer screening and mortality in the UK Collaborative Trial of Ovarian Cancer Screening (UKCTOCS): a randomised controlled trial Lancet, 387 (2016), pp. 945-956

Itamochi, H. et al. Sensitivity to anticancer agents and resistance mechanisms in clear cell carcinoma of the ovary. Jpn. J. Cancer Res. 93, 723–728 (2002).

Jayson GC, Kohn EC, Kitchener HC, Ledermann JA. Ovarian cancer. Lancet 2014;384:1376–88. Jeroen Ooms (2020). magick: advanced graphics and imageprocessing in R. R package version 2.5.2. https://CRAN.Rproject. org/

Jiang S, Zhou Z, Sun Y, Zhang T, Sun L. Coral gasdermin triggers pyroptosis. Sci Immunol. 2020 Dec 4;5(54):eabd2591. https:// doi.org/10.1126/sciimmunol.abd2591.

JJ Allaire and Yihui Xie and Jonathan McPherson and Javier Luraschi and Kevin Ushey and Aron Atkins and Hadley Wickham and Joe Cheng and Winston Chang and Richard Iannone (2022). rmarkdown: Dynamic Documents for R. R package version 2.19. URL https://rmarkdown.rstudio.com.

JJ Allaire and Yihui Xie and Jonathan McPherson and Javier Luraschi and Kevin Ushey and Aron Atkins and Hadley Wickham and Joe Cheng and Winston Chang and Richard Iannone (2020). rmarkdown: dynamic documents for R. R package version 2.6. https://rmarkdown.rstudio.com.

Karlan BY, Dering J, Walsh C, Orsulic S et al. POSTN/TGFBI-associated stromal signature predicts poor prognosis in serous epithelial ovarian cancer. Gynecol Oncol 2014 Feb;132(2):334-42. PMID: 24368280

Kassambara A (2022). _ggpubr: 'ggplot2' Based Publication Ready Plots_. R package version 0.5.0, <https://CRAN.R-project.org/package=ggpubr>.

Katoh M., Katoh M. (2004b). Identification and characterization of human DFNA5L, mouse Dfna5l, and rat Dfna5l genes in silico. Int. J. Oncol. 25 765–770.

Kayagaki N, Stowe IB, Alegre K, Deshpande I, Wu S, Lin Z, Kornfeld OS, Lee BL, Zhang J, Liu J, Suto E, Lee WP, Schneider K, Lin W, Seshasayee D, Bhangale T, Chalouni C, Johnson MC, Joshi P, Mossemann J, Zhao S, Ali D, Goldenberg NM, Sayed BA, Steinberg BE, Newton K, Webster JD, Kelly RL, Dixit VM. Inhibiting membrane rupture with NINJ1 antibodies limits tissue injury. Nature. 2023 May 17. doi: 10.1038/s41586-023-06191-5. Epub ahead of print. PMID: 37196676.

Kayagaki, N. et al. Non-canonical inflammasome activation targets caspase-11. Nature 479, 117–121 (2011).

Kayagaki, N., I.B. Stowe, B.L. Lee, K. O'Rourke, K. Anderson, S. Warming, T. Cuellar, B. Haley, M. Roose-Girma, Q.T. Phung, P.S. Liu, J.R. Lill, H. Li, J. Wu, S. Kummerfeld, J. Zhang, W.P. Lee, S.J. Snipas, G.S. Salvesen, L.X. Morris, L. Fitzgerald, Y. Zhang, E.M. Bertram, C.C. Goodnow, and V.M. Dixit. 2015 Oct 29. Caspase-11 cleaves gasdermin D for non-canonical inflammasome signalling. Nature. 526 (7575): 666–671. https://doi.org/10.1038/nature15541.

Kayagaki, N., O.S. Kornfeld, B.L. Lee, I.B. Stowe, K. O'Rourke, Q. Li, W. Sandoval, D. Yan, J. Kang, M. Xu, J. Zhang, W.P. Lee, B.S. McKenzie, G. Ulas, J. Payandeh, M. Roose-Girma, Z. Modrusan, R. Reja, M. Sagolla, J.D. Webster, V. Cho, T.D. Andrews, L.X. Morris, L.A. Miosge, C.C. Goodnow, E.M. Bertram, and V.M. Dixit. 2021 Mar. NINJ1 mediates plasma membrane rupture during lytic cell death. Nature. 591 (7848): 131–136. https://doi.org/10.1038/s41586-021-03218-7.

Kerr, J. F., Wyllie, A. H. & Currie, A. R. Apoptosis: a basic biological phenomenon with wide-ranging implications in tissue kinetics. Br. J. Cancer 26, 239–257 (1972).

Kersey PJ, Allen JE, Allot A, BarbaM, Boddu S, Bolt BJ, Carvalho- Silva D, Christensen M, Davis P, Grabmueller C, Kumar N, Liu Z, Maurel T, Moore B, McDowall MD, Maheswari U, Naamati G, Newman V, Ong CK, Paulini M, Pedro H, Perry E, Russell M, Sparrow H,

Tapanari E, Taylor K, Vullo A,Williams G, Zadissia A, Olson A, Stein J,Wei S, Tello-RuizM,Ware D, Luciani A, Potter S, Finn RD, UrbanM, Hammond-KosackKE, BolserDM, De Silva N, Howe KL, Langridge N, Maslen G, Staines DM, Yates A. Ensembl Genomes 2018: an integrated omics infrastructure for non-vertebrate species. Nucleic Acids Res. 2018 Jan 4;46(D1):D802-D808. https:// doi.org/10.1093/nar/gkx1011. PMID: 29092050; PMCID: PMC5753204.

Kim MS, Lebron C, Nagpal JK, Chae YK, Chang X, Huang Y, Chuang T, Yamashita K, Trink B, Ratovitski EA, Califano JA, Sidransky D. Methylation of the DFNA5 increases risk of lymph node metastasis in human breast cancer. Biochem Biophys Res Commun. 2008 May 23;370(1):38-43. https://doi.org/10.1016/ j.bbrc.2008.03.026. Epub 2008Mar 17. PMID: 18346456; PMCID: PMC3094717.

Kim, M.S., X. Chang, K. Yamashita, J.K. Nagpal, J.H. Baek, G. Wu, B. Trink, E.A. Ratovitski, M. Mori, and D. Sidransky. 2008 Jun 5. Aberrant promoter methylation and tumor suppressive activity of the DFNA5 gene in colorectal carcinoma. Oncogene. 27 (25): 3624–3634. https://doi.org/10.1038/sj.onc.1211021.

Köbel M, Kalloger SE, Boyd N, McKinney S, Mehl E, Palmer C, et al. Ovarian carcinoma subtypes are different diseases: implications for biomarker studies. PLoS Med. 2008;5:e232.

Kurman RJ, Carcangiu ML, Herrington CS, Young RH (eds). WHO classification of tumours of female reproductive organs, 4th edn. Lyon, France: International Agency for Research on Cancer; 2014.

Kyrgiou, M., G. Salanti, N. Pavlidis, E. Paraskevaidis, and J.P. Ioannidis. 2006. Survival benefits with diverse chemotherapy regimens for ovarian cancer:meta-analysis ofmultiple treatments.JNatl Cancer Inst. 98 (22): 1655–1663. https://doi.org/10.1093/jnci/ djj443.

Li, Z., Mo, F., Wang, Y. et al. Enhancing Gasdermin-induced tumor pyroptosis through preventing ESCRT-dependent cell membrane repair augments antitumor immune response. Nat Commun 13, 6321 (2022). https://doi.org/10.1038/s41467-022-34036-8

Lin, J., Sun, S., Zhao, K. et al. Oncolytic Parapoxvirus induces Gasdermin E-mediated pyroptosis and activates antitumor immunity. Nat Commun 14, 224 (2023). https://doi.org/10.1038/s41467-023-35917-2

Liu, X., Z. Zhang, J. Ruan, Y. Pan, V.G. Magupalli, H. Wu, and J. Lieberman. 2016. Inflammasome-activated gasdermin D causes pyroptosis by forming membrane pores. Nature 535 (7610): 153– 158. https://doi.org/10.1038/nature18629 PMID: 27383986; PMCID: PMC5539988.

Liu, Z. et al. Crystal structures of the full-length murine and human Gasdermin D reveal mechanisms of autoinhibition, lipid binding, and oligomerization. Immunity 51, 43–49.e4 (2019).

Lou, X., Li, K., Qian, B. et al. Pyroptosis correlates with tumor immunity and prognosis. Commun Biol 5, 917 (2022). https://doi.org/10.1038/s42003-022-03806-x

Mabuchi, S., Sugiyama, T. & Kimura, T. Clear cell carcinoma of the ovary: molecular insights and future therapeutic perspectives. J. Gynecol. Oncol. 27, e31 (2016).

Marchetti C, De Felice F, Romito A, Iacobelli V, Sassu CM, Corrado G, et al. Chemotherapy resistance in epithelial ovarian cancer: Mechanisms and emerging treatments. Semin Cancer Biol. 2021;77:144–66.

Martinon F, Tschopp J. Inflammatory caspases and inflammasomes: master switches of inflammation. Cell Death Differ. 2007 Jan;14(1):10-22. doi: 10.1038/sj.cdd.4402038. Epub 2006 Sep 15. PMID: 16977329.

Martinon, F., Burns, K. & Tschopp, J. The inflammasome: a molecular platform triggering activation of inflammatory caspases and processing of proIL-β. Mol. Cell 10, 417–426 (2002).

Matulonis UA, Sood AK, Fallowfield L, Howitt BE, Sehouli J, Karlan BY. Ovarian cancer. Nat Rev Dis Prim. 2016;2:16061.

McMullen, M., Karakasis, K., Rottapel, R. & Oza, A. M. Advances in ovarian cancer, from biology to treatment. Nat. Cancer 2, 6–8 (2021).

Miao, E. A. et al. Caspase-1-induced pyroptosis is an innate immune effector mechanism against intracellular bacteria. Nat. Immunol. 11, 1136–1142 (2010).

Miguchi M, Hinoi T, Shimomura M, Adachi T, Saito Y, Niitsu H, Kochi M, Sada H, Sotomaru Y, Ikenoue T, Shigeyasu K, Tanakaya K, KitadaiY, Sentani K, Oue N, YasuiW, OhdanH. Gasdermin C is upregulated by inactivation of transforming growth factor β receptor type II in the presence of mutated Apc, promoting colorectal cancer proliferation. PLoS One. 2016 Nov 11;11(11):e0166422. doi: https://doi.org/10.1371/journal.pone.0166422. PMID: 27835699; PMCID: PMC5105946.

Mikuła-Pietrasik J, Witucka A, Pakuła M, Uruski P, Begier-Krasińska B, Niklas A, Tykarski A, Książek K. Comprehensive review on how platinum- and taxane-based chemotherapy of ovarian cancer affects biology of normal cells. Cell Mol Life Sci. 2019 Feb;76(4):681-697.

doi: 10.1007/s00018-018-2954-1. Epub 2018 Oct 31. PMID: 30382284; PMCID: PMC6514066.

Miller RE, Leary A, Scott CL, Serra V, Lord CJ, Bowtell D, et al. ESMO recommendations on predictive biomarker testing for homologous recombination deficiency and PARP inhibitor benefit in ovarian cancer. Ann Oncol. 2020;31:1606–1622.

Millstein, J. et al. Prognostic gene expression signature for high-grade serous ovarian cancer. Ann. Oncol. 31, 1240–1250 (2020).

Mirza MR, Monk BJ, Herrstedt J, Oza AM, Mahner S, Redondo A, et al. Niraparib maintenance therapy in platinum-sensitive, recurrent ovarian cancer. N Engl J Med. 2016;375:2154–2164.

Mohammadian M, Ghafari M, Khosravi B, et al. Variations in the incidence and mortality of ovarian cancer and their relationship with the human development index in European Countries in 2012. Biomed Res Ther. 2017;4(08):1541–1557. doi: 10.15419/bmrat.v4i08.228

Mok SC, Bonome T, Vathipadiekal V, Bell A, Johnson ME, Wong KK, Park DC, Hao K, Yip DK, Donninger H, Ozbun L, Samimi G, Brady J, RandonovichM, Pise-Masison CA, Barrett JC,WongWH, Welch WR, Berkowitz RS, Birrer MJ. A gene signature predictive for outcome in advanced ovarian cancer identifies a survival factor: microfibril-associated glycoprotein 2. Cancer Cell. 2009 Dec 8;16(6):521-32. doi:https://doi.org/10.1016/j.ccr.2009.10.018. PMID: 19962670; PMCID: PMC3008560.

Momenimovahed Z, Tiznobaik A, Taheri S, Salehiniya H. Ovarian cancer in the world: epidemiology and risk factors. Int J Womens Health. 2019 Apr 30;11:287-299. doi: 10.2147/IJWH.S197604. PMID: 31118829; PMCID: PMC6500433.

Morales J, Li L, Fattah FJ, Dong Y, Bey EA, Patel M, Gao J, Boothman DA. Review of poly (ADP-ribose) polymerase (PARP) mechanisms of action and rationale for targeting in cancer and other diseases. Crit Rev Eukaryot Gene Expr. 2014;24(1):15-28. doi: 10.1615/critreveukaryotgeneexpr.2013006875. PMID: 24579667; PMCID: PMC4806654.

Morgan M, Obenchain V, Hester J, Pagès H (2022). _SummarizedExperiment: SummarizedExperiment container_. R package version 1.26.1, <https://bioconductor.org/packages/SummarizedExperiment>.

Morgan M, Shepherd L (2022). _ExperimentHub: Client to access ExperimentHub resources_. R package version 2.4.0.

Mulvihill E, Sborgi L, Mari SA, Pfreundschuh M, Hiller S, Müller DJ. Mechanism of membrane pore formation by human gasdermin-D. EMBO J. 2018 Jul 13;37(14):e98321. doi: 10.15252/embj.201798321. Epub 2018 Jun 13. PMID: 29898893; PMCID: PMC6043855.

Murata T, Haisa M, Uetsuka H, Nobuhisa T, Ookawa T, Tabuchi Y, et al. Molecular mechanism of chemoresistance to cisplatin in ovarian cancer cell lines. Int J Mol Med. 2004;13:865–8. Mylavarapu S, Das A, Roy M. Role of BRCA Mutations in the Modulation of Response to Platinum Therapy. Front Oncol. 2018 Feb 5;8:16. doi: 10.3389/fonc.2018.00016. PMID: 29459887; PMCID: PMC5807680.

Nagy Á, Munkácsy G, Győrffy B. Pancancer survival analysis of cancer hallmark genes. Sci Rep. 2021;11(1):6047. https://doi.org/10.1038/s41598-021-84787-5.

Odunsi K. Immunotherapy in ovarian cancer. Ann Oncol. 2017 Nov 1;28(suppl_8):viii1-viii7. doi: 10.1093/annonc/mdx444. PMID: 29232467; PMCID: PMC5834124.

Oltra SS, Colomo S, Sin L, Pérez-López M, Lázaro S, Molina-Crespo A, Choi KH, Ros-Pardo D, Martínez L, Morales S, González-Paramos C, Orantes A, Soriano M, Hernández A, Lluch A, Rojo F, Albanell J, Gómez-Puertas P, Ko JK, Sarrió D, Moreno-Bueno G. Distinct GSDMB protein isoforms and protease cleavage processes differentially control pyroptotic cell death and mitochondrial damage in cancer cells. Cell Death Differ. 2023 Mar 11. doi: 10.1038/s41418- 023-01143-y. Epub ahead of print. PMID: 36899106.

Ooms J (2021). _magick: Advanced Graphics and Image-Processing in R_. R package version 2.7.3, <https://CRAN.R-project.org/package=magick>.

Orning P, Weng D, Starheim K, Ratner D, Best Z, Lee B, Brooks A, Xia S, Wu H, Kelliher MA, Berger SB, Gough PJ, Bertin J, Proulx MM, Goguen JD, Kayagaki N, Fitzgerald KA, Lien E. Pathogen blockade of TAK1 triggers caspase-8-dependent cleavage of gasdermin D and cell death. Science. 2 0 1 8 Nov 30;362(6418):1064-1069. doi: https://doi.org/10.1126/science.aau2818. Epub 2018 Oct 25. PMID: 30361383; PMCID: PMC6522129.

Papadopoulos, S., Jurgens, K. D. & Gros, G. Protein diffusion in living skeletal muscle fibers: dependence on protein size, fiber type, and contraction. Biophys. J. 79, 2084–2094 (2000).

Pennington KP, Walsh T, Harrell MI, Lee MK, Pennil CC, Rendi MH, et al. Germline and somatic mutations in homologous recombination genes predict platinum response and survival in ovarian, fallopian tube, and peritoneal carcinomas. Clin Cancer Res. 2014;20:764–775.

PF Pinsky, K Yu, BS Kramer, et al. Extended mortality results for ovarian cancer screening in the PLCO trial with median 15 years follow-up Gynecol Oncol, 143 (2016), pp. 270-275

Pujade-Lauraine E, Fujiwara K, Ledermann JA, Oza AM, Kristeleit R, Ray-Coquard IL, et al. Avelumab alone or in combination with chemotherapy versus chemotherapy alone in platinum-resistant or platinum-refractory ovarian cancer (JAVELIN Ovarian 200): An open-label, three-arm, randomised, phase 3 study. Lancet Oncol. 2021;22:1034–46.

Pujade-Lauraine E, Ledermann JA, Selle F, Gebski V, Penson RT, Oza AM, et al. Olaparib tablets as maintenance therapy in patients with platinum-sensitive, relapsed ovarian cancer and a BRCA1/2 mutation (SOLO2/ENGOT-Ov21): a double-blind, randomised, placebo-controlled, phase 3 trial. Lancet Oncol. 2017;18:1274–1284.

Qiao, L., X. Wu, J. Zhang, L. Liu, X. Sui, R. Zhang, W. Liu, F. Shen,Y. Sun, andX.Xi. 2019 Nov. α-NETA induces pyroptosis of epithelial ovarian cancer cells through the GSDMD/caspase-4 pathway. FASEB J. 33 (11): 12760–12767. https://doi.org/10.1096/ fj.201900483RR.

R Core Team (2022). R: A language and environment for statistical computing. R Foundation for Statistical Computing, Vienna, Austria. URL https://www.R-project.org/.

Rana, N. et al. GSDMB is increased in IBD and regulates epithelial restitution/repair independent of pyroptosis. Cell https://doi.org/10.1016/j.cell.2021.12.024 (2022).

Ray, M., Hostetter, D. R., Loeb, C. R., Simko, J. & Craik, C. S. Inhibition of Granzyme B by PI-9 protects prostate cancer cells from apoptosis. Prostate 72, 846–855 (2012).Return to ref 84 in article

Rogers C, Fernandes-Alnemri T, Mayes L, Alnemri D, Cingolani G, Alnemri ES. Cleavage of DFNA5 by caspase-3 during apoptosis mediates progression to secondary necrotic/pyroptotic cell death. Nat Commun. 2017 Jan 3;8:14128. doi: https://doi.org/10.1038/ncomms14128. PMID: 28045099; PMCID: PMC5216131.

Rogers, C. et al. Cleavage of DFNA5 by caspase-3 during apoptosis mediates progression to secondary necrotic/pyroptotic cell death. Nat. Commun. 8, 14128 (2017).

Ruan, J., Xia, S., Liu, X., Lieberman, J. & Wu, H. Cryo-EM structure of the gasdermin A3 membrane pore. Nature 557, 62–67 (2018).

Rubin SC, Randall TC, Armstrong KA, Chi DS, Hoskins WJ. Ten-year follow-up of ovarian cancer patients after second-look laparotomy with negative findings. Obstet Gynecol. 1999;93:21–24.

Rühl, S. et al. ESCRT-dependent membrane repair negatively regulates pyroptosis downstream of GSDMD activation. *Science* 362, 956–960 (2018).

Saeki, N., T. Usui, K. Aoyagi, D.H. Kim, M. Sato, T. Mabuchi, K. Yanagihara, K. Ogawa, H. Sakamoto, T. Yoshida, and H. Sasaki. 2009 Mar. Distinctive expression and function of four GSDM family genes (GSDMA-D) in normal and malignant upper gastrointestinal epithelium. *Genes Chromosomes Cancer.* 48 (3): 261–271. https://doi.org/10.1002/gcc.20636.

Saeki, N., Y. Kuwahara, H. Sasaki, H. Satoh, and T. Shiroishi. 2000 Sep. Gasdermin (Gsdm) localizing to mouse Chromosome 11 is predominantly expressed in upper gastrointestinal tract but significantly suppressed in human gastric cancer cells. Mamm Genome. 11 (9): 718–724. https://doi.org/10.1007/s003350010138.

Sagulenko, V. et al. AIM2 and NLRP3 inflammasomes activate both apoptotic and pyroptotic death pathways via ASC. Cell Death Differ. 20, 1149–1160 (2013).

Sanjo, H., J. Nakayama, T. Yoshizawa, H.J. Fehling, S. Akira, and S. Taki. 2019 Aug 15. Cutting edge: TAK1 safeguards macrophages against proinflammatory cell death. *J Immunol.* 203 (4): 783–788. https://doi.org/10.4049/jimmunol.1900202.

Sankaranarayanan R, Ferlay J. Worldwide burden of gynaecological cancer: the size of the problem. Best Pract Res Clin Obstet Gynaecol. 2006;20:207–25.

Santa Cruz Garcia AB, Schnur KP, Malik AB, Mo GCH. Gasdermin D pores are dynamically regulated by local phosphoinositide circuitry. Nat Commun. 2022 Jan 10;13(1):52. doi: 10.1038/s41467-021-27692-9. PMID: 35013201; PMCID: PMC8748731.

Sarhan J, Liu BC, Muendlein HI, Li P, Nilson R, Tang AY, Rongvaux A, Bunnell SC, Shao F, Green DR, Poltorak A. Caspase-8 induces cleavage of gasdermin D to elicit pyroptosis during Yersinia infection. Proc Natl Acad Sci U S A. 2018 Nov 13;115(46):E10888-E10897. doi: https://doi.org/10.1073/ pnas.1809548115. Epub 2018 Oct 31. PMID: 30381458; PMCID: PMC6243247.

Sborgi L, Rühl S, Mulvihill E, Pipercevic J, Heilig R, Stahlberg H, Farady CJ, Müller DJ, Broz P, Hiller S. GSDMD membrane pore formation constitutes the mechanism of pyroptotic cell

death. EMBO J. 2016 Aug 15;35(16):1766-78. doi: 10.15252/ embj.201694696. Epub 2016 Jul 14. PMID: 27418190; PMCID: PMC5010048.

Schloerke B, Cook D, Larmarange J, Briatte F, Marbach M, Thoen E, Elberg A, Crowley J (2021). _GGally: Extension to 'ggplot2'_. R package version 2.1.2, <https://CRAN.R-project.org/package=GGally>.

Seidman JD, Horkayne-Szakaly I, Haiba M, Boice CR, Kurman RJ, Ronnett BM. The histologic type and stage distribution of ovarian carcinomas of surface epithelial origin. Int J Gynecol Pathol. 2004;23:41–4.

Shi, J., Y. Zhao, K. Wang, X. Shi, Y. Wang, H. Huang, Y. Zhuang, T. Cai, F. Wang, and F. Shao. 2015 Oct 29. Cleavage of GSDMD by inflammatory caspases determines pyroptotic cell death. *Nature.* 526 (7575): 660–665. https://doi.org/10.1038/nature15514.

Shih IeM, Kurman RJ. Ovarian tumorigenesis: a proposed model based on morphological and molecular genetic analysis. Am J Pathol. 2004;164:1511–8.

Siddik ZH. Cisplatin: mode of cytotoxic action and molecular basis of resistance. Oncogene 2003;22:7265–79.

Siegel R, Jemal A. Cancer statistics, 2020. CA Cancer J Clin. 2020;70:7–30.

Siegel, R. M. Caspases at the crossroads of immune-cell life and death. Nat. Rev. Immunol. 6, 308–317 (2006).

Silge J, RobinsonD (2016). "tidytext: textmining and analysis using tidy data principles in R." JOSS, 1(3). doi: https://doi.org/10.21105/ joss.00037.

Society AC Cancer Facts & Figures 2019. Atlanta, GA: American Cancer Society; 2019.
SS Buys, E Partridge, A Black, et al. Effect of screening on ovarian cancer mortality: the Prostate, Lung, Colorectal and Ovarian (PLCO) cancer screening randomized controlled trial JAMA, 305 (2011), pp. 2295-2303

Stockwell, B. R. et al. Ferroptosis: a regulated cell death nexus linking metabolism, redox biology, and disease. Cell 171, 273–285 (2017).

Sugiyama, T. et al. Clinical characteristics of clear cell carcinoma of the ovary: a distinct histologic type with poor prognosis and resistance to platinum-based chemotherapy. Cancer 88, 2584–2589 (2000).

Sun Q, Yang J, Xing G, Sun Q, Zhang L, He F. Expression of GSDML associates with tumor progression in uterine cervix cancer. Transl Oncol. 2008 Jul;1(2):73-83. doi: https://doi.org/10.1593/ tlo.08112. PMID: 18633457; PMCID: PMC2510814.

Sung H, Ferlay J, Siegel RL, Laversanne M, Soerjomataram I, Jemal A, et al. Global cancer statistics 2020: GLOBOCAN estimates of incidence and mortality worldwide for 36 cancers in 185 countries. CA Cancer J Clin. 2021;71:209–49.

Taabazuing CY, Okondo MC, Bachovchin DA. Pyroptosis and apoptosis pathways engage in bidirectional crosstalk in monocytes and macrophages. Cell Chem Biol. 2017 Apr 20;24(4):507-514.e4. https://doi.org/10.1016/j.chembiol.2017.03.009. Epub 2017 Apr 6. PMID: 28392147; PMCID: PMC5467448.

Takenaka M, Saito M, Iwakawa R, Yanaihara N, Saito M, Kato M, Ichikawa H, Shibata T, Yokota J, Okamoto A, Kohno T. Profiling of actionable gene alterations in ovarian cancer by targeted deep sequencing. Int J Oncol. 2015;46(6):2389-98. doi: 10.3892/ijo.2015.2951. Epub 2015 Apr 3. PMID: 25846456.

Tang, R. et al. Ferroptosis, necroptosis, and pyroptosis in anticancer immunity. J. Hematol. Oncol. 13, 110 (2020).

Tomiyoshi, G., Horita, Y., Nishita, M., Ohashi, K. & Mizuno, K. Caspase-mediated cleavage and activation of LIM-kinase 1 and its role in apoptotic membrane blebbing. Genes Cells 9, 591–600 (2004).

Tsuruo T, Hamilton TC, Louie KG, Behrens BC, Young RC, Ozols RF. Collateral susceptibility of adriamycin-, melphalan- and cisplatin-resistant human ovarian tumor cells to bleomycin. Jpn J Cancer Res. 1986 Sep;77(9):941-5. PMID: 2429947.

Vathipadiekal, V., V. Wang, W. Wei, L. Waldron, R. Drapkin, M. Gillette, S. Skates, and M. Birrer. 2015 Nov 1. Creation of a human secretome: a novel composite library of human secreted proteins: validation using ovarian cancer gene expression data and a virtual secretome array. Clin Cancer Res. 21 (21): 4960–4969. https:// doi.org/10.1158/1078-0432.CCR-14-3173.

Vercammen, D., Vandenabeele, P., Beyaert, R., Declercq, W. & Fiers, W. Tumour necrosis factor-induced necrosis versus anti-Fas-induced apoptosis in L929 cells. Cytokine 9, 801–808 (1997).

Wang C, Ruan J. An ancient defense mechanism: Conservation of gasdermin-mediated pyroptosis. PLoS Biol. 2023 May 4;21(5):e3002103. doi: 10.1371/journal.pbio.3002103. PMID: 37141191; PMCID: PMC10159131.

Wang, Q., Peng, H., Qi, X., Wu, M. & Zhao, X. Targeted therapies in gynecological cancers: a comprehensive review of clinical evidence. Signal Transduct. Target Ther. 5, 137 (2020).

Wang, Y., and F. Shao. 2021 Apr 1. NINJ1, rupturing swollen membranes for cataclysmic cell lysis. Mol Cell. 81 (7): 1370– 1371. https://doi.org/10.1016/j.molcel.2021.03.005.

Wang, Y., W. Gao, X. Shi, J. Ding, W. Liu, H. He, K. Wang, and F. Shao. 2017 Jul 6. Chemotherapy drugs induce pyroptosis through caspase-3 cleavage of a gasdermin. *Nature.* 547 (7661): 99–103. https://doi.org/10.1038/nature22393.

Watabe K, Ito A, Asada H, Endo Y, Kobayashi T, Nakamoto K, Itami S, Takao S, Shinomura Y, Aikou T, Yoshikawa K, Matsuzawa Y, Kitamura Y, Nojima H. Structure, expression and chromosome mapping ofMLZE, a novel gene which is preferentially expressed in metastatic melanoma cells. Jpn J Cancer Res. 2001 Feb;92(2):140- 51. doi: https://doi.org/10.1111/j.1349-7006.2001.tb01076.x. PMID: 11223543; PMCID: PMC5926699.

Watson, P. R. et al. Salmonella enterica serovars Typhimurium and Dublin can lyse macrophages by a mechanism distinct from apoptosis. Infect. Immun. 68, 3744–3747 (2000).

Whisstock JC, Law RHP. The role of NINJ1 protein in programmed cellular destruction. Nature. 2023 May 17. doi: 10.1038/d41586-023-01602-z. Epub ahead of print. PMID: 37198463.

Wickham H, Averick M, Bryan J, Chang W, McGowan LD, François R, Grolemund G, Hayes A, Henry L, Hester J, Kuhn M, Pedersen TL, Miller E, Bache SM, Müller K, Ooms J, Robinson D, Seidel DP, Spinu V, Takahashi K, Vaughan D, Wilke C, Woo K, Yutani H (2019). "Welcome to the tidyverse." _Journal of Open Source Software_, *4*(43), 1686. doi:10.21105/joss.01686 <https://doi.org/10.21105/joss.01686>.

Wickham H, Bryan J (2022). _readxl: Read Excel Files_. R package version 1.4.1, <https://CRAN.R-project.org/package=readxl>.

Wickham, et al. 2019. Welcome to the tidyverse. Journal of Open Source Software 4 (43): 1686. https://doi.org/10.21105/joss.

Wickham, H., Grolemund, G. (2017). R for Data Science: Import, Tidy, Transform, Visualize, and Model Data. O'Reilly Media. ISBN: 1491910399

Wilke C, Wiernik B (2022). _ggtext: Improved Text Rendering Support for 'ggplot2'_. R package version 0.1.2, <https://CRAN.R-project.org/package=ggtext>.

Wu R, Hendrix-Lucas N, Kuick R, Zhai Y et al. Mouse model of human ovarian endometrioid adenocarcinoma based on somatic defects in the Wnt/beta-catenin and PI3K/Pten signaling pathways. Cancer Cell 2007 Apr;11(4):321-33. PMID: 17418409

Wu R, Zhai Y, Kuick R, Karnezis AN, Garcia P, Naseem A, Hu TC, Fearon ER, Cho KR. Impact of oviductal versus ovarian epithelial cell of origin on ovarian endometrioid carcinoma phenotype in the mouse. J Pathol. 2016 Nov;240(3):341-351. doi: https://doi.org/10.1002/path.4783. PMID: 27538791; PMCID: PMC5071155.

Xia X et al. The role of pyroptosis in cancer: pro-cancer or pro-"host"? Cell death dis. 10, 650 (2019).

Yacobi-Sharon, K., Namdar, Y. & Arama, E. Alternative germ cell death pathway in Drosophila involves HtrA2/Omi, lysosomes, and a caspase-9 counterpart. Dev. Cell 25, 29–42 (2013).

Yihui Xie (2014) knitr: A Comprehensive Tool for Reproducible Research in R. In Victoria Stodden, Friedrich Leisch and Roger D. Peng, editors, Implementing Reproducible Computational Research. Chapman and Hall/CRC. ISBN 978-1466561595.

Yihui Xie (2015) Dynamic Documents with R and knitr. 2nd edition. Chapman and Hall/CRC. ISBN 978-1498716963.

Yihui Xie (2020). knitr: a general-purpose package for dynamic report generation in R. R package version 1.30.

Yihui Xie (2022). knitr: A General-Purpose Package for Dynamic Report Generation in R. R package version 1.41.

Yihui Xie and Christophe Dervieux and Emily Riederer (2020). R Markdown Cookbook. Chapman and Hall/CRC. ISBN 9780367563837. URL https://bookdown.org/yihui/rmarkdown-cookbook.

Yihui Xie and J.J. Allaire and Garrett Grolemund (2018). R Markdown: The Definitive Guide. Chapman and Hall/CRC. ISBN 9781138359338. URL https://bookdown.org/yihui/rmarkdown.

Yokoi, A. et al. Malignant extracellular vesicles carrying MMP1 mRNA facilitate peritoneal dissemination in ovarian cancer. Nat. Commun. 8, 14470 (2017).

Yokomizo, K., Y. Harada, K. Kijima, K. Shinmura, M. Sakata, K. Sakuraba, Y. Kitamura, A. Shirahata, T. Goto, H. Mizukami, M. Saito, G. Kigawa, H. Nemoto, and K. Hibi. 2012 Apr. Methylation of the DFNA5 gene is frequently detected in colorectal cancer. Anticancer Res. 32 (4): 1319–1322.

Yoshihara,K., A. Tajima,D. Komata, T.Yamamoto, S.Kodama,H. Fujiwara, M. Suzuki, Y. Onishi, M. Hatae, K. Sueyoshi, H. Fujiwara, Y. Kudo, I. Inoue, and K. Tanaka. 2009 Aug. Gene expression profiling of advanced-stage serous ovarian cancers distinguishes novel subclasses and implicates ZEB2 in tumor progression and prognosis. Cancer Sci. 100 (8): 1421–1428. https://doi.org/ 10.1111/j.1349-7006.2009.01204.x.

Zerbino DR,Achuthan P, Akanni W,AmodeMR, Barrell D, Bhai J, Billis K, Cummins C, Gall A, Girón CG, Gil L, Gordon L, Haggerty L, Haskell E, Hourlier T, Izuogu OG, Janacek SH, Juettemann T, To JK, Laird MR, Lavidas I, Liu Z, Loveland JE, Maurel T, McLaren W, Moore B,Mudge J, Murphy DN, Newman V, Nuhn M, Ogeh D, Ong CK, Parker A, Patricio M, Riat HS, Schuilenburg H, Sheppard D, SparrowH, Taylor K, Thormann A,Vullo A, Walts B, ZadissaA, Frankish A, Hunt SE, Kostadima M, Langridge N, Martin FJ, Muffato M, Perry E, Ruffier M, Staines DM, Trevanion SJ, Aken BL, Cunningham F, Yates A, Flicek P. Ensembl 2018. Nucleic Acids Res. 2018 Jan 4;46(D1):D754-D761. https://doi.org/ 10.1093/nar/gkx1098. PMID: 29155950; PMCID: PMC5753206.

Zhang Z, Zhang Y, Xia S, Kong Q, Li S, Liu X, Junqueira C, Meza- Sosa KF, Mok TMY, Ansara J, Sengupta S, Yao Y, Wu H, Lieberman J. Gasdermin E suppresses tumour growth by activating anti-tumour immunity. Nature. 2020 Mar;579(7799):415-420. doi: https://doi.org/10.1038/s41586-020-2071-9. Epub 2020 Mar 11. PMID: 32188940; PMCID: PMC7123794.

Zhang, Y., Chen, X., Gueydan, C. & Han, J. Plasma membrane changes during programmed cell deaths. Cell Res. 28, 9–21 (2018).

Zhong, X., Zeng, H., Zhou, Z. et al. Structural mechanisms for regulation of GSDMB pore-forming activity. Nature 616, 598–605 (2023). https://doi.org/10.1038/s41586-023-05872-5

Zhou Z, He H, Wang K, Shi X, Wang Y, Su Y, Wang Y, Li D, Liu W, Zhang Y, Shen L, Han W, Shen L, Ding J, Shao F. Granzyme A from cytotoxic lymphocytes cleaves GSDMB to trigger pyroptosis in target cells. Science. 2020 May 29;368(6494):eaaz7548. doi: https://doi.org/10.1126/science.aaz7548. Epub 2020 Apr 16.